AD-A087 002 NAVAL RESEARCH LAB WASHINGTON DC F/G 20/11
PIPING INELASTIC FRACTURE MECHANICS ANALYSIS.(U)
JUN 80 C I CHANG, M NAKAGAKI, C A GRIFFIS NRC-03-79-116
UNCLASSIFIED NRL-MR-4259 NUREG-CR-1119 NL

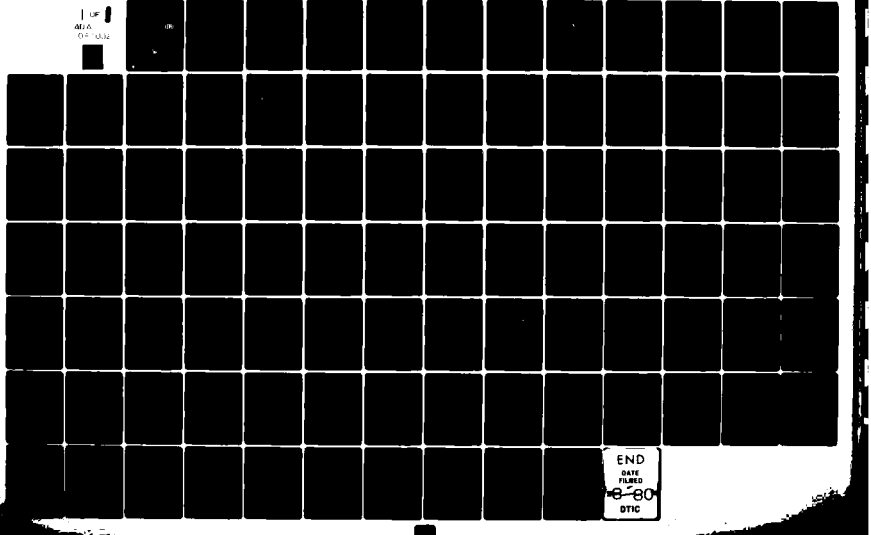

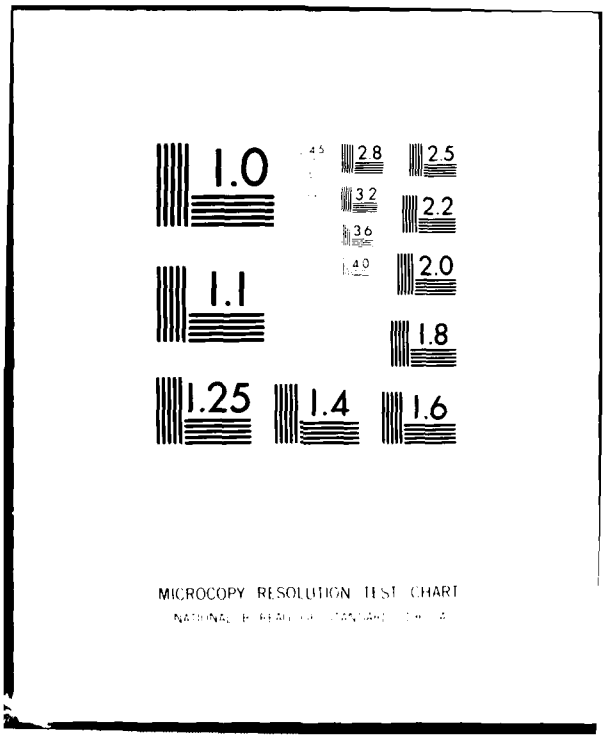
1.0
2.8
2.5
3.2
2.2
3.6
4.0
2.0
1.1
1.8
1.25
1.4
1.6
MICROCOPY RESOLUTION TEST CHART

LEVEL II

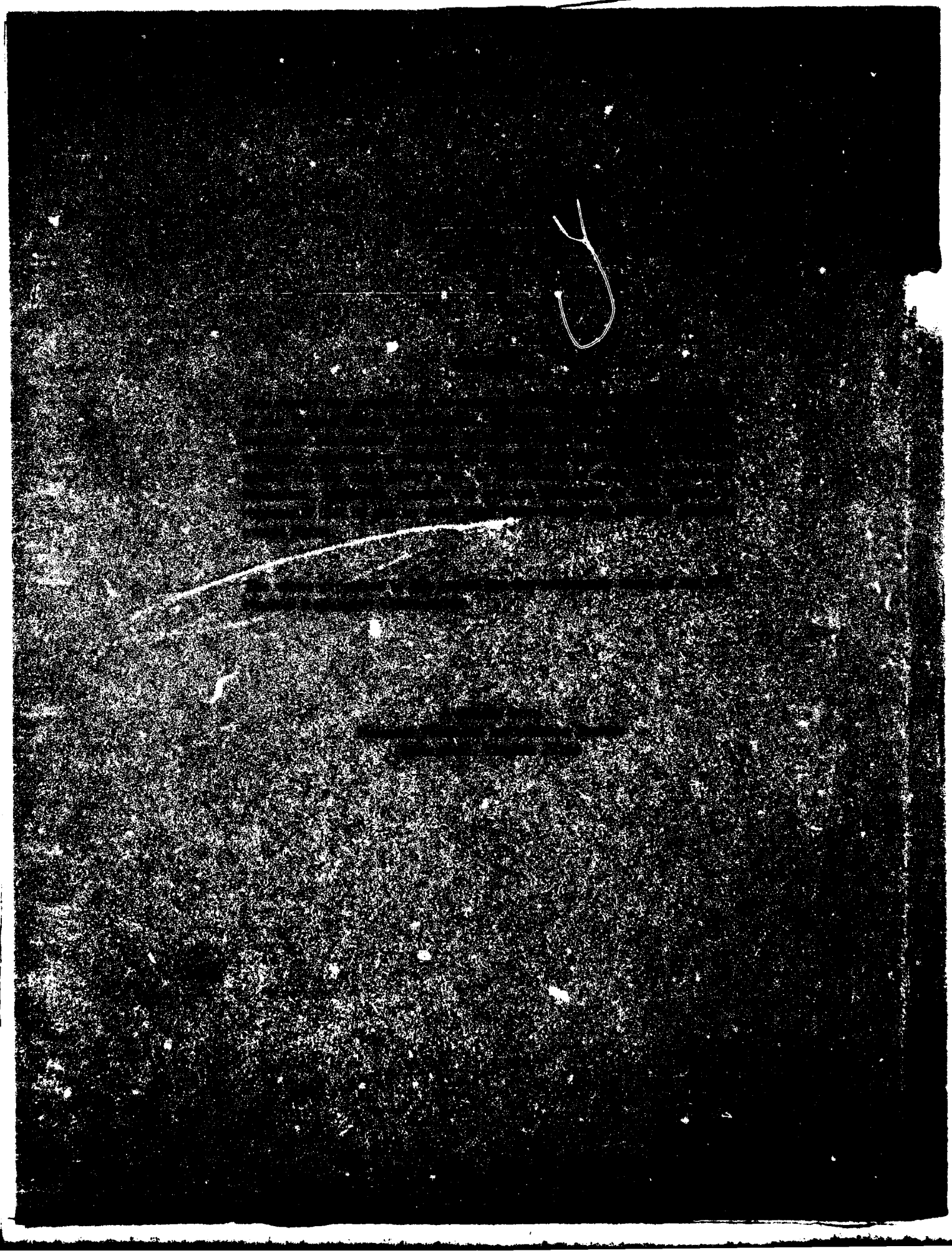

(9) Memorandum Rept.

SECURITY CLASSIFICATION OF THIS PAGE (When Data Entered)

REPORT DOCUMENTATION PAGE

READ INSTRUCTIONS BEFORE COMPLETING FORM

1. REPORT NUMBER
NUREG/CR 1119
NRL Memorandum Report 4259

2. GOVT ACCESSION NO.
AD-A087002

3. RECIPIENT'S CATALOG NUMBER

4. TITLE (and Subtitle)
(6) PIPING INELASTIC FRACTURE MECHANICS ANALYSIS

5. TYPE OF REPORT & PERIOD COVERED
Interim report on a continuing NRL problem.

6. PERFORMING ORG. REPORT NUMBER
(15)

7. AUTHOR(s)
(10) C. I. Chang, M. Nakagaki, C. A. Griffis and R. A. Masumura

8. CONTRACT OR GRANT NUMBER(s)
NRC-03-79-116,
NRC-FIN-B6587

9. PERFORMING ORGANIZATION NAME AND ADDRESS
Naval Research Laboratory
Washington, D.C. 20735

10. PROGRAM ELEMENT, PROJECT, TASK AREA & WORK UNIT NUMBERS
NRL Problem 63-1002-0

11. CONTROLLING OFFICE NAME AND ADDRESS
U.S. Nuclear Regulatory Commission
Office of the Controller
Washington, D.C. 20555

(11) 30

12. REPORT DATE
June 1980

13. NUMBER OF PAGES
90

14. MONITORING AGENCY NAME & ADDRESS(if different from Controlling Office)
(12) 91

15. SECURITY CLASS. (of this report)
UNCLASSIFIED

15a. DECLASSIFICATION/DOWNGRADING SCHEDULE

16. DISTRIBUTION STATEMENT (of this Report)

Approved for public release; distribution unlimited.

(14) NRL-MR-4259

17. DISTRIBUTION STATEMENT (of the abstract entered in Block 20, if different from Report)

(18) NUREG, SBIE

(19) CR-1119, AD-A000 423

18. SUPPLEMENTARY NOTES

Prepared for the U.S. Nuclear Regulatory Commission, Office of Nuclear Regulatory Research, Reactor Safety Research Division under Interagency Agreement DE-AI14-80FF37115. NRC Distribution Category R1 and R5.

19. KEY WORDS (Continue on reverse side if necessary and identify by block number)

LWR pipe rupture	Tearing modulus	Leak-before-break
Fracture toughness	Crack opening angle	
Pseudo toughness theory	J-resistance	
Flow stress theory	Stability index	
J-controlled crack growth	Energy release (or dissipation) rate	

20. ABSTRACT (Continue on reverse side if necessary and identify by block number)

Available experimental data and the analytical methods for predicting rupture of LWR piping are assembled and assessed. The analytical techniques investigated can be catologued into three major groups: structural response, semiempirical methods, and the J-controlled growth approach. A leak-before-break condition is also investigated.

DD FORM 1 JAN 73 1473 EDITION OF 1 NOV 65 IS OBSOLETE
S/N 0102-014-6601

SECURITY CLASSIFICATION OF THIS PAGE (When Data Entered)

251 250

CONTENTS

PIPING INELASTIC FRACTURE MECHANICS ANALYSIS

1.0 SUMMARY

This report summarizes the results and conclusions of Task 1 and 2 of the study on "Piping Inelastic Fracture Mechanics Analysis", Contract Number (NRC-03-79-116). In these tasks, available experimental data and the analytical methods for predicting rupture of LWR piping have been assembled and assessed. The analytical techniques investigated can be catalogued into three major groups. These are gross structural response analysis, semiempirical methods, and the J-controlled growth approach.

The gross structural response is computed using numerical techniques when dynamic behavior of both the piping and the fluid is considered. The LWR piping stability is modeled by allowing a preassigned crack to propagate under a certain toughness criterion such as K_{Ic}, K_{Id} or maximum strain at the crack tips. In this analysis, the accuracy of the results depends very heavily on the crack growth criterion about which little information is known. When brittle failure is observed, K_{Ic} or K_{Id} may be adequate. For a pipe that fails plastically or in a mixed brittle/ductile failure mode, well established fracture criteria are not yet available. In addition, a single computer run frequently provides numerical results which may not be extrapolated to other cases where computing costs prevent additional runs to be made.

Depending upon the piping materials and their service temperature, a semiempirical approach has been proposed to study elastic/plastic fracture of LWR piping. A pseudo-toughness parameter, K_c, has been derived from classical fracture mechanics theory and modified to describe the toughness of the piping made of low to medium toughness materials. Unfortunately, poor correlation was found between the pseudo-toughness, K_c, and experimental results. For high-toughness materials, a flow

Manuscript submitted April 30, 1980.

stress theory has been proposed. In this case, the theory characterizes the piping stability by its limit load carrying capability and contains no fracture parameter of any type. By properly adjusting the flow stress value, experimental results from tests on piping made of high toughness materials suggest that the flow stress theory may be adequate. However, upon further evaluation, it is revealed that structural stability is influenced by both crack tip conditions as well as structural geometry. Therefore, more conclusive analytical or experimental evidence is needed before any conclusion can be drawn regarding the adequacy and the applicability of the semiempirical methods in LWR rupture prediction.

One of the most promising and most rigorous predictive methods to date is the J-control growth. J_{Ic} has been accepted as an elastic/plastic fracture initiation criterion and the existence of a HRR (Hutchinson-Rice-Rosengren) field has been identified as the necessary condition of a J-dominated stress field. Once a crack starts to propagate, however, large deformations and unloading near the crack tip region are expected; these factors are not accounted for in the original J-theory formation where infinitesimal deformation and deformation theory of plasticity (no unloading) are assumed. Nevertheless, extensive research effort has been directed to extend J to a governing crack propagation criterion in spite of its underlying assumptions. Other crack extension criteria, closely associated with the J-controlled growth, include crack opening angle (COA), tearing modulus (T), finite stretch and stability index (λ_I). It is noted that these extension criteria are all related and permissible in treating a limited amount of crack growth.

A leak before break condition is expected for high toughness materials as well as medium to high toughness materials at shelf temperature. The large critical flaw sizes associated with these materials suggest that extensive leaking, as well as general yielding, will precede attainment of a critical fracture condition. There are simplified methods to compute mouth opening for pipes of these materials in transition region; however, their accuracy remains to be established.

2.0 INTRODUCTION

The purpose of this work is to study nuclear reactor pipe failure due to elastic/plastic fracture. The scope of this study includes definition of critical flaw size-stress level conditions necessary to induce structural instability. Subcritical growth mechanisms, such as fatigue and stress-corrosion, as well as crack arrest will not be discussed. A primary objective here is to assemble and to ultilize existing experimental data and analytical tools toward the study of elastic/plastic pipe rupture. Therefore, no basic research in the fundamentals of elastic/plastic fracture mechanics or experiments in generating new data are included. Only limited amount of information is included for the analytical methods presented in this report. Details of the formulation and justification should be referred to the original work which are included in the references. In this report, vast amount of experimental data has been collected for later use; but details of experimental techniques and variables are partially omitted.

2.1 LWR Cracking Experience

Cracking of LWR piping was first observed Dec. 1965, when a leakage was found in a 6 in. bypass line of the recirculation loop in Dresden I. Between 1965 and 1975, cracks were discovered on many 4 in. diameter 304 s.s. pipes for recirculation loop valve bypass, and on 10 in. diameter 304 s.s. reactor core spray lines (Figs. 1 and 2) in six domestic Boiling Water Reactors. These BWRs are Dresden 2, Quad City 1 and 2, Millstation 1, Peach Bottom 3 and Monticello. Subsequent investigation [1] has concluded these flaws were produced by intergranular stress corrosion cracking (IGSCC) and are due to the combined effects of stress, oxidization, sensitization and fatigue growth. Subsequent to 1975, IGSCC has also been found in other location such as reactor-water-clean up lines and control-rod-drive-return lines. In 1978, cracks in large diameter pipes (greater than 20 in O.D) were discovered. In this case, extensive cracking was found on a 24 in. diameter recirculation-inlet-nozzle safe end (Fig. 3) at the Duane Arnold Plant. Following intensive investigation, NRC's pipe crack study group [2]

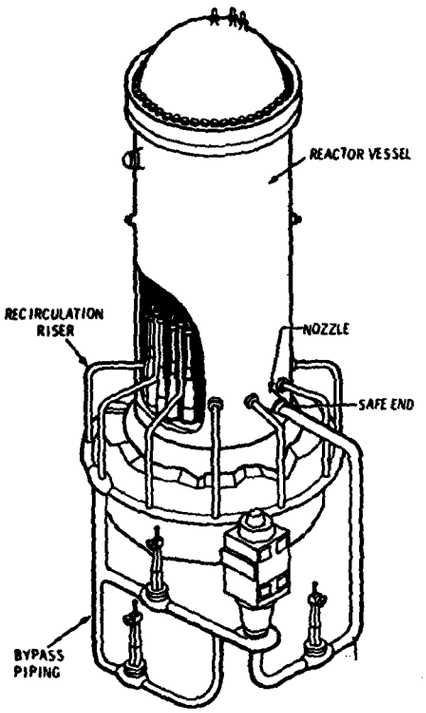

Fig. 1—BWR Recirculation System

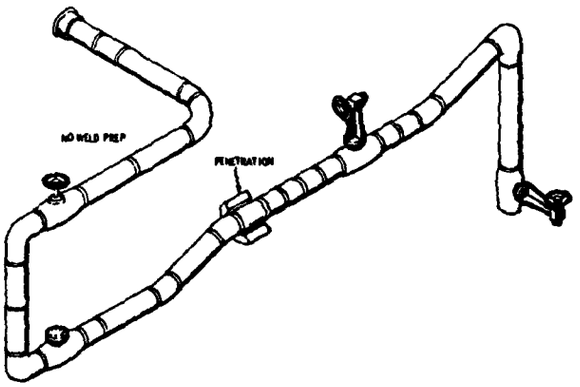

Fig. 2—Dresden-2 core spray-loop A (north)

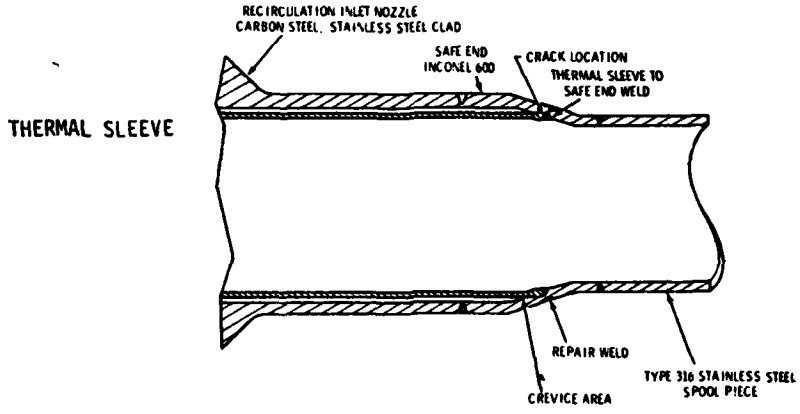

Fig. 3.1—Duane Arnold recirculation-inlet-nozzle safe end configuration

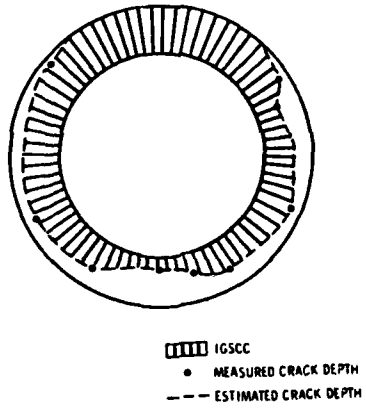

Fig. 3.2—Representation of IGSCC in Duane Arnold leaking recirculation-inlet-Nozzle safe end

concluded that the crevice geometry at this location and the sensitized material enhanced the IGSCC mechanism even on these larger pipes.

The stress corrosion problem in PWR is not as severe as that in BWR due to low oxygen content in the water and fewer furnace-sensitized safe ends. Therefore, no problem has been experienced in PWR primary systems. Nevertheless, in the secondary system, inter and transgranular stress corrosion cracking has been observed in these locations where relatively stagnant boric acid solution are present.

The impurities were introduced by safety injection and borated water make-up systems. At Arkansas 1, Ginna and Surry 1 plants, the piping involved were Type 304 s.s. in 8 in. and 10 in. sizes.

A detail complication of the LWR failure experience can be found in References 3 and 4.

2.2 Materials, Geometry and Environment

The most commonly used materials in the LWR piping system are Types 304 and 316 austenitic stainless steel (cast/wrought). However, for various reasons, such as intergranular stress corrosion prevention or others, ferrific steels such as SA-333, SA-106 and SA-516 have also been used. Feed water lines in PWR and steam lines in BWR are typical examples. Table 1 is a comparison of the tensile properties of these materials. In addition, low carbon stainless steel 304L or 306L and other stress corrosion resistant materials have been recommended for piping applications [1].

The piping system in LWR is very complex and a typical 4-loop Westinghouse configuration is shown in Fig. 4 [2]. It can be classified by its functional requirements or by the material, geometry and environment to which it is subjected. In this report, since only the consequence of the existence of a flaw is to be investigated, a pipe is referred by its size, material composition, and the loading on it. At this point, it should be noted that nearly all the cracks discovered to date are located in the weldment or HAZ where the piping is connected to the nozzle. These connections may be to the reactor vessel, steam generator, feedwater system pressurizer, or other components. Although the major loads on the system are pressure, thermal and mechanical loads (e.g. seismic and water hammering), the contribution of the residual stress due to the welding plays a very important role in initiation and propagation characteristics of cracks. If pressure stress dictates the pipe failure, only axial cracks resulting from large hoop stress are possible. However, the combined effects of material sensitization, residual stress

TABLE 1. Material Tensile Properties of Ferritic Steels

Material	Impact Requirement		Tensile						
A-333 (Seamless and Welded steel pipe for low temperature service)	Yes!	Grade	1	3	4	6	7	8	9
		σ_u	55	65	60	60	65	100	63
		σ_y	30	35	35	35	35	75	46
A-106 (Seamless carbon steel pipe for high temperature service- 1/8 to 26 inches)	No!	Grade	A		B		C		
		σ_u	48		60		70		
		σ_y	30		35		40		
A-516 (pressure vessel plates, carbon steel, for moderate and low temperature service)	Improved notch toughness	Grade	55		60		65	70	
		σ_u	55-75		60-80		65-85	70-90	
		σ_y	30		32		35	35	

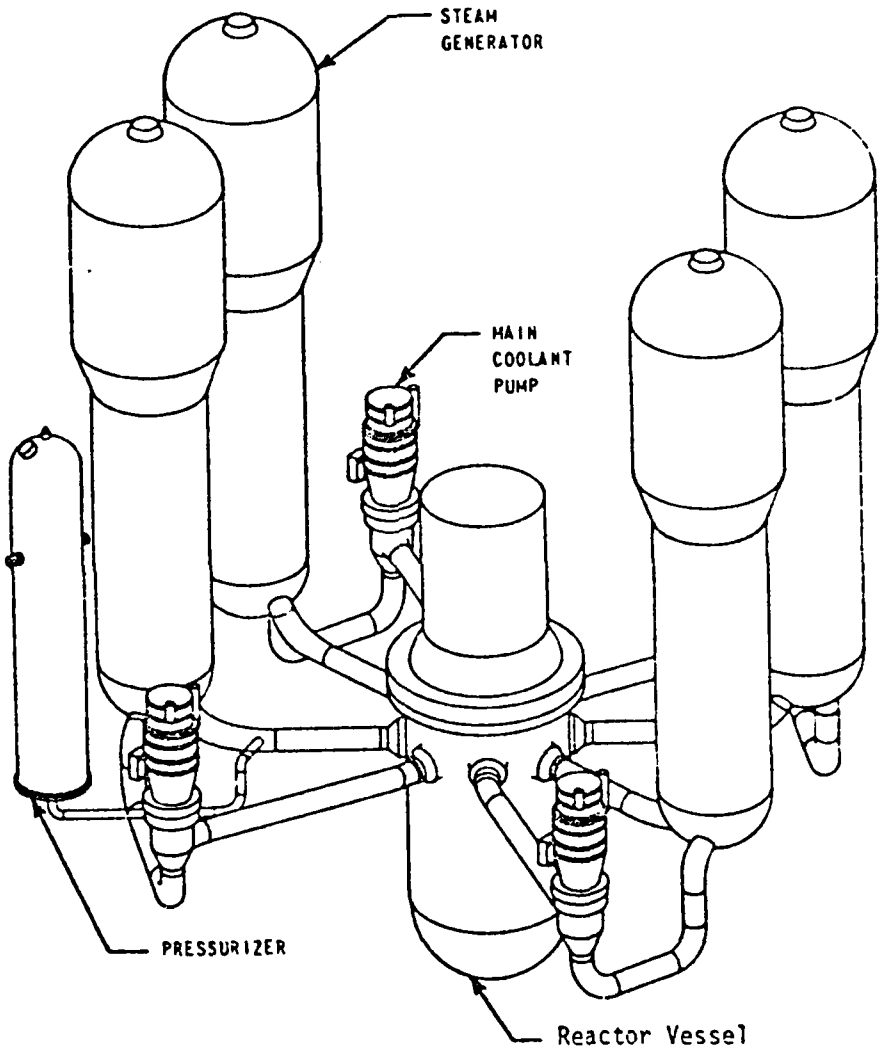

Fig. 4— Primary pressure boundary of a typical 4-loop Westinghouse Nuclear Power Plant

from welding processes, pressure and bending stress often initiate and propagate cracks in the circumferential directions. In addition, because both bending and residual stresses are self-equilibrating quantities, failure generally initiates at the surface where the combined stress is the largest. In the study of pipe integrity, both surface and through-wall cracks are of equal importance.

The operating conditions of a typical Pressure Water Reactor (PWR) is at a pressure of 2235 psi and at temperature of 650°F. The Boiling Water Reactor (BWR) is operated at around 1035 psi and 550°F. The size of these pipes are approximately 30 in. diameter for main loop and steam generator loop, and 6 to 14 in. diameter for the other large branches.

2.3 Material Characteristics and Fracture Toughness

Toughness is one of the material properties that is essential to the integrity of a structure. The actual material toughness is both geometry dependent and temperature sensitive. Because of the microstructural variation and different constraint condition surrounding a sharp flaw, a component can have brittle failure, ductile rupture or mixture of both.

To illustrate this phenomeon, a schematic Dynamic Tearing (DT) test result of fixed thickness specimens are shown in Fig. 5. At the Nil Ductility Transition (NDT) temperature, the fracture is brittle and shows a flat, featureless surface. A rapid increase in fracture energy is recorded at temperatures above NDT as more ductility is developed which is evidenced by increase in lateral contraction and development of shear lips. As the temperature exceeds shelf temperature, brittle cleavage appearance is replaced by ductile dimple type failure and there is no further increase in fracture resistance above this point. The basics of this fracture energy/temperature relationship can be explained from the differences in microstructural failure modes. Brittle failure at temperatures considerably below the shelf involves pure cleavage of the individual grains and is a high-speed process. However, upon increasing

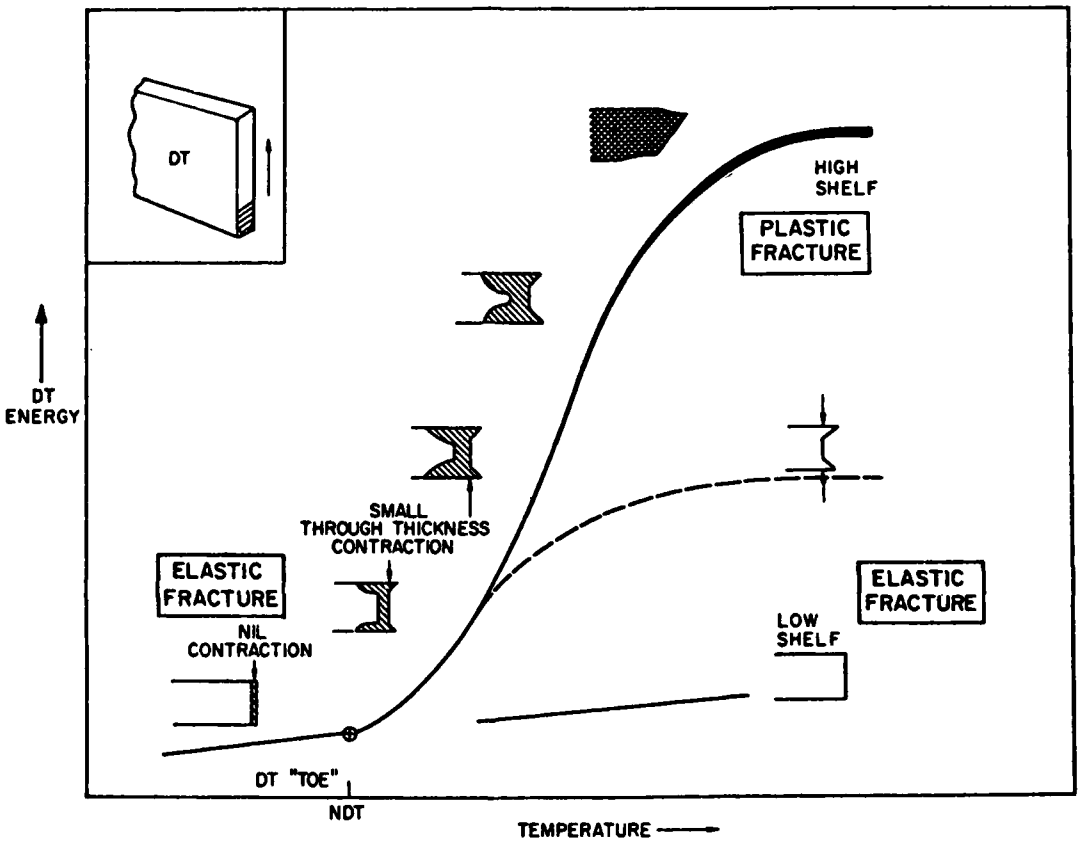

Fig. 5—DT test transitions to various levels of shelf fracture toughness. Note that with a decrease in shelf level fracture energy there is a corresponding change from fractures with large lateral contraction to flat fractures with nil contraction features. The decrease in shelf energy marks a transition from plastic (plane stress) to elastic (plane strain) fracture conditions.

in temperature, cleavage separation of individual grains competes with slip processes. More energy is requried for attaining higher stress needed for cleavage because more strain is required for elevating flow stress to the level of the cleavage stress. Macroscopically, in the transition region, the increase in fracture toughness is accompanied by the development of shear lips at the fracture surface. Finally, at the upper shelf temperature, fracture process is defined by microvoid coalescence; when small voids between grains, or of inclusions or impurities, are opened and the metal bridges between these voids

are stretched as tiny tensile specimens which finally rupture in a progressive ductile mode. The transition temperature and the sharpness of transition region depends on the specimen thickness (Fig. 6). Generally, the thinner specimen exhibits lower transition temperatures.

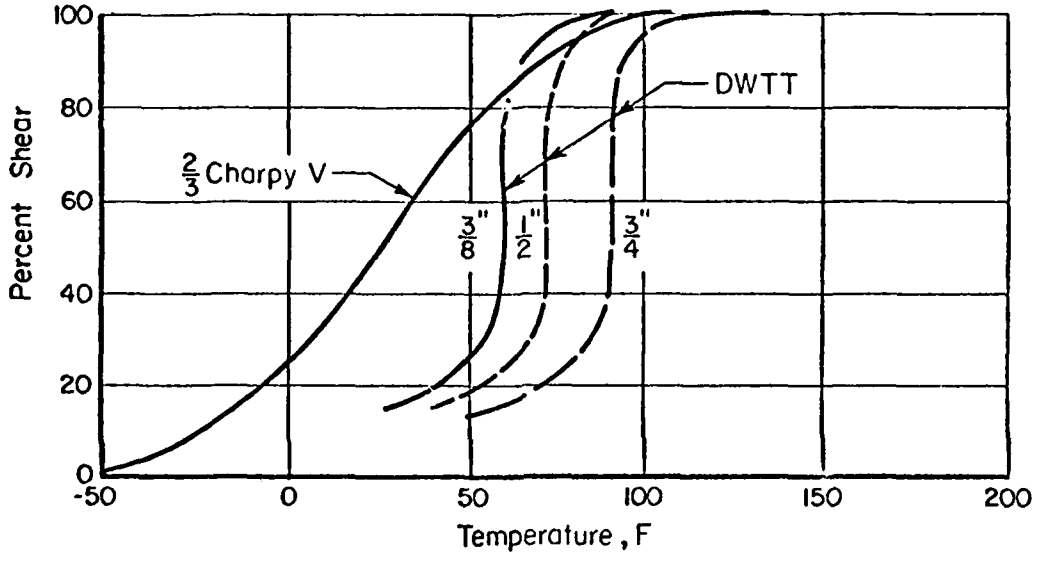

Fig. 6—Effect of plate thickness on DWTT and Charpy shear area results

The validity of linear elastic fracture mechanics (LEFM) is limited to small scale yielding. When the size of plastic zone developed in the specimen exceeds a prescribed limit (Fig. 7) due to changes in service loading or increase in temperature, K_{Ic} [6] or K_{Id} looses its usefulness. The region of valid LEFM toughness determination is restricted to the temperature (T) and energy level (S) limits indicated in Fig. 8. Fortunately, the J-integral [7-16] approach has extended the material toughness measurement to upper shelf region. The development of J-integral concept and testing technique not only has reduced K testing effort by using smaller specimens but also has enabled structural engineers to characterize a flawed body subjected to large scale yielding. However, the validity of J-integral approach is limited theoretically due to its basic assumptions [7] such as infinitesimal deformation, deformation theory of plasticity etc.

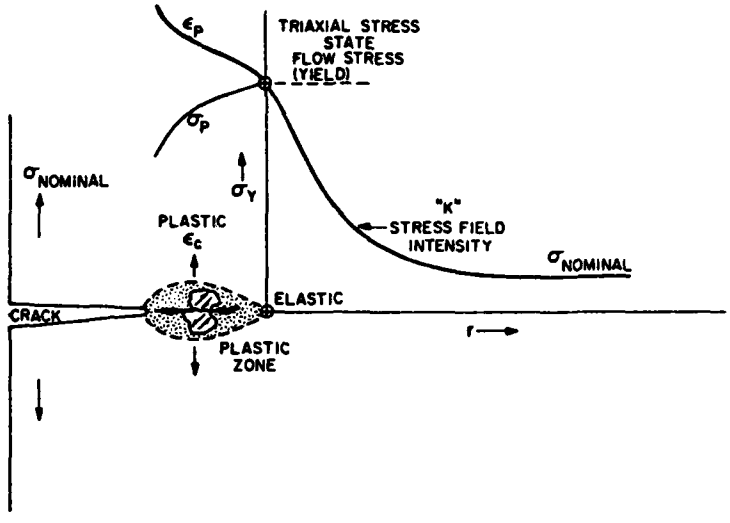

Fig. 7—Relationships of elastic and plastic stress fields to the plastic zone at crack tips for the case of plane strain constraint. As plastic relaxation is developed (large plastic zone and crack tip blunting), the elastic stress fields are replaced by plastic strain fields. Elastic stress field K definitions are not possible for these conditions.

Under normal reactor operating conditions, materials that have been used for nuclear piping construction can be identified as those exhibiting no transition temperature and those having a definite transition temperature. Austenitic stainless steel, 304 and 316 s.s., are examples of the first kind and ferritic steels are the second type. Therefore, austenitic stainless steels are materials having very high toughness and the structural failure is generally related to limit load conditions. Figure 9 illustrates the J-R curves of 304 and 316 s.s. at room temperature as well as 600°F [17]. The J_{Ic} (critical initiation value) ranges from 5000 in. lb/in.^{2} at RT to 3500 in. lb/in.^{2} at 600°F. Using the K_{Ic}-J_{Ic} relationship:

$$K_{Ic}^2 = \frac{EJ_{Ic}}{1-\nu^2}$$

where E is the modulus and ν is Poisson's ratio, the critical stress intensity factors K_{Ic} are 375 ksi $\sqrt{\text{in.}}$ and 300 ksi $\sqrt{\text{in.}}$, respectively. With such high toughness values, it is obvious that these materials have high tolerance against brittle fracture, and the structural failure must be controlled by ductile tearing.

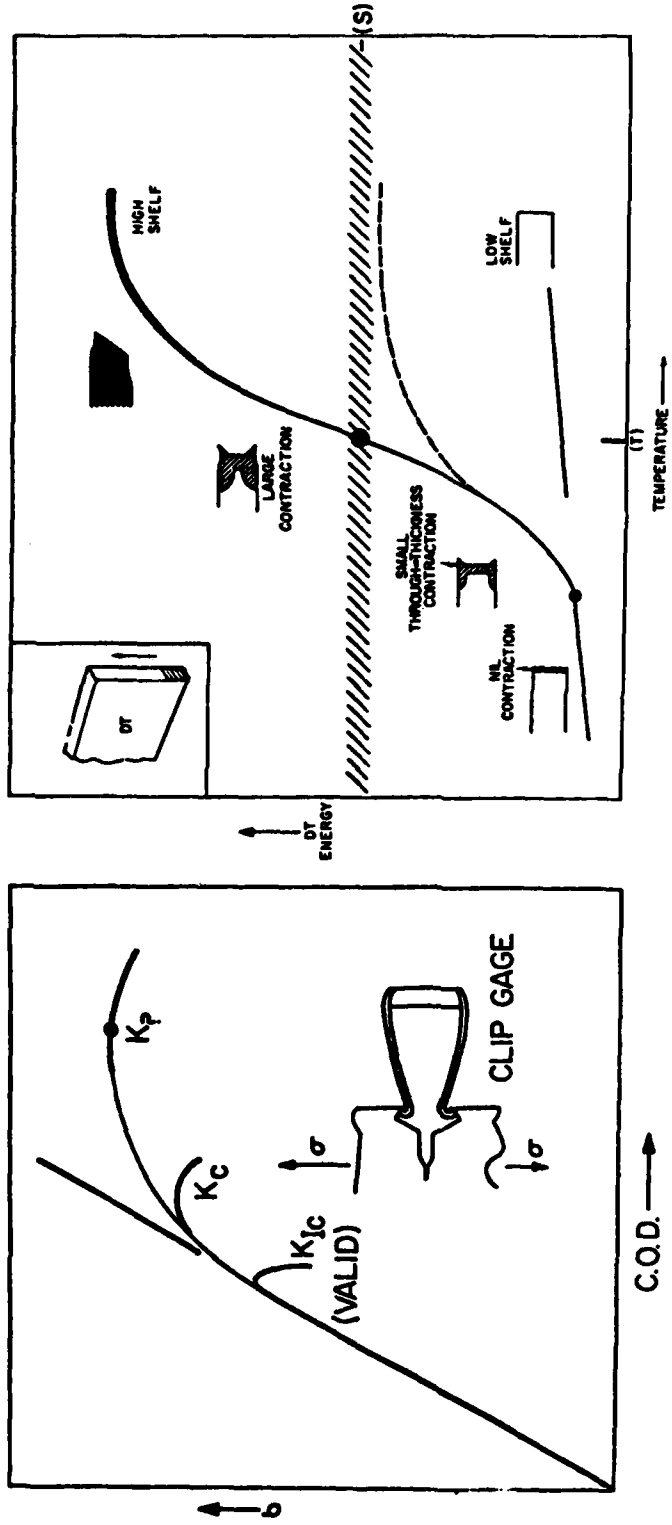

Fig. 8—Relationships of Crack Opening Displacement (COD) features of K_{Ic} test specimens to DT energy transition curves featuring high- and low-shelf characteristics. Valid K_{Ic} values involving elastic COD instability can be attained only to temperature (T) and shelf (S) limits of the DT test which involve small amounts of lateral contraction. Fractures of DT test specimens involving plastic deformation document plane stress conditions (K_c or K_r).

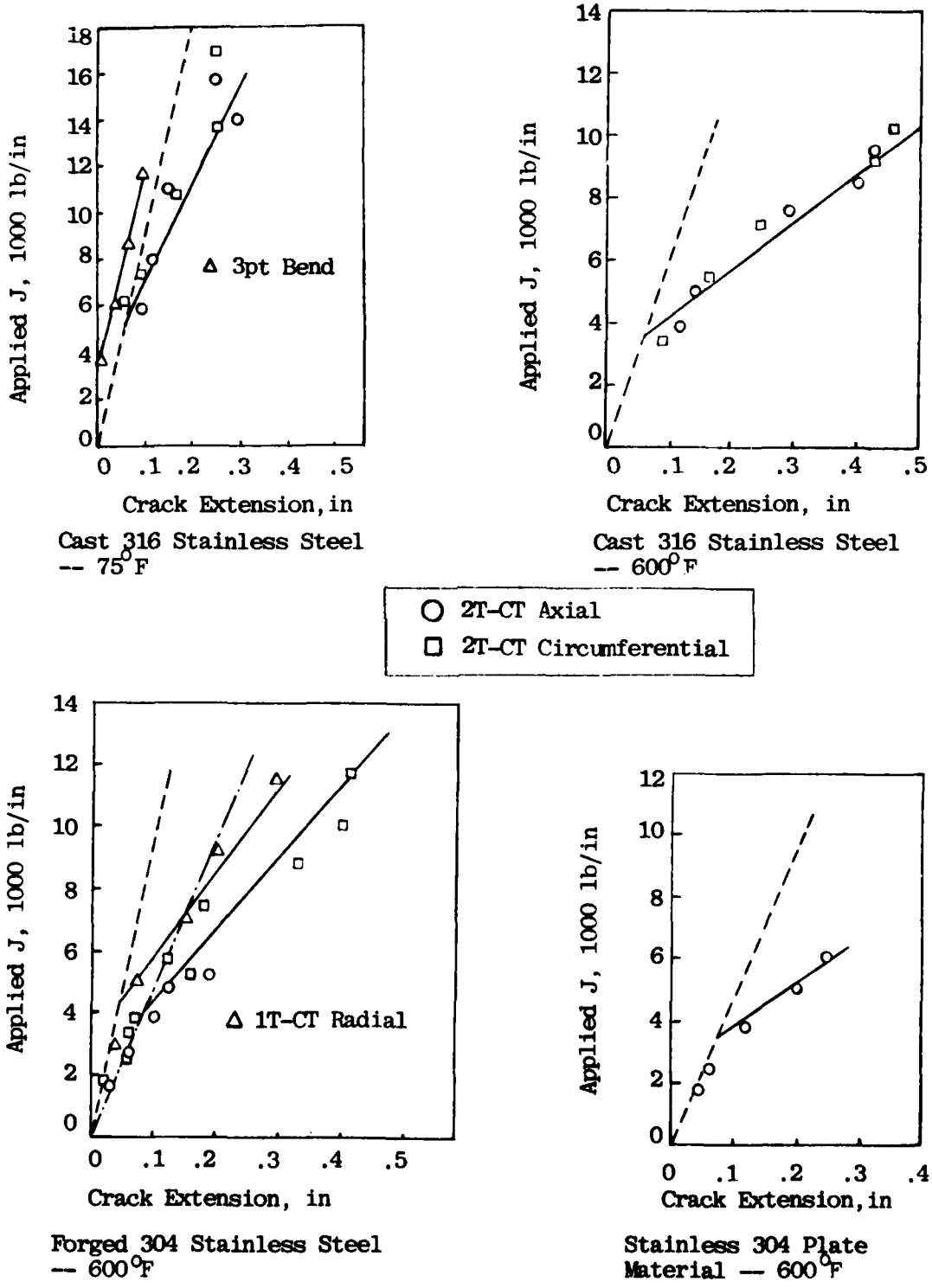

Fig. 9—J_{Ic} determination

When attention is directed to the materials of second type which have lower toughness and exhibit a definite transition temperature, the structure failure is no longer controlled by ductile tearing alone. Depending on the operating temperature regime of the material and the geometry of the structure (thickness, pipe size and surface flaw or through-wall flaw), brittle fracture and/or ductile tearing is possible. Generally, the material toughness characterization tests and structural failure analyses of these types of materials are more complicated and less conclusive.

3.0 COMPUTATIONAL METHODS OF NUCLEAR REACTOR PIPE RUPTURE

Typically, the pipe rupture study can be classified as near field or far field study. The terms, near and far, denote the relative size of the region around the crack tip where the analysis is employed. In the far field computational method, a considerable amount of effort is directed to model the overall structural response of piping system, and the crack tip behavior enters into the analysis only as a simple fracture criterion. On the other hand, near field study deals with the materials and structural response locally near the cracked region. The overall structural response affects the local stability only in the compliance formulation.

In the far field computation, the whole piping system is generally modeled by 3-D solid or shell finite elements. The dynamic behavior, produced by an advancing crack, of the piping system and the fluid inside are considered. Because of the computational complexity in dealing with the overall structural dynamics of the piping system, only the simple crack extension criterion can be included in the iterative process without prohibitive computational time. The commonly used criteria are either maximum strain or K_{Ic}.

In the LEFM analysis, toughness can be considered as a material property. The stability of a flawed structure is conservatively assured when the applied stress intensity factor is less than the critical

value, K_{Ic}. This is the basic philosophy that the ASME boiler and pressure vessel code has adopted. Because the structural stability is measured by a near field parameter K, this type of analysis can be considered as a near field analysis. Another example of the near field approach is the fracture mode transition temperature method, where the operating temperature is used to control structural failure against fracture initiation and propagation of existing flaws. However, when cracks advance into material resulting in large deformation, stability against fracture may depend on material as well as geometry and loading conditions. In this case, better failure description is needed. The J-integral approach is rigorous in defining fracture initiation under gross plastic yielding. Evidence to date indicates that the J-R resistance curve may be useful in studying crack propagation under monotonic loading. If one accepts this assumption, the J-R resistance curve approach can also be considered as a near field analysis method.

Both near field and far field methods assume that the local instability criteria are dependent only on the material. However, the structural geometry and the loading are needed in the structural/material response computation. To make this complicated problem more trackable, much effort has been directed to develop a simple analytical formulation which considers the material properties as well as structural geometry and loading conditions. The technique used in generating these formulations is generally semi-empirical in nature. Starting from a known solution for a flawed plate, modifications to account for plasticity and geometry effects are first incorporated. The final simplified solution is derived by verification and adjustment of the modified formulation using a vast amount of experimental data.

In the next several sections, detailed discussion of each computational method will be presented.

3.1 Gross Structural Response

This type of computational method is far field study because the analysis includes a very large region of the piping system. In addition, the computational emphasis is on the overall response of the structural rather than local region surrounding an existing crack. With improved numerical computation capabilities, pipe rupture can be very easily modeled by finite element or finite difference computer programs. In these analysis, typical shell elements are used to model the piping. Elastic, elastic/plastic, or even viscoelastic constitutive behavior can be employed. In addition, the dynamics of crack opening, coupled with the escape of the internal fluid, can also be included. Depending on the requirement, a very costly program may be developed to model some postulated event. One of the key ingredients in simulating the piping rupture is the requirement of an adequate fracture criterion such as maximum strain or K_{Ic}. References 18 & 22 are typical research results of this kind. However, the accuracy of these analytical results depends heavily on a poorly-defined quantity, viz., the fracture toughness of the material. When brittle failure is observed, K_{Ic} or K_{Id} may be adequate. For a pipe that fails plastically or in a mixed brittle/ductile failure mode, the analytical prediction can be misleading. In addition, the numerical results of one costly numerical analysis may not be extrapolated to other cases where the prohibitive costs prevent additional runs. The need for this type of analysis is apparent when dynamic fracture (static initiation/dynamic propagation) governs the fracture processes. However, based on the documented nuclear reactor piping field failure experience, there is very little evidence that a pipe failure due to dynamic propagation is likely. The primary reason for a non-propagating crack is the fluid (water) does not enhance dynamic growth in piping. In general, gross structureal analysis is not a very widely accepted method in pipe rupture analysis.

3.2 Semi–Empirical Methods

Before an acceptable inelastic pipe rupture analytical method is developed, the most logical means to study the problem is to rely on known technology. In this case, the existing technology is linear

elastic fracture mechanics. However, one immediately faced with the task of circumventing the inherent limitations built within LEFM. The test specimen thickness requirement is one example. The constraint requirement imposed by ASTM E-399 with respect to determination of the plane strain critical stress intensity factor, K_{Ic}, is

$$B \geqslant 2.5 \left(\frac{K_{Ic}}{\sigma_{ys}}\right)^2. \tag{1}$$

For materials having yield strength σ_{ys}, the thickness (B) must be in excess of the actual reactor piping thickness to have an adequate K_{Ic} measurement. Since K_{Ic} is very sensitive to thickness variation, experimentally generated K_{Ic} values can be misleading. Another important consideration in adopting the LEFM approach is extensive plastic yielding during the failure process. If pipe failure is due to gross plastic yielding, the elastically-generated fracture toughness value becomes meaningless.

To account for the LEFM limitations as well as the geometry and loading conditions on a pipe, semi-empirical methods have been proposed. In this respect, either a pseudo-toughness value, K_c, or flow stress theory is applicable, depending upon the fracture mode (brittle, brittle/ductile, ductile). The pseudo-toughness value, K_c, is an equivalent critical toughness parameter for a piping application. It is derived by modifying elastic fracture mechanics solutions of a flawed plate through curvature correction, plasticity consideration, and extensive experimental pipe rupture data correlation. When pipe failure is dictated by gross plastic yielding, a flow stress theory is derived by assuming that pipe instability is governed by the limit load of the pipe.

It will become apparent in subsequent sections that these semi-empirical methods are easy to use but do not assure good correlation with the actual pipe test results.

3.2.1 Axial Cracks

For an axial crack in gas transmission line pipe, equation (2) has been proposed [23] to compute K_c.

$$K_c^2 = \frac{\pi c \sigma_h^2}{\cos\theta}\left[1 + 1.61\frac{c^2}{Rt}\right]\left[\frac{4-K}{2}\right] \tag{2}$$

$$K_c^2 = \frac{\pi c \sigma_h^2}{\cos\theta}(M^2)\left[\frac{4-K}{2}\right], \tag{2a}$$

where

K_c = critical stress intensity, ksi$\sqrt{\text{in.}}$

c = half axial through-wall crack length, in.

R = average radius of vessel, in.

t = wall thickness, in.

$\theta = \frac{\pi}{2}\frac{\sigma_h}{\sigma_c}$

$\sigma_h = \frac{Pr}{t}$, nominal hoop stress at failure, ksi

P = vessel failure pressure, ksig

r = inside radius of vessel, in.

σ_c = failure stress for unflawed vessel, ksi
($M\sigma_h$ was used for this value)

K = $(3 - 4\nu)$ plane strain; $(3 - \nu)/(1 + \nu)$ plane stress

ν = Poisson's ratio

M = stress magnification factor for an axial through crack in a cylinder which is a function of λ (see Figure 10; M_{exact} exact was used herein)

$$\lambda^2 = \frac{c^2}{Rt}\sqrt{12(1-\nu^2)}.$$

For axial cracks in an intermediate wall thickness vessel or pipe, Folias [24] and Goodier & Field [25] proposed equation (3) for low to medium toughness materials with relatively long crack. Hahn [26] derived equation (4) for high toughness materials with short cracks.

$$K_c = \sigma^* \left[\frac{8c}{\pi} \ln \sec \frac{\pi M \sigma_h}{2\sigma^*}\right]^{1/2}, \tag{3}$$

where

σ^* is the flow stress of the material, which according to Hahn can be taken as $1.04\,\sigma_y + 10.0$ (ksi) or with less accuracy by $0.51\,(\sigma_y + \sigma_u)$

σ_y = yield stress, ksi

σ_u = tensile stress, ksi

$M = \left(1 + 1.61\,\frac{c^2}{Rt}\right)^{1/2}$ or from Figure 10 for a better estimate

$$\sigma^* = \sigma_h M \tag{4}$$

where $M = \left(1 + 1.61\,\frac{c^2}{Rt}\right)^{1/2}$ or M_{exact} from Figure 10 for a better estimate. The relationship between equations (3) and (4) is illustrated in Fig. 11. It is seen that equation (4) is the upper limit for the high toughness (ductile) behavior.

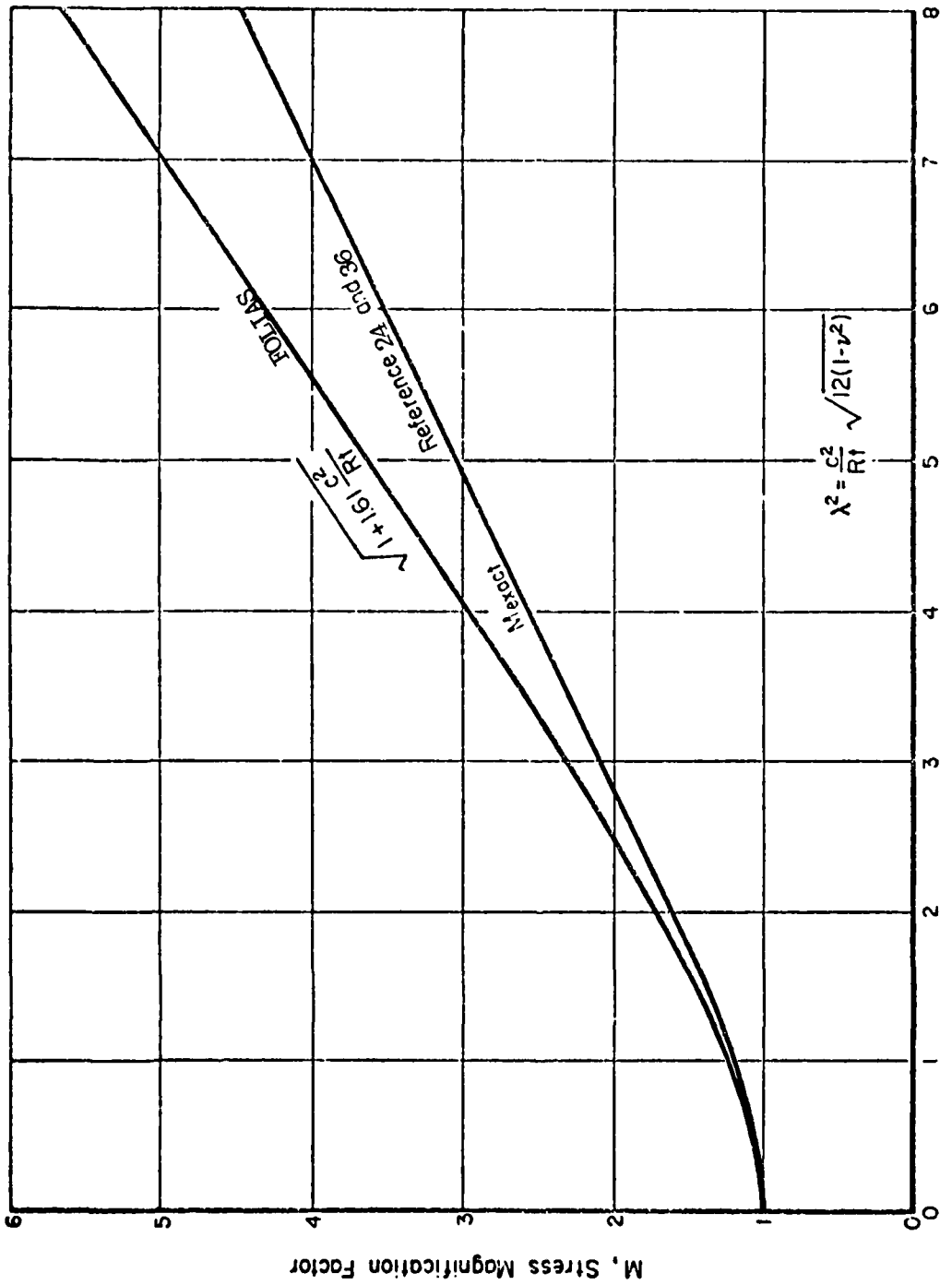

Fig. 10—Relationship between λ and stress magnification factor *M*

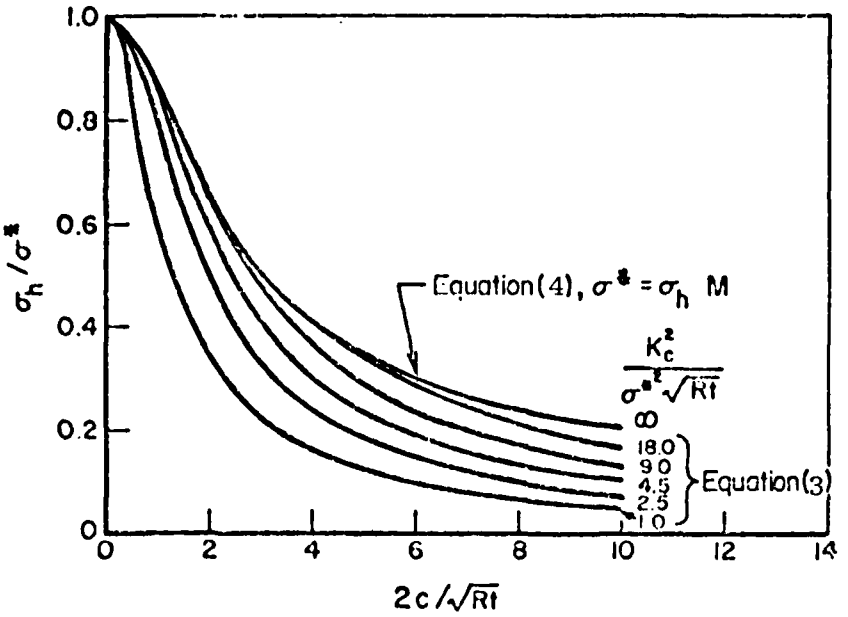

Fig. 11—Dimensionless failure curves for Eq. (3) and (4)

To describe the failure of low to medium toughness materials, Newman [27] proposed a two-parameter fracture criterion to include material yielding as well as brittle failure. These two parameters, m and K_f, are computed from laboratory test results (N tests) and are related to the net section failure stress S_n, of a specimen having half crack length c, width W, and ultimate strength σ_u.

$$m = \frac{\sum_{i-1}^{N} \frac{S_n}{\sigma_u} \sum_{i-1}^{N} K_{Ie}^2 - \sum_{i-1}^{N} K_{Ie} \sum_{i-1}^{N} K_{Ie} \left(\frac{S_n}{\sigma_u}\right)}{\sum_{i-1}^{N} \left(\frac{S_n}{\sigma_u}\right)^2 \sum_{i-1}^{N} K_{Ie}^2 - \left[\sum_{i-1}^{N} K_{Ie} \left(\frac{S_n}{\sigma_u}\right)\right]^2} \tag{5}$$

and

$$K_f = \frac{\sum_{i-1}^{N} K_{Ie}^2}{\sum_{i-1}^{N} K_{Ie} - m \sum_{i-1}^{N} K_{Ie} \left(\frac{S_n}{\sigma_u}\right)} \tag{6}$$

where K_{Ie} is the computed elastic stress intensity based on gross section stress S to failure equation

$$K_{Ie} = S\sqrt{\pi c \sec(\pi c/w)}. \tag{7}$$

For plane strain behavior m approaches zero $K_f \rightarrow K_{Ie} \rightarrow K_{Ic}$ (the plane strain fracture toughness). For notch insensitive materials, m becomes unitv so K_f relates failure to the ultimate tensile strength. In the range covered by mixed mode and plane stress fracture, the failure stress is a function of both K_f and m. To account for the curvature effect of a cylindrical structure, Adams [28] proposed a revised failure equation which gives the failure stress, S_{cal}, as

$$S_{cal} = \frac{K_f}{C_c\sqrt{\pi c - sec\,(\pi c/w)} + \dfrac{mK_f}{\sigma_u}\left(\dfrac{Ag}{An}\right)}, \tag{8}$$

where A_g and A_n are cross sectional area and net section area, respectively. A curvature correction factor, C_c, is defined by:

$$C_c = 0.614 + 0.48\lambda + 0.386e^{(-1.25\lambda)}, \tag{9}$$

where

$$\lambda = [12(1 - \nu^2)^{1/4}c]/\sqrt{Rt}. \tag{10}$$

Figure 12 [29] illustrates the comparison of equations (2), (3) and (8) for a 42 in., 3 in. wall thickness pipe. Approximations made in equation (8) were $m \sim 1.0$ and $\pi c/w \sim 0.0$. It is noted that for K_c less than 200 ksi $\sqrt{\text{in.}}$, all three equations have similar toughness (K_c) and flaw size ($2c$) relationship. This observations is encouraging because most reactor piping materials, displaying brittle to ductile transition ıperature response, exhibit toughness ranges from 50 to 200 KSI $\sqrt{\text{in.}}$

Other semi-empirical equations to define piping toughness have been described by Folias [31] and Quirk [30]. However, a detailed assessment program using A 106 B pipe experiments [31] indicated that equations (3) and (4) are the most suitable equations to be used. There is evidence, however, that the scatter of the K_c computation may be much larger than that indicated in Ref. [31] when materials or different pipe sizes are considered. It is concluded that the pseudo-fracture toughness, K_c, can be used as a toughness indication and it is accurate under specific conditions. More discussions on this point will be followed in a subsequent portion of the text.

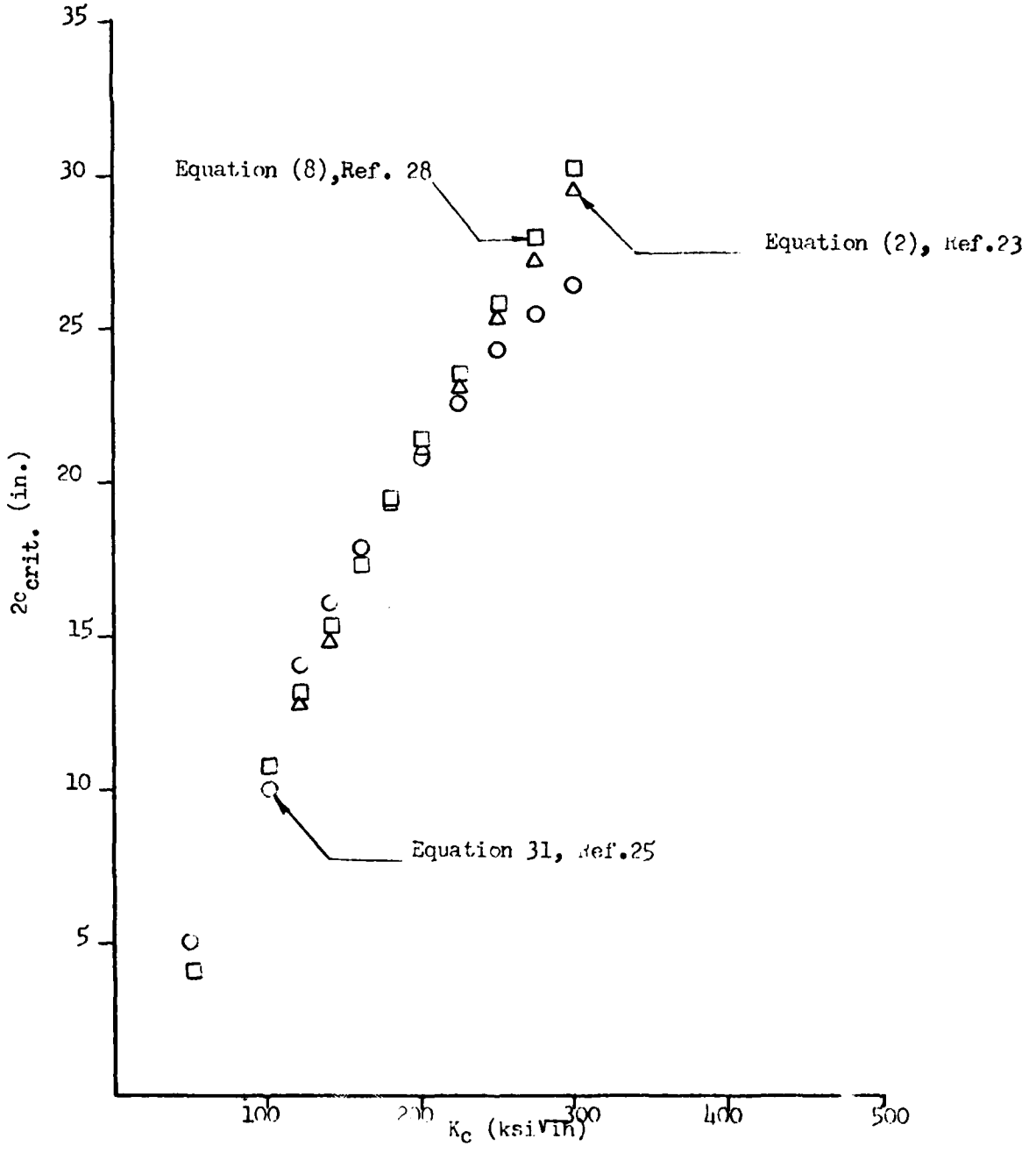

Fig. 12—$2c_{crit}$ vs K_c for a 42 in. OD, 3 in. wall thickness

3.2.2. Circumferential Cracks

Circumferential cracks can only be initiated and propagated by large axial stress. Therefore, the necessary condition associated with these types of cracks is the presence of high secondary stresses (thermal, bending, expansion and residual stresses). Although most pipe failures in the field are due to circumferential flaws [5], no rigorous analytical method is available to date. Laboratory tests on medium to high toughness materials [32,33,34,35] revealed that for short circumferential flaws the propagation was axial from the crack tips. This result indicated that prototype tests were not good simulations to account for the complicated stress state and microscopic material degradation of the materials in service. However, when longer circumferential flaws were studied, circumferential propagation was observed. In this case, tests on high toughness materials seem to correlate well with an ultimate strength theory. This theory suggests that pipe rupture is produced when the axial stress, due to pressure and bending, reaches the material ultimate strength. The bending stress in the pipe is derived by accounting for the shifting of the section's neutral axis due to the presence of a flaw. One of the formulations [3] gives the corresponding limit moment (Fig. 13) as:

$$M = \frac{4(\pi - \alpha)^2 R_m^2 t^2 \sigma_0^2 - \pi^2 R_c^2 P^2}{2(\pi - \alpha)^2 R_m^2 t \sigma_0} [R_0^2 (2\cos\beta - \sin\alpha)] \tag{11}$$

where

σ_0 = flow stress

R_m = mean radius

R_i = inside radius

R_0 = outside radius

T = thickness

P = internal pressure

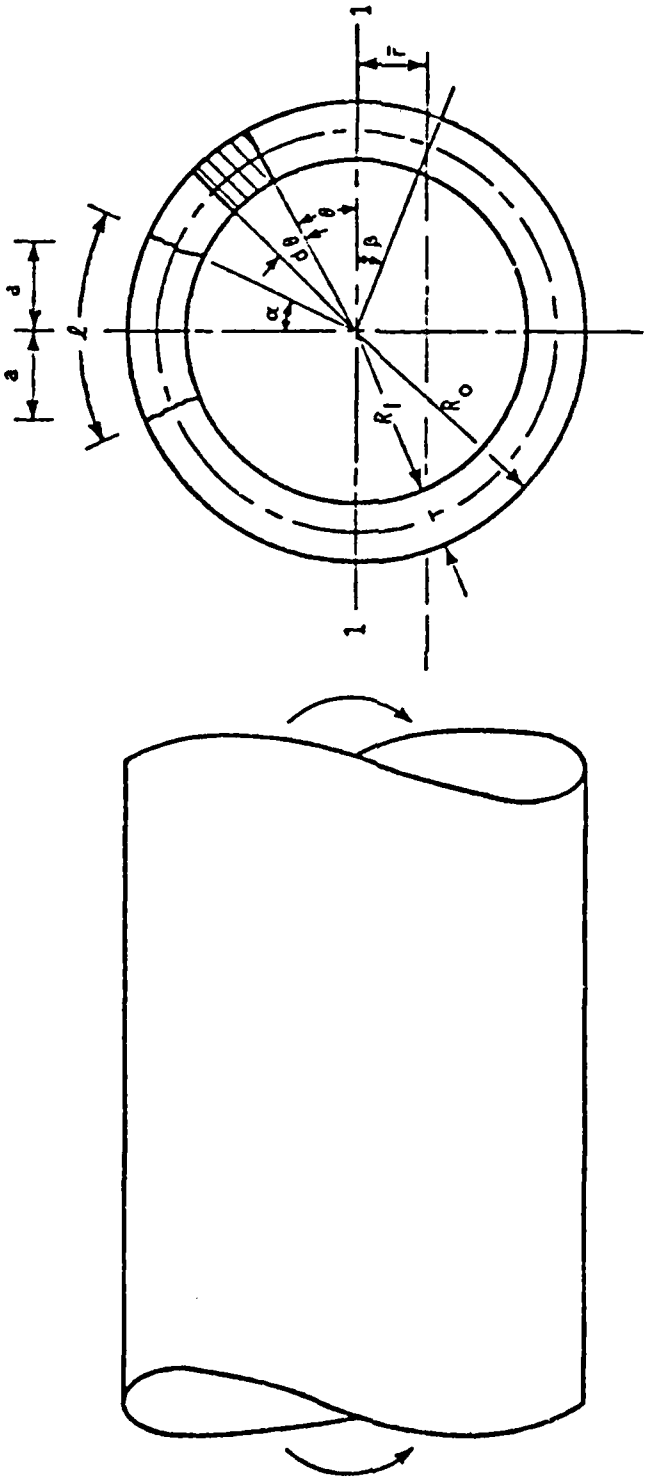

Fig. 13—Pipe with a through wall crack in bending

Another method that may be useful is the solution developed by Erdogan and Kibler [36]. In their work, stress intensity factors have been computed as a function of the parameter λ (Eq. 10). The cylinder is subjected to both axial and bending loads. However, lack of a plastic zone correction factor renders their formulation somewhat unrealistic.

3.3 Semi-Empirical Methods Correlation

The adequacy of the proposed semi-empirical methods are highly dependent on the material being considered. Namely, the pseudo-toughness method, K_c, is for medium to high toughness materials, whereas the flow stress theory is suited for high toughness material applications. In the following discussion, correlations between analysis methods and experimental test data are given for each type of material. Both axial and circumferential cracks are addressed. It will become apparent that both methods can not be used indiscriminately. Lack of good correlation between test data and projections according to the pseudo-toughness, K_c, method raises doubts about the adequacy of this approach. On the other hand, even with limited success, the flow stress theory is still a questionable method to predict inelastic pipe rupture. Specifically, because the flow stress theory is toughness independent and most of all, geometry independent. It is felt that the flow stress theory can be used with success for most of the cases. But before one adapts its methodology, careful consideration should be given to the specific piping system studied and the assumptions and limitations of the theory.

3.3.1 High Toughness Materials

High toughness materials, such as 304 and 316 stainless steels exhibit no brittle to ductile transition temperature and generally fail by ductile rupture. The measured high toughness (Fig. 9) seems to rule out the possibility of brittle fracture initiation. However, cracks have been found in these materials due to various causes. When this material is subjected to heat treatment between 800°F and 1200°F, chromium is depleted from the matrix by precipitation at the grain boundaries in the from of

chromium carbide. The material, having undergone this metallurgical change, is said to be sensitized. When the proper agent, such as oxidizing element, is introduced to the sensitized material, stress corrosion cracking can be developed under imposed thermal and mechanical loads. In this case, the objective is not only to devise techniques to reduce stress corrosion possibility, but also to evaluate the piping stability due to the presence of critical flaws in various orientations.

It has been suggested [37,38,39,40] that the flow stress theory (Eq. 4) may be an adequate method in predicting ductile fracture failure of high toughness materials. As suggested in the following sections, the limited experimental results appear to correlate well with the theory. However, because no crack-tip parameter is considered in the formulation, it is premature to conclude that this theory is applicable regardless of piping geometry or applied loads. Also, Tada and Paris [65] have demonstrated, using J integral techniques, the importance of pipe length/diameter (L/R) ratio in a ductile stability analysis of a circumferential crack in reactor piping.

3.3.1.1 Axial Cracks

Battelle [37,38] carried out 4 experiments on 24 in. diameter 316 stainless steel pipes of 1.5 in. thickness. The length of these pipes was between 8 to 22 ft. The pipes were heated between 470-680°F and pressurized to 5000 psi to induce failure. Both surface cracks and through-wall cracks were introduced in the specimens (Fig. 14). Using equation (4), corrected for reductions in area due to existance of surface flaw, the flow stress equation becomes [37]

$$\sigma_h = \sigma^* \frac{t/d - 1}{t/d - 1/M} \tag{12}$$

where σ_h is the hoop stress at failure; σ^* is the flow stress; M is the stress magnification factor as defined in Fig. 10; and, t and d are pipe thickness and flaw depth, respectively. When very long flaws are considered, $1/M$ approaches zero and the equation (12) is reduced to

$$\sigma_h = \sigma^*(t - d)/t. \tag{13}$$

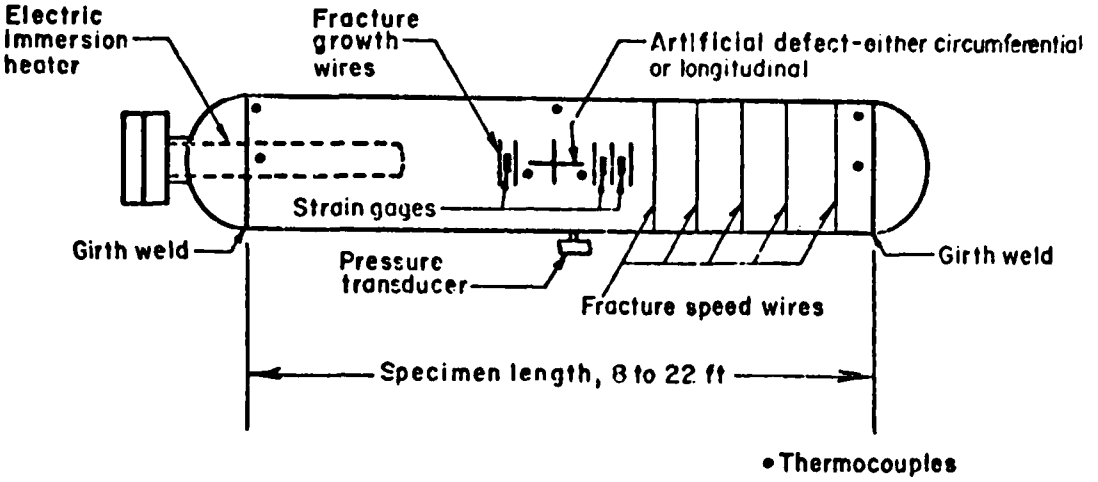

Fig. 14—Type A specimen configuration

In this case failure stress is proportional to the remaining ligament thickness. On the other hand, when deep flaws are considered, equations (12) reduces to the flow stress equation (4) for through-wall cracks. Figure 15 illustrates the correlation between test points and computed values; and it is evident that good agreement was obtained. Since 316 s.s is a very high toughness material, even at room temperature, gross plastic deformation before failure is expected. Therefore, for the pipe geometry studied, the flow stress criterion is adequate.

3.3.1.2 Circumferential Cracks

To investigate the austentic stainless steel toughness against circumferential flaws, Battelle [39,40] undertook a series of experiments performed on type 304 stainless steel plate and pipes. Flat plate specimens containing center cracks were used to evaluate the effect of HAZ (sensitization) and crack tip sharpness on the gross behavior of the material. It was found that extensive blunting practically overshadows the effect of initial crack tip geometry on the final instability. Also, the propagation characteristics were very similar in HAZ and base metal. Because the exhibited high toughness values of 304 s.s., the results from the plate tests suggested that the flow stress theory is an adequate criterion

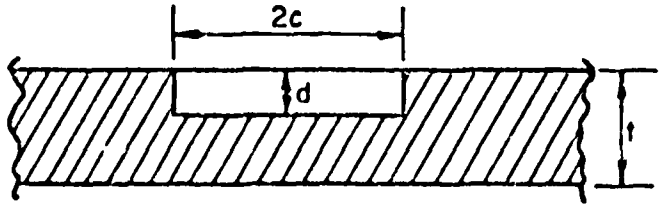

IDEALIZED SURFACE FLAW CONFIGURATION FOR EQUATION (12)

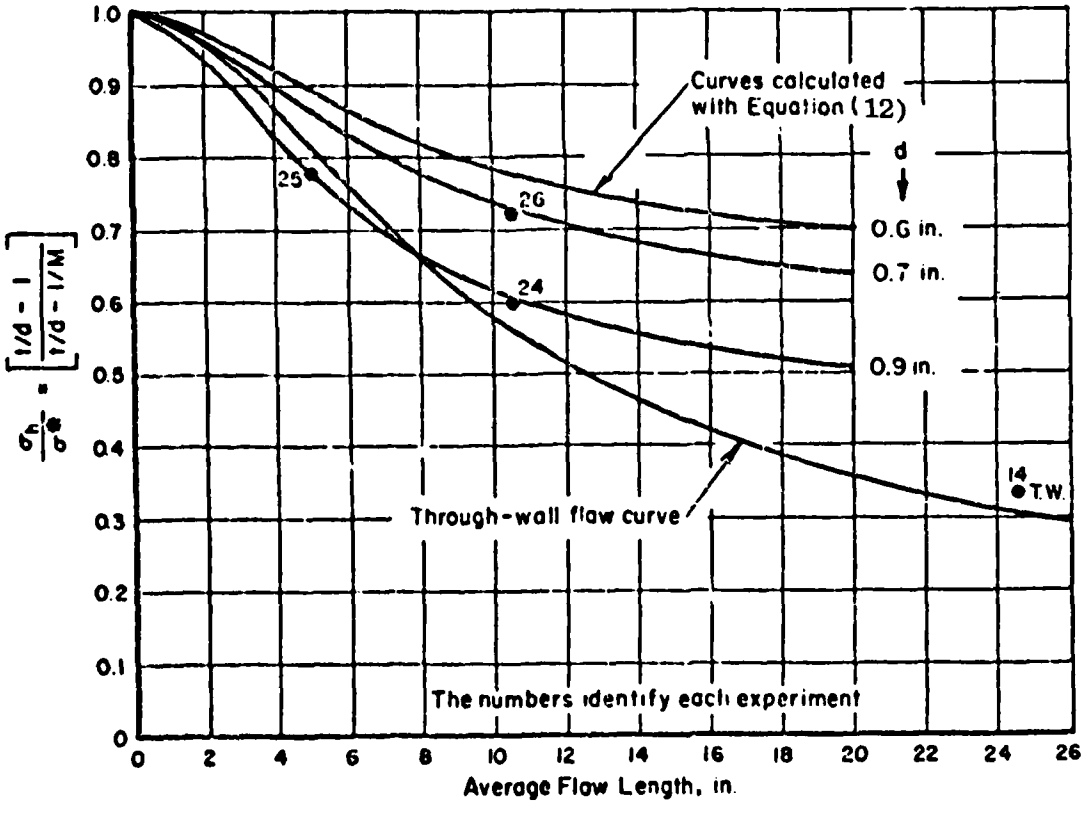

Fig. 15—Surface flaw behavior in 24 × 1.50 Type 316 stainless steel pipe

to predict collapse loads. Ultilizing the computed flow stress values from the plate tests and equation (11), the limiting moment versus flaw length relationship is plotted for internal pressures of 1050 psi and 2500 psi (Fig. 16). Experimental points were obtained from full-scale pipe experiments on two 4-in.-diameter schedule 80 type 304 stainless steel pipes. Initial circumferential flaws subtended arcs over 135° and 75.8°, and testing was performed at a temperature of approximately 3°C. A good correlation between test results and flow stress projections was observed.

For the case of surface cracks, equation (12) can be modified by including the ligament area in the derivation of the cross sectional area characteristics [38].

3.3.2 Medium to High Toughness Materials

In nuclear piping applications, this type of material exhibits a brittle to ductile transition temperature. It can be considered as high toughness material when it is operated at or above the shelf temperature. Therefore, the failure modes, and consequently the analysis methods, are temperature dependent. For this reason, more sub-scale and full-scale experiments have been performed on piping and vessels of this type of material. It is evident from the discussion presented in following sections, that there are a number of technical questions which remain unanswered. The limited evidence to date indicates that when these materials are operating at or above shelf temperature flow stress theory (Eq. 4) is adequate in collapse load prediction. Nevertheless, the inherent simplicity in the flow stress theory (Section 3.3.1) prevents one from adopting this theory for arbitrary pipe geometry and the imposed system loadings. When the operating temperature drops into transition region, the pseudo-fracture toughness, K_c, method may be used for selected axial flaws; however no adequate analytical solution currently exists for circumferential cracks. Furthermore, the poor correlation between K_c and test data raises the question of the general adequacy of the pseudo-toughness theory for piping analysis. An additional practical consideration that contributes towards the difficulty in analyzing these materials is the scatter in material

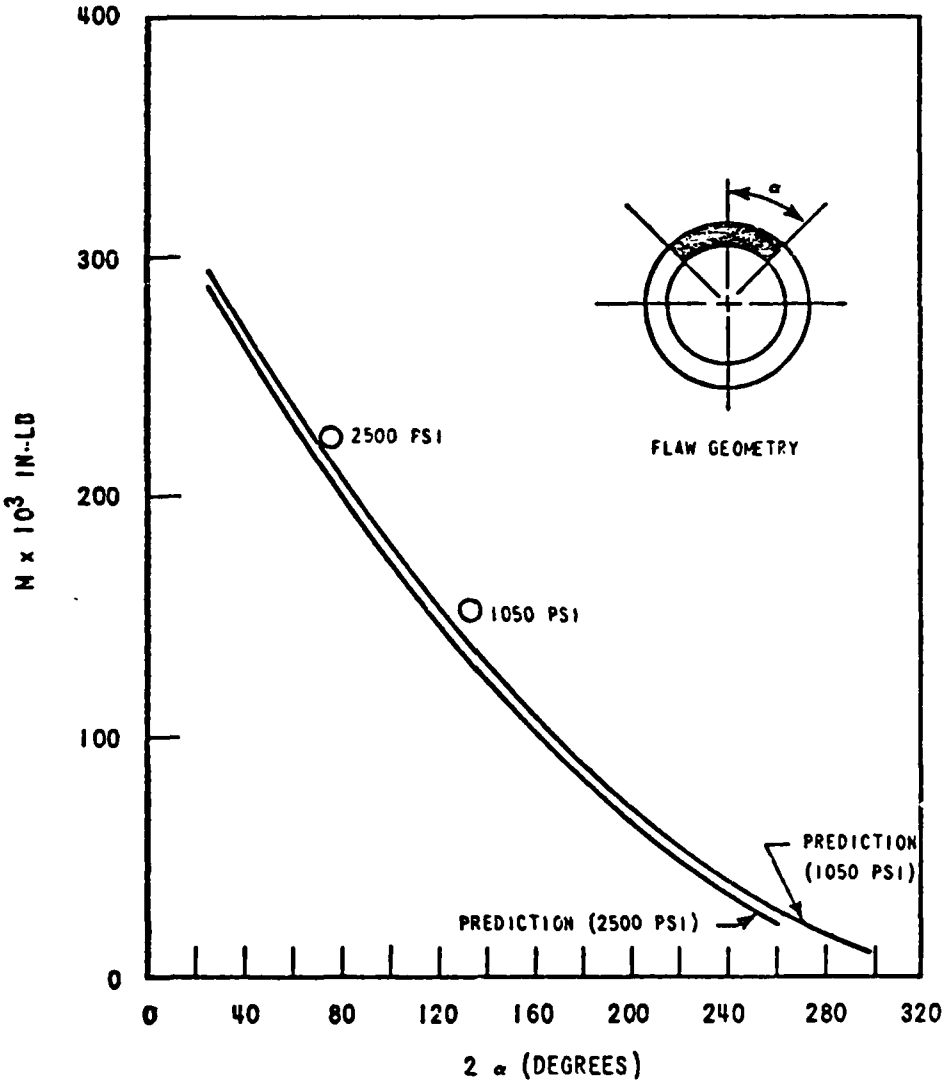

Fig. 16—Comparison on limit moment predictions with experimental results—AISI 304 piping

property data. For materials with identical specifications, significant differences in transition temperature are apparent due to metallurgical variations within a given class of steels. This difference can be observed on the same material from different suppliers or even from same supplier shipped at a different time. Typical materials in this category include A106, A333, and A516.

3.3.2.1 Axial Cracks

For materials containing axial cracks and operating at shelf temperatures, the flow stress theory (Eq. 4) seems to be appropriate for the selected cases investigated. Battelle's [37,38] work on A106 B carbon steel is a typical example of on-the-shelf behavior. A total 22 experiments were conducted on 12.75 in. diameter and 24 in. diameter pipes containing surface and through-wall cracks. These pipes were heated above 450°F under internal pressure (Table 2). According to the Charpy-V-Notch test data contained in the Appendix A [24], 450°F may be considered to be a shelf-level temperature. Figure 17 illustrates the excellent agreement between test point and the flow stress criterion, (Eq. 4).

The on-the-shelf behavior of surface flaws on A106 B steel pipes can also be assessed from other experimental programs. *Table 3 contains the test conditions of Battelle's work on surface flaws* [37]. To investigate the validity of flow stress criterion, failure stress to flow stress ratios (σ_h/σ^*) are computed for experimental results. Corresponding theoretical σ_h/σ^* values are also computed from Eq. 12 for the d/t rations tested. In Fig. 18 a perfect correlation line at 45 degrees is shown, and the excellent agreement between theory and experiment is noted.

For ferritic piping materials operating in the brittle to ductile transition region, experimental data have been generated to characterize the fracture response. General trends have been observed for specific materials and specific pipe geometries. Figure 19 illustrates the failure stress vs. temperature relationships generated from UKAEA data [5,41] (Tables 4, 5) on 0.36% carbon steel. It is noted that 6-in.-flaw failure stress curve crosses the yield strength curve at 135°F, whereas larger flaws push the crossover point to higher temperatures. Because smaller flaws produce full ductile rupture at lower temperature, this implies that smaller flawed structures have lower transition temperatures. GE results [5,42] on schedule 40 A106 B pipe at room temperature (Table 6) indicated that larger pipe have higher

TABLE 2 CRITICAL CRACK EXPERIMENTS ON CARBON STEEL PIPE WITH THROUGH-WALL FLAWS

A106B

Pipe	Experiment	Test Temperature, F	Total Axial Crack Length, in.	σ_h, Nominal Hoop Stress at Failure, ksi	Tensile Data: Yield Stress, ksi	Tensile Data: Ultimate Stress ksi	Outside Radius, in.	Wall Thickness, in.	λ	K_c[a], from Equation (3), ksi$\sqrt{in.}$	σ^*, from Equation (4) ksi	$\left(\frac{K_c}{\sigma_y}\right)^2 \frac{1}{c}$
C1	3	575	24.5	13.49	33.0	75.4	12	1.735	5.08	270	42.2	5.4
C1	1	575	18.5	19.74	33.0	75.4	12	1.674	3.90	300	50.5	8.25
C1	2	587	18.5	18.03	32.8	75.0	12	1.593	3.98	273	46.8	7.5
C2	5	675	13.5	16.48	30.6	75.0	12	1.64	3.94	242	42.2	6.8
C2	7	670	18.5	17.05	30.6	75.0	12	1.635	3.94	252	43.6	7.35
C5	10	661	18.5	17.75	32.6	77.9	12	1.64	3.93	264	45.4	7.1
C5	15	639	18.5	19.85	32.6	77.9	12	1.64	3.94	313	50.8	7.9
C2	6	554	11.6	24.50	34.1	81.5	12	1.715	2.40	222	44.2	7.3
C2	17	642	6.0	33.94	33.6	82.3	12	1.65	1.278	168	44.1	8.3
				Averages	32.5	77.5						
C8	13	555	14.5	17.3	36.5	74.7	12	0.700	4.65	253	50.1	6.6
C8	11	547	10.25	23.55	36.5	74.7	12	0.705	3.26	247	52.7	9.4
C8	12	561	5.25	33.0	36.5	74.7	12	0.710	1.66	202	47.9	11.6
C7	16	581	2.5	42.8	36.5	74.7	12	0.700	0.797	382	49.4	43.6
				Averages	36.5	74.7						
C10	23	567	10.25	15.8	42.8	74.0	6.375	0.700	4.54	190	45.4	3.9
C10	22	538	5.25	24.8	42.8	74.0	6.375	0.707	2.32	148	43.8	4.55
C10	21	605	2.5	39.0	42.8	74.0	6.375	0.710	1.10	166	42.9	12.0
				Averages	42.8	74.0						

(a) σ_c was taken as $(\sigma_u + \sigma_y)/2.4$.

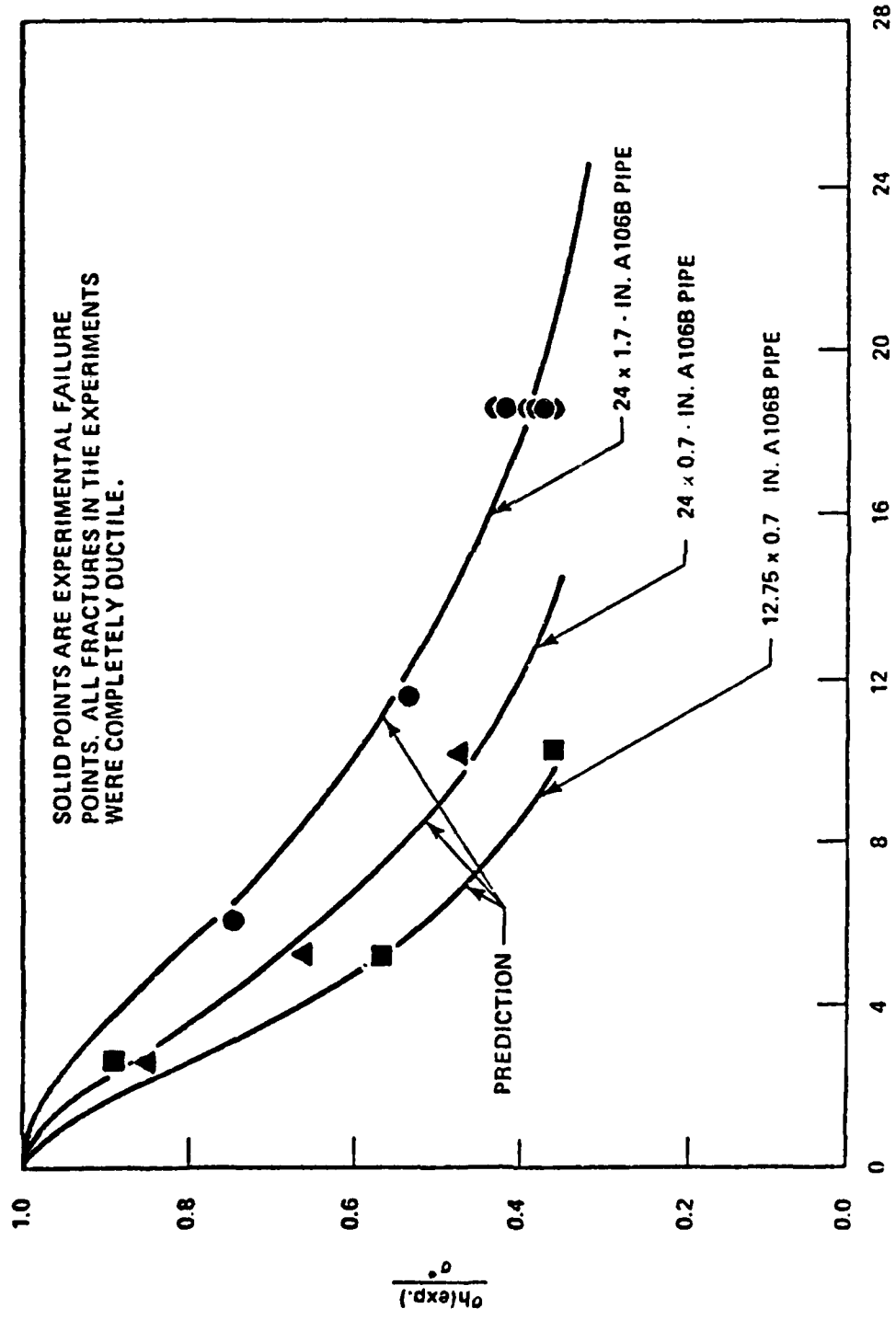

Fig. 17—Comparison of experimental critical flaw size data with calculated behavior for three pipe sizes

TABLE 3 EXPERIMENTAL AND PREDICTED FAILURE STRESSES FOR SURFACE FLAWS

Pipe	Experiment	Test Temperature, F	Surface Length, in.	Depth, d, in.	Wall Thickness, t, in.	Experimental Hoop Stress at Failure σ_h, ksi	Average Crack Length[a] in.	Flow Stress, σ^*, ksi: Based on Equation (12)	Flow Stress, σ^*, ksi: Based on Tensile Tests[b]	Failure Mode	Predicted Hoop Stress at Failure[c] Based on Equation (12) ksi
C2	4	596	28.4	1.30	1.703	15.1	27.18	49.6	45.4	Break	13.8
C4	8	696	24.5	1.27	1.720	16.7	23.24	48.3	45.4	Break	15.8
C4	9	584	24.5	1.45	1.650	8.5	23.21	49.8	45.4	Leak	7.8
C5	19	623	11.6	1.05	1.619	27.6	10.37	48.8	45.4	Break	25.5
C6	18	469	10.25	0.355	0.700	26.2	9.39	41.4	46.0	Break	23.1
C6	20	504	5.25	0.350	0.682	32.5	4.39	42.5	46.0	Break	35.1
S1	24	584	11.6	0.900	1.500	22.5	10.55	37.0	35.6	Leak[d]	21.6
S1	25	670	6.0	0.900	1.500	28.4	4.95	36.0	35.1	Leak	27.7
S1	26	670	11.6	0.700	1.500	25.1	10.51	35.2	35.1	Break	25.2

(a) Because these flaws have semicircle ends, the average crack length was determined such that the flaw area and depth remained the same.
(b) $(\sigma_u + \sigma_y)/2.4$.
(c) Predicted stresses are based on σ^* from tensile test results.
(d) This leaked because $\sigma_{cat.}$ was too low.

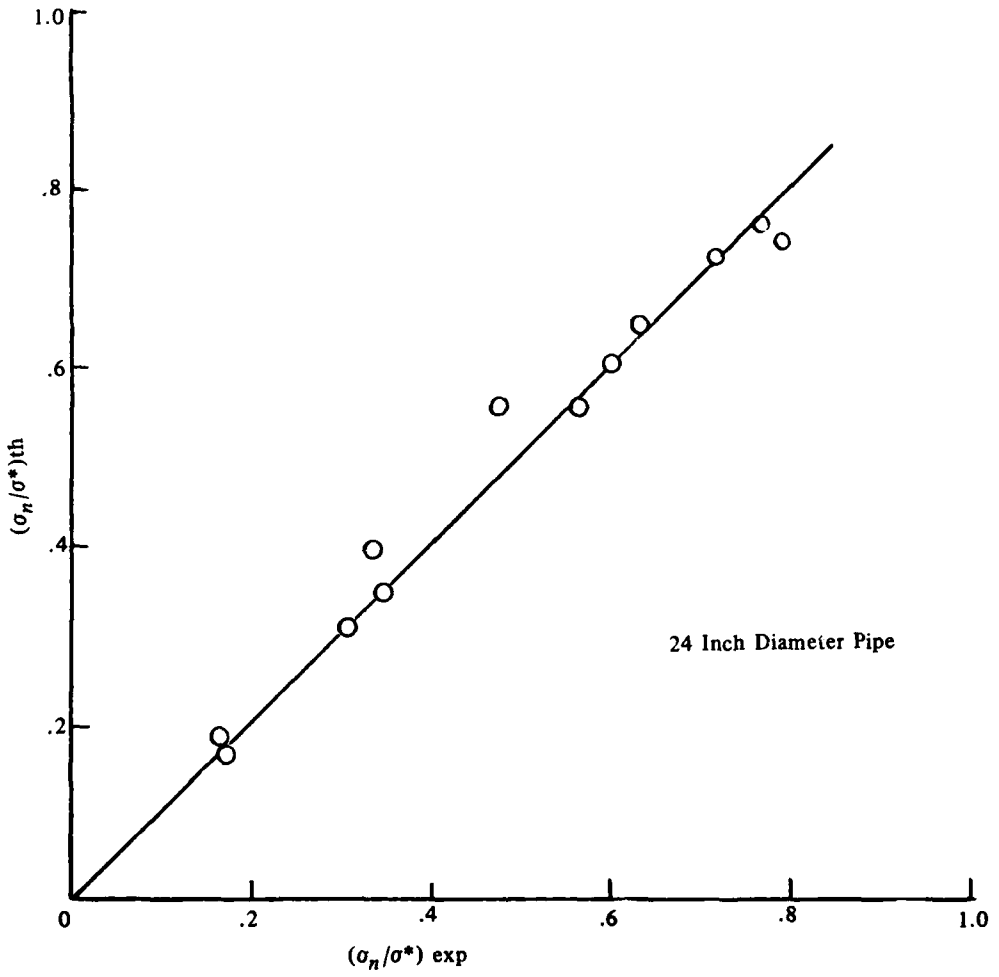

Fig. 18—Experimental/analytical correlation of surface flaws on A106B pipes (refer to Table 3). (On shelf behavior).

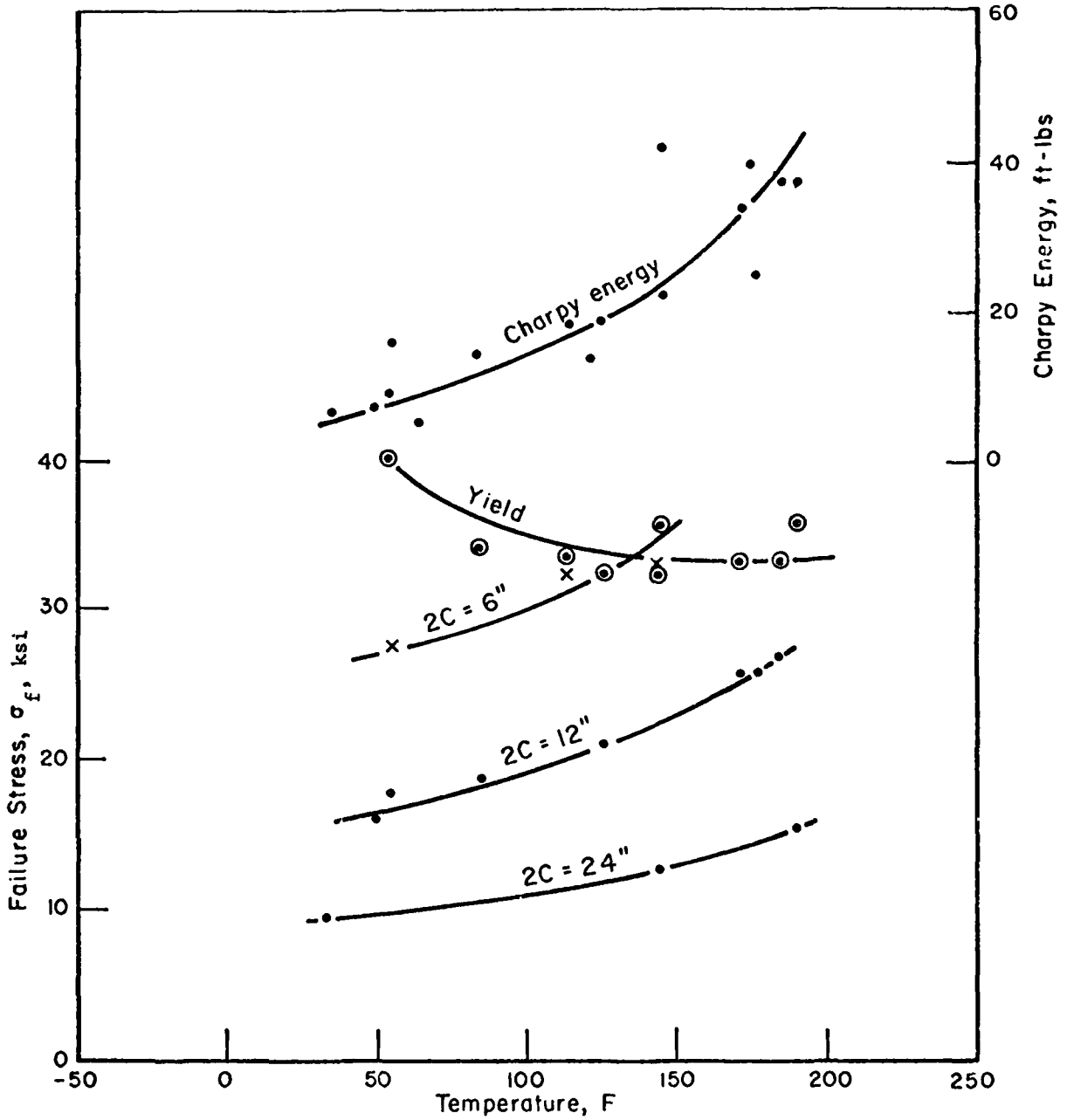

Fig. 19—Relationship of failure stress, Charpy energy and yield strength with temperature for UKAEA 0.36 percent carbon steel pipes

TABLE 4. UNAEA AXIAL THROUGH-WALL FLAW DATA ON STEEL CYLINDRICAL VESSELS

Specimen Number	Diameter, inches D_o	Wall Thickness, inch t	Tensile Stress Data: Yield, ksi	Tensile Stress Data: Ultimate, ksi	Tensile Stress Data: Elong, percent	Burst Hoop Stress Flowed, ksi σ_h	Flaw Length, inches 2c	Test Temperature, F	Fracture Mode (D-Ductile, B-Brittle)	$\frac{2c}{\sqrt{Rt}}$	$\frac{\sigma_b}{\sigma_h}$ (b)	Air Gap, percent	M_T	$M_T\sigma_h$	Type of Steel
V13T1	36	1.0	(24.8)	(69.7)(a)	NA	13.9	12.00	50	B	2.87	(5.01)	0	1.88	26.1	0.36% C steel , NDT +60 F to +95 F
V12T1	36	1.0	(34.8)	(69.7)	NA	23.4	12.00	176	D	2.87	(2.98)	0	1.88	43.9	Ditto
V12T3	36	1.0	(34.8)	(69.7)	NA	17.5	12.00	122	B	2.87	(3.98)	0	1.88	32.9	"
V13T2	60	1.0	40.1	70.1	33	27.6	6.00	54	B	1.10	2.54	0	1.17	32.4	"
V5XT1	60	1.0	33.6	71.7	35	32.4	6.00	113	B	1.10	2.21	10	1.17	38.0	"
V-T1	60	1.0	32.3	65.4	39	33 0	6.00	144	--	1.10	1.98	0	1.17	38.7	"
V2T1	60	1.0	34.0	71.7	35	18.7	12.00	84		2.21	3.83	0	1.59	29.6	"
W-T4	60	1.0	32.3	65.4	39	21.0	12.00	125	B	2.21	3.11	0	1.59	33.5	"
V6T3	60	1.0	33.2	69.4	30	25.8	12.00	171	D	2.21	2.69	20	1.59	40.9	"
V5T1	60	1.0	33.6	71.7	35	26.7	12.00	183	D	2.21	2.69	0	1.59	42.3	"
V3T2	60	1.0	(34.8)	(69.7)	--	17.9	12.00	55	B	2.21	(3.89)	0	1.59	28.4	"
V7T11	60	1.0	(34.8)	(69.7)	--	15.9	12.00	50	B	2.21	(4.38)	0	1.59	25.2	"
V1:T6	60	1.0	(34.8)	(69.7)	--	25.8	12.00(c)	176	D	2.21	(2.7)	0	1.59	40.4	"
V7T3	60	1.0	42.1	64.1	41	29.8	12.00	61	D	2.21	2.15	0	1.59	47.2	Al-grain-refined steel 0.13% C, NDT +6 F
V8T1	60	1.0	(39.9)	(63.2)	--	31.8	12.00	64	D	2.21	(1.99)	10	1.59	50.4	Ditto
V7T2	60	1.0	37.6	62.3	43	29.3	12.00	120	D	2.21	2.13	0	1.59	46.4	"
V:0T2	60	1.0	(39.9)	(63.2)	--	31.8	12.00	176	D	2.21	(1.99)	10	1.59	50.4	"
V7T4	60	1.0	30.9	64.1	40	28.4	12.00	102	D	2.21	2.26	0	1.59	45.0	Si-killed steel 0.16% C, NDT +43 F
V3T1	60	1.0	35.8	79.7	29	12.7	24.00	145	B	4.42	6.28	0	2.61	33.1	0.36% C steel
V3XT1	60	1.0	35.8	79.7	29	15.3	24.00	190	D	4.42	5.21	20	2.61	39.9	0.36% C steel
V3T3	60	1.0	(39.9)	(63.2)	--	19.5	24.00	66	D	4.42	(3.24)	10	2.61	50.9	Al-grain-refined steel 0.13% C
V7T6	60	1.0	70.3	89.6	29	17.0	24.00	48	B	4.42	5.27	0	2.61	44.4	Low alloy steel 0.155% C
V7T10	60	1.0	75.3	94.5	27	20.6	24.00	133	D	4.42	4.59	0	2.61	53.8	Ditto
V11T3	60	1.0	(72.8)	(92.1)	--	23.4	24.00	73	D	4.42	(3.94)	0	2.61	61.1	"
V7T1	60	1.0	(34.8)	(69.7)	--	9.7	24.75	35	B	4.56	(7.18)	0	2.68	25.9	0.36% C steel
V11T4	60	1.0	(72.8)	(92.1)	--	13.2	29.00	104	B	5.34	(6.98)	0	3.04	40.2	Low alloy steel 0.155% C
V14T2	114	1.0	(34.8)	(69.7)	--	20.2	12.00	83	B	1.58	(3.46)	0	1.34	27.0	0.36% C steel
V14T1	114	1.0	(34.8)	(69.7)	--	27.1	12.00	176	D	1.58	(2.57)	0	1.34	36.2	0.36% C steel

Chemical Analysis of Test Materials, weight percent

	C	Mn	Si	S	P	Ni	Cr	Mo	Cu	V
0.36 % C	0.36	0.44-0.46	0.10-0.13	0.038-0.024	0.015-0.026	--	--	--	--	--
Al-grain-refined steel	0.13	0.16	0.12	0.033	0.013	--	--	--	--	--
Si-killed steel	0.16	1.22	0.20	0.03	0.014	--	--	--	--	--
Low-alloy steel	0.155	1.30	0.22	0.02	0.022	0.22	0.63	0.255	0.07	0.09

(a) Flaw 45 degrees to surface.

(b) Used ultimate tensile value for σ_b.

(c) ( ) means estimated.

TABLE 5. AXIAL THROUGH-WALL FLAW DATA ON STEEL CYLINDRICAL VESSELS EXPERIMENTS CONDUCTED BY UKAEA

Specimen Number	Diameter, inches	Wall Thickness, inch	Tensile Stress Data: Yield, ksi	Tensile Stress Data: Ultimate, ksi	Tensile Stress Data: Elong, percent	Burst Hoop Stress Flawed, ksi σ_h	Flaw Length, inches 2c	Test Temperature, F	Charpy Energy, ft-lbs	$\frac{2c}{\sqrt{Rt}}$	$\frac{b}{\sigma_h}$	M_T	$M_T\sigma_h$	Type of Steel
A7	60	1.0	39.0	80.2	29	39.6	6.00	124	22	1.095	2.03	1.17	46.4	0.36% C Steel, NDT of +68 F to +77 F 60 ft-lb charpy shelf energy
A20	60	1.0	45.5	81.1	31	29.9	6.00	-18	6.5	1.095	2.71	1.17	35.1	Ditto
A2	60	1.0	30.0	67.2	31	27.0	12.00	194	51	2.19	2.49	1.58	42.6	"
A6	60	1.0	29.6	67.2	32	22.2	12.00	122	23	2.19	3.03	1.58	35.0	"
A3	60	1.0	43.9	82.0	29	21.3	12.00	50	13	2.19	3.85	1.58	33.6	"
A16	60	1.0	48.4	86.0	34	19.5	12.00	-22	6.5	2.19	4.41	1.58	30.7	"
A23	60	1.0		--	--	20.6	12.00	-49	--	2.19		1.58	32.5	"
A17	60	1.0	36.1	68.1	42	29.4	6.00	-18	4.5	1.095	2.32	1.17	34.5	B.S. 1501-151, NDT of +32 F, 75 ft-lb charpy shelf energy
A5	60	1.0	28.7	57.1	39	>24.6	12.00	194	74	2.19	<2.32	1.58	>38.8	Ditto
A8	60	1.0	32.0	64.1	37	28.8	12.00	122	52	2.19	2.23	1.58	45.4	"
A9	60	1.0	31.6	63.0	37	23.7	12.00	46	10	2.19	2.66	1.58	37.4	"
A12	60	1.0	34.7	66.1	38	19.7	12.00	16	6	2.19	3.36	1.58	31.1	"
A11	60	1.0	38.5	70.1	43	18.7	12.00	-22	3	2.19	3.75	1.58	29.5	"
A19	60	1.0	38.5	68.1	42	11.1	24.00	-18	5	4.38	6.14	2.59	28.8	"
A22	60	1.0	74.1	90.7	30	30.5	6.00	-33	8	1.095	2.97	1.17	35.8	Mo-B Steel, NDT of -31 F, 80 ft-lb charpy shelf energy
A10	60	1.0	72.8	88.0	26	>36.6	12.00	117	43	2.19	<2.40	1.58	>57.7	Ditto
A13	60	1.0	70.1	84.0	27	>37.1	12.00	59	21	2.19	<2.26	1.58	>58.5	"
A24	60	1.0		--	--	>36.5	12.00	45	--	2.19		1.58	>57.5	"
A14	60	1.0	73.2	88.0	29	18.9	12.00	-18	7.5	2.19	4.66	1.58	29.8	"
A10A	60	1.0	75.0	90.9	26	8.0	24.00	49	16	4.38	11.36	2.59	20.7	"
A13A	60	1.0	70.1	84.0	27	12.6	24.00	52	21	4.38	6.67	2.59	32.6	"
A21	60	1.0	71.0	86.0	28	8.1	24.00	45	22	4.38	10.62	2.59	21.0	"

Properties of Steel Plates

(A) Chemical Analyses, weight percent

Steel	C	Si	S	P	Mn	Ni	Cr	Mo	B	Remarks
0.36% C normalized	0.35/0.36	0.10/0.22	0.038/0.047	0.012/0.024	0.44/0.46					Range of analysis of two casts
B.S.1501-151 as-rolled	0.25	0.045	0.028	0.008	0.70					Plate analysis
Mo-B normalized	0.12	0.35	0.023	0.014	0.77	0.05	0.03	0.46	0.004	Plate analysis

TABLE 6. THROUGH-WALL FLAW DATA ON A106B PIPE FROM REYNOLDS

Specimen	Diameter in.	Wall Thickness, in.	Temperature, F	Half Flaw Length[a], in.	Failure Stress, ksi	σ^*, Calculated Using Equation (3), ksi	σ_b, Burst Strength from Vessel Test[b], ksi	Tensile Test Data, ksi		$\frac{\sigma_u + \sigma_y}{2.4}$ ksi	K_c[c], Based on Equation (2), ksi$\sqrt{in.}$	$\left(\frac{K_c}{\sigma_y}\right)^2 \frac{1}{c}$
								Yield	Ultimate			
6-39	6.67	0.430	60	5.00	8.5	45.8	NA	45.3	NA	~46.5	183	3.26
6-31F	6.67	0.430	60	4.32	9.3	36.5	58.8	47.4	66.9	47.5	138	1.96
6-31	6.67	0.430	60	4.00	10.3	38.2	58.8	47.4	66.9	47.5	139	2.15
6-32F	6.67	0.430	60	3.27	13.4	42.1	58.8	47.4	66.9	47.5	141	2.72
6-30F	6.67	0.431	30	2.43	21.0	52.5	58.8	47.4	66.9	47.5	165	5.00
6-30	6.67	0.429	60	2.00	20.3	42.0	58.8	47.4	66.9	47.5	119	3.15
6-38	6.67	0.430	60	1.50	27.8	49.8	NA	46.5	66.5	47.2	138	5.88
6-33F	6.67	0.430	60	1.24	29.1	46.3	58.8	47.4	66.9	47.5	121	5.28
6-35	6.67	0.430	60	0.75	37.8	47.3	NA	46.5	66.5	47.2	129	10.2
6-36	6.67	0.430	60	0.43	42.7	47.0	NA	46.5	66.5	47.2	138	20.5
8-34	8.66	0.32	60	5.00	11.1	49.0	69.4	50.3	76.3	52.8	200	3.15
8-33	8.66	0.32	60	4.76	11.5	48.9	69.4	50.3	76.3	52.8	195	3.14
8-32	8.66	0.32	60	2.50	19.6	50.3	69.4	50.3	76.3	52.8	154	3.74
8-31	8.66	0.32	60	1.50	31.9	54.3	69.4	50.3	76.3	52.8	154	6.25
8-30	8.66	0.32	60	0.75	42.6	53.6	69.4	50.3	76.3	52.8	152	12.2
12-30	12.75	0.71	60	4.75	14.7	39.7	61.2	44.3	68.3	47.0	163	2.85
12-32	12.75	0.71	60	3.49	19.3	41.5	61.2	44.3	68.3	47.0	153	3.41
12-33	12.75	0.71	60	2.25	28.1	45.5	61.2	44.3	68.3	47.0	158	5.66
12-31	12.75	0.71	60	1.01	38.4	44.6	61.2	44.3	68.3	47.0	149	10.1

(a) All flaws were through-wall flaws.

(b) It is not known if these burst tests were conducted on these lengths of pipe or on other lengths from the same heat. NA = not available.

(c) σ_c was taken as $(\sigma_u + \sigma_y)/2.4$.

tolerance to the existence of larger axial flaws (Fig. 20). To date, macroscopic observations and analytical solutions have been able to establish flawed structural behavior with limited success. Specifically, a non-dimensional parameter β seems to be one of the variables that can be ultilized to correlate the laboratory results. The shape parameter, β, is defined by:

$$\beta = \frac{2c}{\sqrt{Rt}} \tag{14}$$

where

$2c$ = flaw length

R = pipe radius

t = pipe wall thickness

To test this assumption, a correlation between failure stress and β is made on Fig. 21 [37]. On this graph (all test data are reproduced in Appendix A), the flow stress theory (Eq. 4) is shown as solid lines and McDermott's [43] limit analysis is shown as dotted lines. A general trend is seen, but the scattered data points signal the importance of other variables which have not been incorporated into the definition of β.

As stated previously, the uncertainty in as-received material properties, flaw geometry, pipe size and pipe geometry play a very important role in the precise location of the brittle to ductile transition temperature of a specific structure. When the temperature is below NDT, LEFM is adequate and when the shelf temperature is reached, flow stress criterion may be appropriate. However, in the transition region, mixed mode of failure occurs. The degree of ductility associated with failure is affected by various factors and it is very difficult to express fracture response in the framework of present elastic/plastic fracture mechanics technology.

Among the existing criteria, pseudo-toughness (K_c) and flow stress (σ^*) theories seem to be favored by researchers because of their simplicity. However, if a material fails in mixed mode manner,

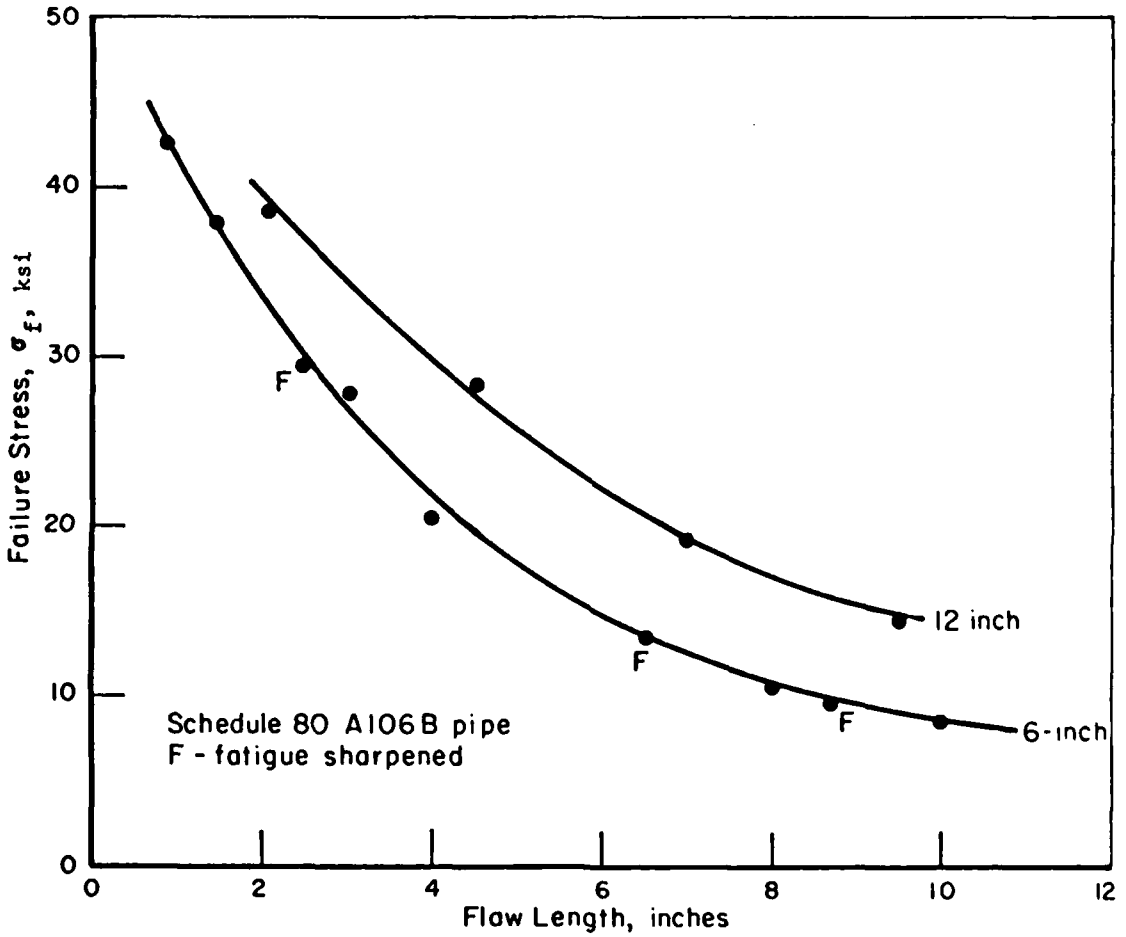

Fig. 20—Effect of pipe size and notch acuity on axial through-wall flaws in schedule 80 A106B pipe

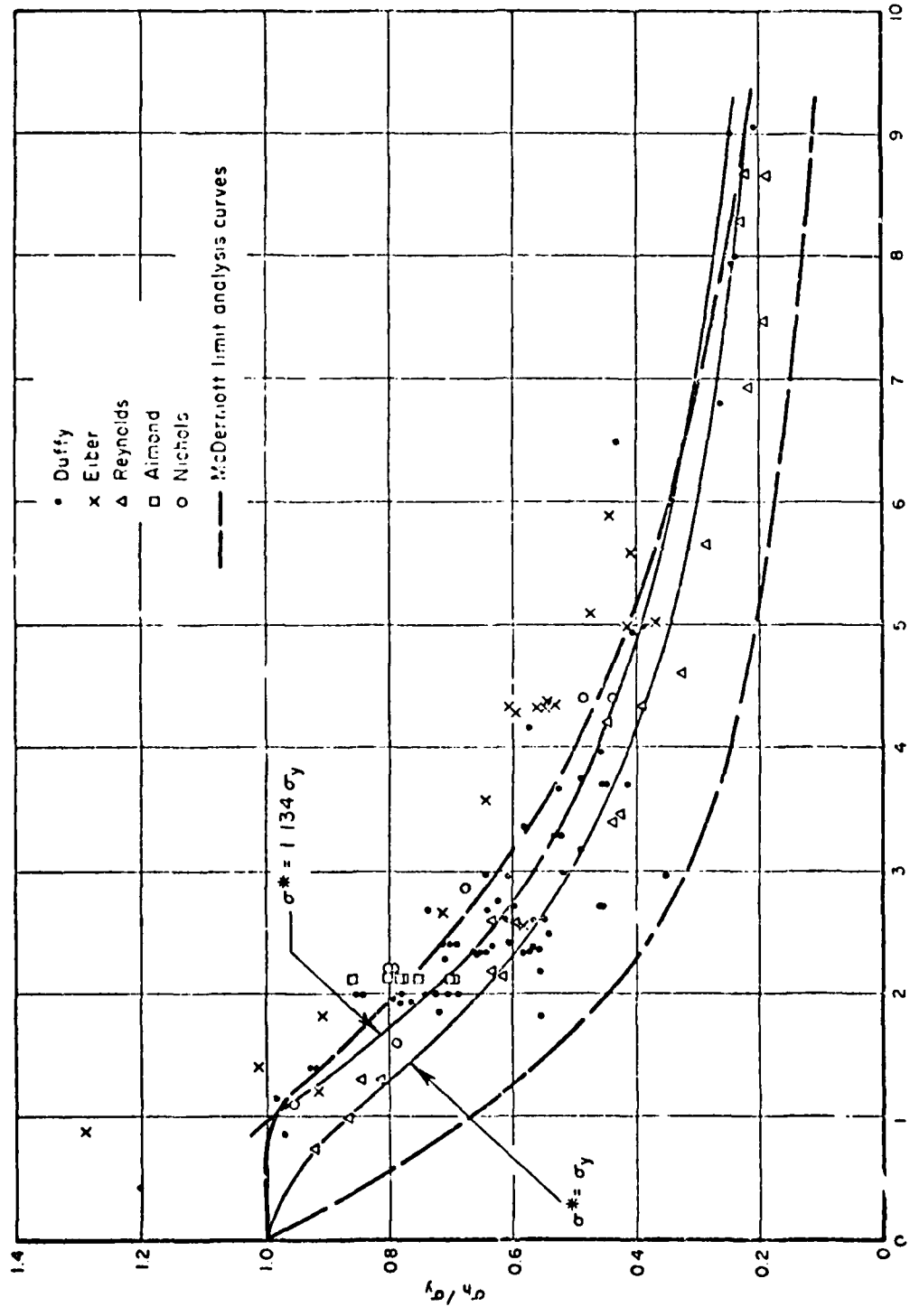

Fig. 21—Analytical curves and 122 ductile-fracture data points for pressure vessels containing through-wall axial flaws

application of the flow stress theory is tenuous due to its underlying assumption of full ductility. On the other hand, the pseudo-toughness formulation has the capability to rigorously treat brittle failure and also incorporates a plasticity correction. Unfortunately, the semi-empirical nature of K_c requires extensive experimental data to justify its validity and also limits its ability to extrapolate to different materials, structures, and service conditions. To test the adequacy of K_c and flow stress criterion, test data from UKAEA (Tables 4 & 5) and GE (Table 6) have been used to compute K_c, σ^*; the results are shown in Figs. 22 and 25. If the pseudo-toughness, K_c, can be considered as a criterion, it should be a constant for different flaw lengths (geometry independent). Similarly, if the flow stress criterion is workable, a close correlation should exist between the flow to failure stress ratio, σ^*/σ_h, and the M factor (Eq. 4). Unfortunately, the expected behavior is not apparent in these figures.

For the case of surface flaws, complexities similar to those for through-wall flaws also exist. However, it has been pointed out by Kiefner [5] that surface flaws have much lower transition temperature than through-wall flaws. This is a reasonable observation because the ligament is subjected to much less constraint than a full thickness section. Consequently, for the same material operating at the same temperature, surface flaws are more likely to undergo ductile rupture rather than a through-wall flaw. Unfortunately evidence on testing of A106 B pipes [34] having inner or outer surface flaws does not substantiate this suggestion (Tables 7, 8). The flow stress, computed from the equation:

$$\sigma^* = \frac{\sigma_{yield} + \sigma_{ult}}{2.4}, \tag{15}$$

ranges from 44 ksi to 45 ksi. If the surface flaws behave in ductile manner, $M_p \sigma_h$ values on these two tables should be within this range in order for the flow stress theory (Eq. 4) to hold. Figures 26 and 27 summarize this comparison and two observations are noted. First, the scattered data points indicate lack of correlation; and second, the definition for the "flow stress" is not optimal. If the constant 2.4 in the above equation is reduced, i.e. higher flow stress is computed, better correlation can be attained. In

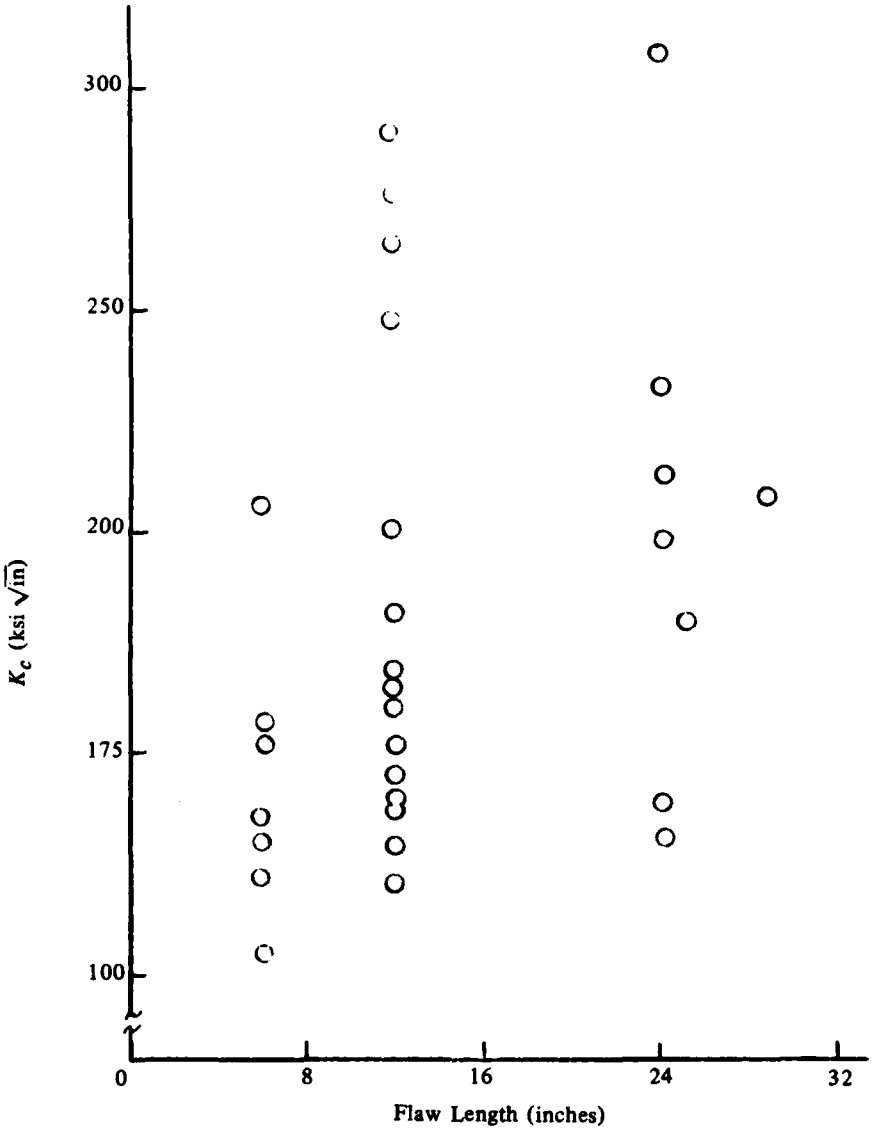

Fig. 22—UKAEA axial through-wall flaw

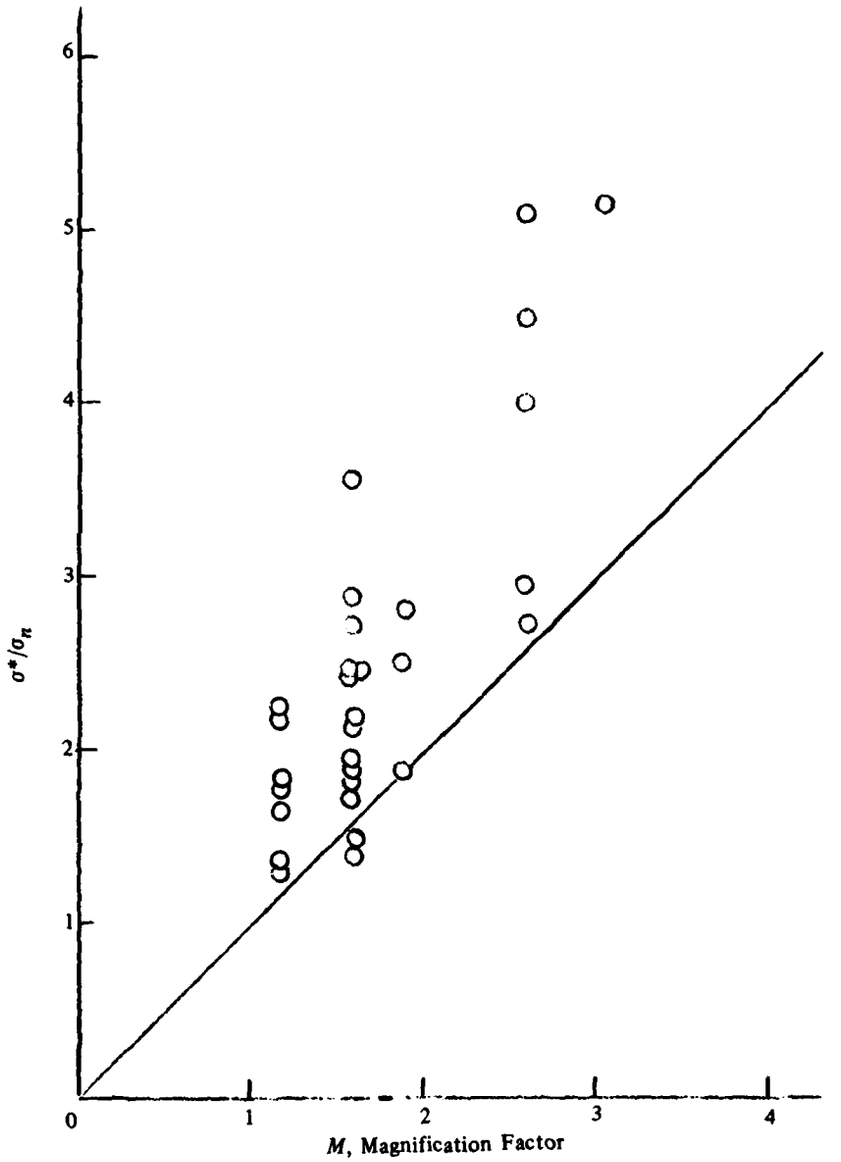

Fig. 23—UKAEA axial through-wall flaw

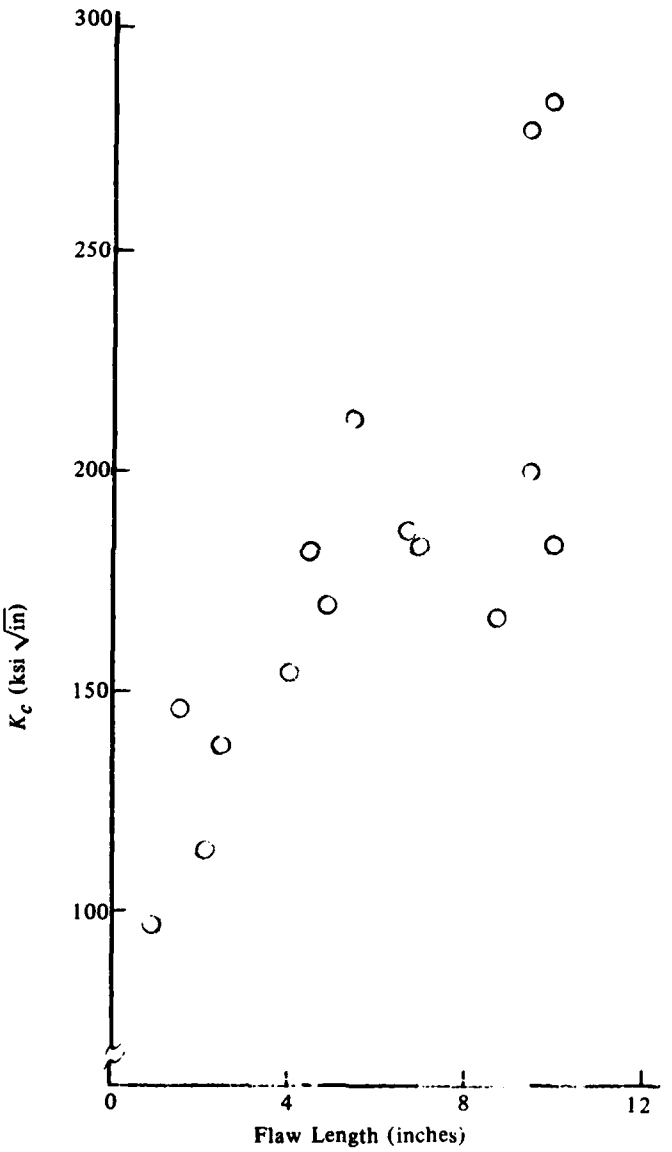

Fig. 24—GE axial through-wall flaw

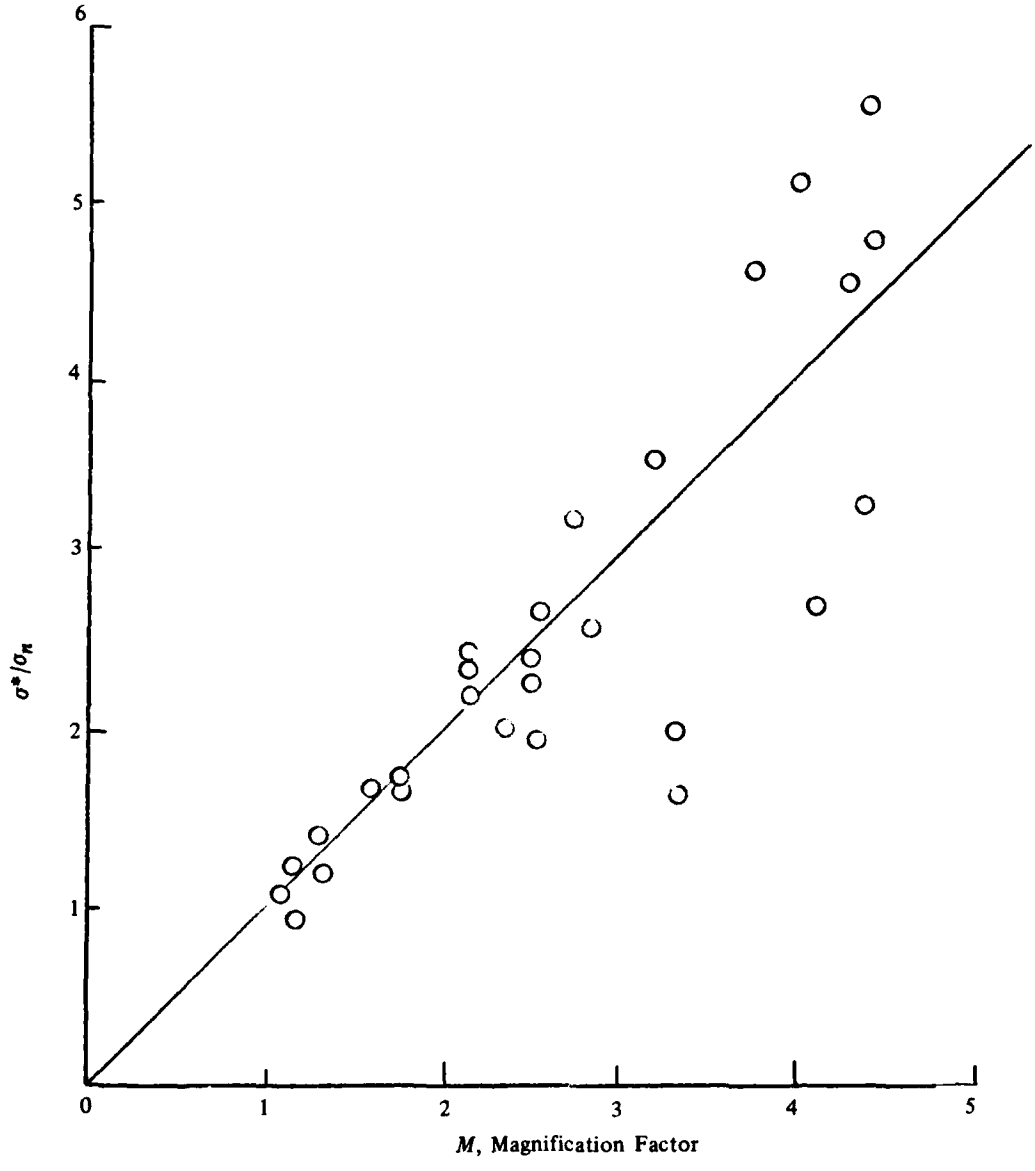

Fig. 25—GE axial through-wall flaw

TABLE 7. AXIAL INSIDE SURFACE FLAW DATA ON A106B PIPE, 6 INCHES, SCHEDULE 80, 0432 INCH WALL

Test Number	Specimen Number	Tensile Stress Data: Yield, ksi	Tensile Stress Data: Ultimate, ksi	Hoop Stress at Failure, ksi σ_h	Flaw Data: Depth, inch d	Flaw Data: Length, inches 2c	$\frac{d}{t}$	$\frac{2c}{\sqrt{Rt}}$	$\frac{\sigma_b}{\sigma_h}$ (a)	M_T	M_p	$M_p\sigma_h$
21	6-51	62.1	73.8	52.6	0.279	2.00	0.65	1.73	1.40	1.39	1.52	80.00
22	6-52	62.1	73.8	54.5	0.139	4.00	0.32	3.46	1.35	2.15	1.25	68.23
23	6-53	62.1	73.8	29.1	0.335	8.00	0.78	6.92	2.54	3.75	3.60	104.79
24	6-54	62.1	73.8	50.6	0.216	3.00	0.50	2.59	1.46	1.75	1.43	72.31
25	6-55	62.1	73.8	45.5	0.231	5.03	0.53	4.35	1.62	2.58	1.69	76.89
26	6-56	62.1	73.8	54.9	0.143	6.12	0.33	5.29	1.34	3.02	1.33	72.99
27	6-70	53.9	69.2	53.5	0.072	11.91	0.17	10.30	1.29	4.98	1.16	62.26
28	6-71	53.9	69.2	42.8	0.173	8.10	0.40	7.00	1.62	3.79	1.49	63.80
29	6-72	53.9	69.2	32.6	0.261	8.16	0.60	7.06	2.12	3.81	2.11	68.68
30	6-73	53.9	69.2	60.6	0.046	3.00	0.11	2.59	1.14	1.75	1.05	63.81
31	6-74	54.4	68.3	21.2	0.326	12.00	0.75	10.38	3.22	5.00	3.40	72.08
32	6-75	54.4	68.3	51.2	0.116	4.90	0.27	4.24	1.33	2.52	1.22	62.63
33	6-76	54.4	68.3	31.3	0.334	4.89	0.77	4.23	2.18	2.52	3.02	94.48
34	6-77	54.4	68.3	40.6	0.317	3.00	0.73	2.59	1.68	1.75	2.16	87.69
35	6-78	54.4	68.3	37.3	0.218	9.37	0.50	8.10	1.83	4.24	1.76	65.80

NOTES: Flaws cut with 2.75-inch diameter milling cutter, 45 degree included angle, 0.010-inch tip radius.

Test temperature ~ 60 degrees F.

(a) Used ultimate tensile for σ_b.

TABLE 8. AXIAL OUTSIDE SURFACE FLAW DATA ON A106B PIPE, 6 INCH, SCHEDULE 80, 0.432 INCH WALL

Test Number	Specimen Number	Tensile Data: Yield, ksi	Tensile Data: Ultimate, ksi	Hoop Stress at Failure, ksi σ_h	Flaw Data: Depth, inch d	Flaw Data: Length, inches 2c	Flaw Data: Type	Leak Failure, L	$\frac{d}{t}$	$\frac{2c}{\sqrt{Rt}}$	$\frac{\sigma_b}{\sigma_h}$	M_T	M_p	$M_p\sigma_h$
1	6-10	56.5	58.5	43.2	0.112	23.00	a		.26	19.89	1.35	--	--	--
2	6-11	56.5	58.5	27.2	0.230	22.00	a		.53	19.02	2.15	--	--	--
3	6-2	56.5	58.5	44.8	0.230	1.75	b	L	.53	1.51	1.31	1.31	1.27	56.70
4	6-3	49.5	58.5	35.2	0.230	4.00	b		.53	3.46	1.66	2.15	1.60	56.46
5	6-4	49.5	58.5	29.6	0.243	6.00	b		.56	5.19	1.98	2.97	1.84	54.60
6	6-5	49.5	58.5	37.5	0.248	4.10	a		.57	3.54	1.56	2.19	1.72	64.52
7	6-12	47.7	58.5	21.0	0.321	26.00	b	L	.74	22.48	2.79	--	--	--
8	6-13	47.7	58.5	24.0	0.295	26.00	b	L	.68	22.48	2.44	--	--	--
9	6-8	47.7	58.5	29.2	0.235	8.00	a	L	.54	6.92	2.00	3.75	1.86	54.35
10	6-9	47.7	58.5	19.3	0.345	8.00	a		.80	6.92	3.03	3.75	3.93	75.93
11	6-40	--	58.5	10.4	0.382	8.00	a	L	.88	6.92	5.63	3.75	6.38	66.35
12	6-41	52.1	65.4	49.0	0.108	8.00	a		.25	6.92	1.33	3.75	1.24	60.98
13	6-42	52.1	65.4	46.9	0.124	5.00	a		.29	4.32	1.39	2.56	1.25	58.58
14	6-43	52.1	65.4	35.0	0.292	5.00	a		.68	4.32	1.87	2.56	2.30	80.34
15	6-44	52.1	65.4	19.6	0.410	5.00	a	L	.95	4.32	3.34	2.56	12.58	246.62
16	6-45	52.1	65.4	49.1	0.184	3.00	a		.43	2.59	1.33	1.75	1.32	64.99
17	6-46	52.1	65.4	39.9	0.318	3.00	a	L	.74	2.59	1.64	1.75	2.22	88.61
18	6-48	52.1	65.4	34.5	0.330	4.00	a	L	.76	3.46	1.90	2.15	2.70	93.01
19	6-49	52.1	65.4	46.5	0.337	2.00	a	L	.78	1.73	1.41	1.39	1.99	92.74
20	6-50	52.1	65.4	62.9	0.047	6.50	a		.11	5.62	1.04	3.17	1.08	68.22
36	6-79	53.9	69.2	54.6	0.083	11.87	a		.19	10.26	1.27	4.97	1.19	64.83
37	6-80	53.9	69.2	41.0	0.185	8.18	a		.43	7.07	1.69	3.82	1.56	63.63
38	6-81	53.9	69.2	29.8	0.278	8.12	a		.64	7.02	2.32	3.80	2.31	68.82
39	6-82	53.9	69.2	60.7	0.071	3.02	a		.16	2.61	1.14	1.76	1.08	65.69
40	6-83	54.4	68.3	19.5	0.356	11.98	a		.82	10.36	3.50	5.00	4.64	90.55
41	6-84	54.4	68.3	47.9	0.138	4.92	a		.32	4.25	1.43	2.53	1.28	61.53
42	6-85	54.4	68.3	39.6	0.340	3.01	a	L	.79	2.60	1.72	1.76	2.62	103.72
43	6-86	54.4	68.3	35.6	0.225	9.37	a		.52	8.10	1.92	4.24	1.83	65.06

NOTE: Test temperature ~ 60 degrees F.

(a) Flaw cut with 2.75-inch diameter milling cutter, 45 degree included angle, 0.010-inch tip radius.

(b) Flaw cut with 0.020-inch thick slitting saw.

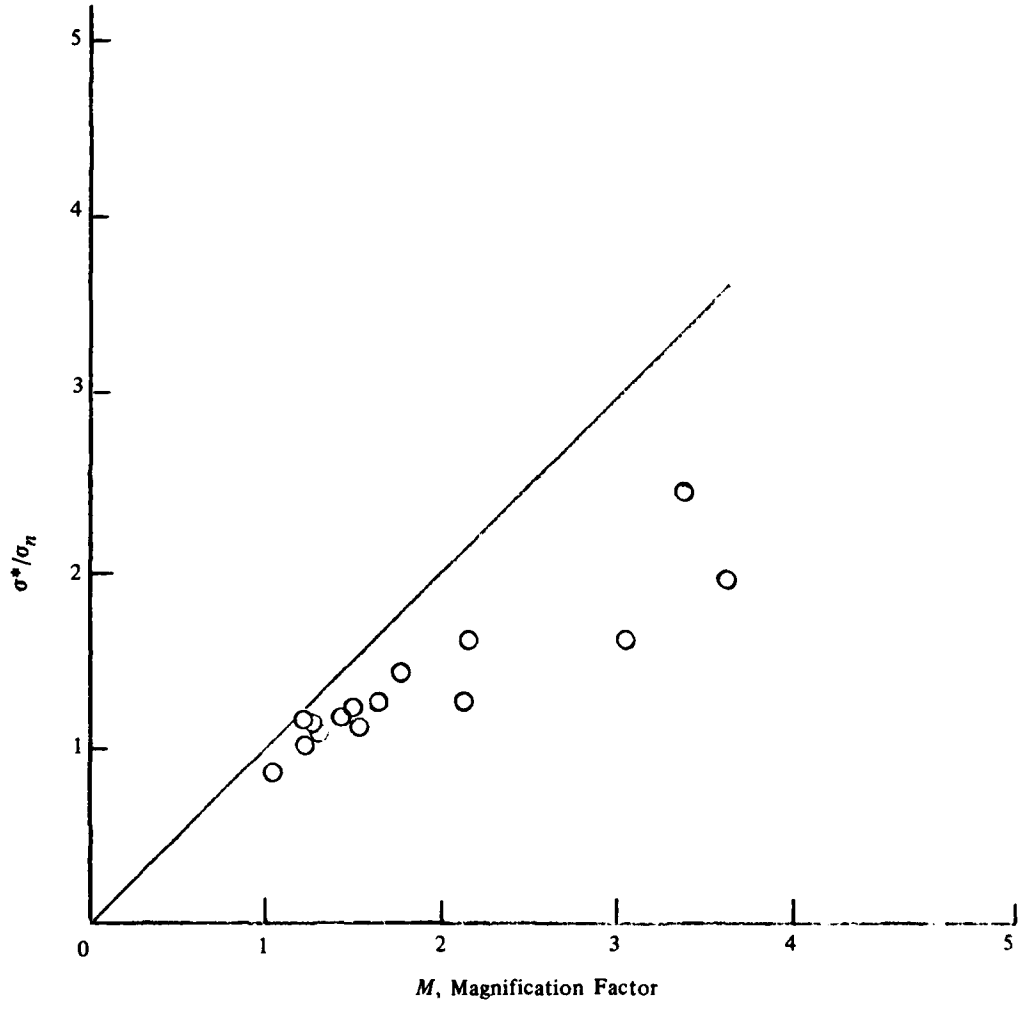

Fig. 26—GE axial *inside* surface flaw

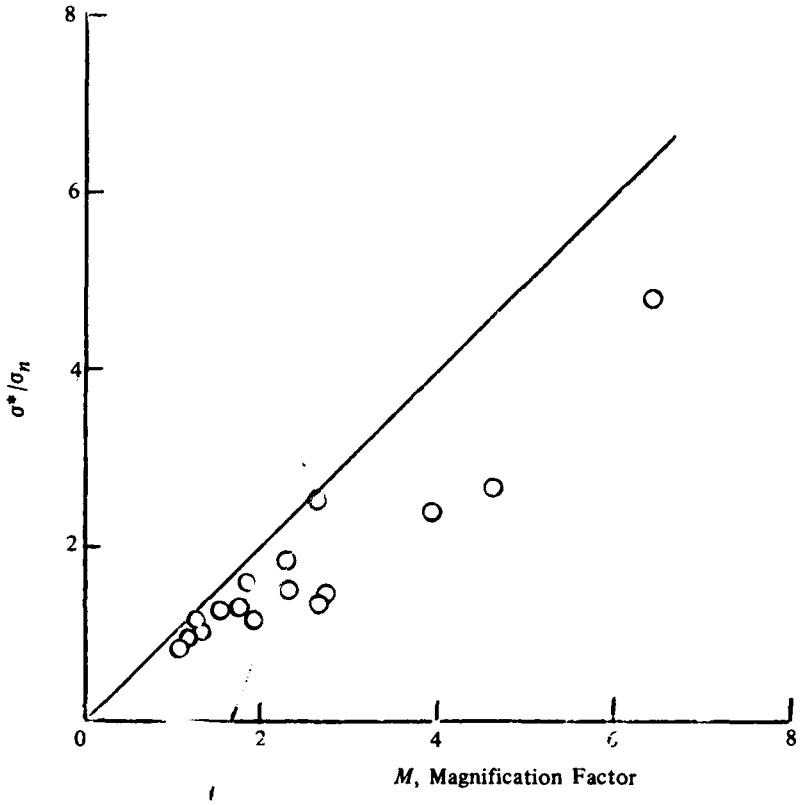

Fig. 27—GE axial *outside* surface flaw

comparing through-wall flaws (Fig. 25) with surface flaws (Figs. 26 & 27), it is interesting to note that if higher flow stress value are used, the surface flaw results display better correlation. This may indicate the surface flaw have higher ductility, lower transition temperature, as discussed previously.

3.3.2.2. Circumferential Cracks

When a material is operating on the shelf, ductile rupture is expected. The Battelle [38] test on 24 × 0.75 in. A106 B pipes (Table 9) suggest the same limit load analysis as that used for high toughness materials is applicable. In this analysis, the load carrying capability of the flawed pipe is restricted to the limit load. The applied pressure and bending loads are corrected to the new neutral axis position

TABLE 9. SUMMARY OF CIRCUMFERENTIAL SURFACE-FLAW EXPERIMENTS ON 24 X 0.750 A106B PIPE C16

Experiment	t_{net}, in.	$t_{nom.}$, in.	Flaw Length, 2c, in.	P_{fail}, psig	Calculated Data, ksi[c]						Bending Moment, f(P_f)	Temperature, F	Tensile Test Data, ksi	
					σ_L, nom.	$\sigma_{L,net}$[a]	σ_H, nom.	σ_B[b]	σ_{flow} Based on σ_L net	σ_{flow} Based on σ_L nom.			σ_y	σ_u
29	0.175	0.630-0.757, Avg 0.670	37.75	1070	9.74	34.5	19.48	20.2	54.5	28.8	1750P	526	31.8	82.4
30	0.175	0.627-0.775, Avg 0.702	56.625	1390	12.17	44.7	24.34	25.3	70.0	36.6	1690P	505	31.8	82.4
31	0.175	0.658-0.748, Avg 0.700	47.2	940	7.6	30.3	15.2	19.3	49.2	26.9	1840P	523	31.8	82.4
33	0.175	0.621-0.772, Avg 0.695	18.9	1740	14.15	55.9	28.3	6.9	63.0	21.0	1000P	534	31.8	82.4
34	0.175	0.656-0.727, Avg 0.698	65.8	1400	11.35	45.1	22.7	19.3	64.5	30.7	1183P	541	31.8	82.4
								Avg	60.6					

(a) These values were calculated using $\sigma_L = Pr/2t_{net}$.
(b) These values were calculated using the measured wall thicknesses.
(c) σ_L, longitudinal membrane stress, σ_H, hoop membrane stress, σ_B longitudinal bending stress.

due to the existence of a circumferential flaw. The limit load can be computed from the flow stress of the material. Figure 28 is a cross plot of results from Table 9, where both bending moment and failure stress are presented with flaw length. It is noted that maximum bending moment capability does correspond well with minimum failure pressure. This suggests the failure description of circumferential flawed pipes is quantitatively correct.

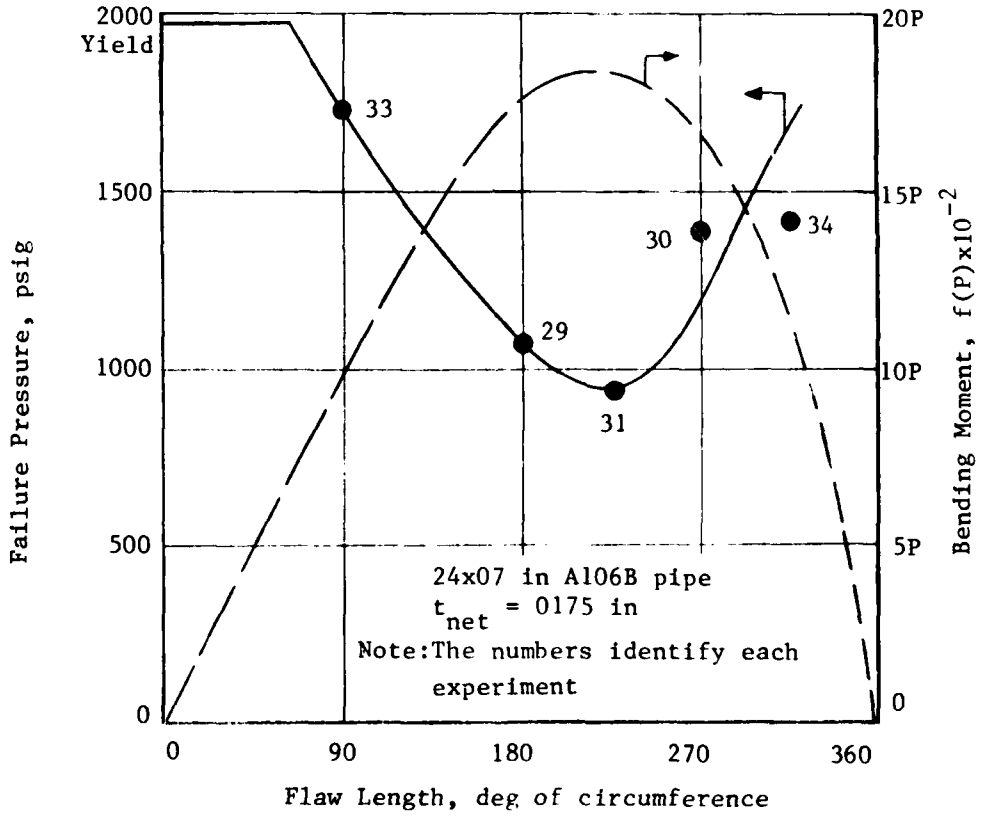

Fig. 28—Failure pressure and calculated bending moments for various circumferential surface flaw length

When the material is operating at room temperature, similar analysis technique may be employed. Test results [45, 46] on 6 in. A106B schedule 80 pipes are tabulated in Tables 10 and 11. To further investigate the adequacy of the limit load theory, a limit moment is computed for 0.0 and 1000.0 psig internal pressure at various through crack lengths (2α). Solid lines in Fig. 29 represents the computed values using Eq. 11, and test points, represented by circles, are from Tables 10 and 11. A fairly good agreement is noted; however when compared with the high toughness material (304 s.s) predictions (Fig. 16), the experimental result displays a larger deviation from theory.

3.4 Recent Advances in Elastic/Plastic Fracture Mechanics

The pseudo-toughness criterion, K_c, was developed from LEFM theory, modified by a large body of experimental data and it has been applied with very limited success to pipe rupture studies on medium toughness materials operating in the brittle to ductile transition region. Previous discussion has also indicated that the flow stress theory may be utilized to compute fracture behavior of piping made of high toughness materials or medium toughness materials operating at shelf temperature. The desirable situation in a piping integrity investigation is to have material criteria that are a counterpart of K_{Ic} for brittle fracture, and are capable of characterizing material at the shelf temperature as well as in transition region.

The importance of recent advancement in elastic-plastic fracture mechanic is not only to provide a better understanding of the fundamentals of fracture propagation processes, but also to clarify the limitations and applicability of simple criteria, e.g., T, COA or "final stretch" that have been derived under assumptions of J initiation criterion [52,53].

TABLE 10. BEHAVIOR OF CIRCUMFERENTIALLY FLAWED 6-INCH A106B SCHEDULE 80 PIPES UNDER BENDING AND PRESSURE STRESSES

Spec. No.	Flaw length, degrees	d/t	Rupture Pressure, ksi	Bending moment at rupture, 10^5 in.-lb	Bending stress in outside fiber, ksi	Flaw Type
6-23-80	34.0	1.00	9.20	0	--	0.050 in. wide
6-27-8B	42.7	1.00	6.00	5.49	44.6	0.045 in. wide
6-25-80	68.0	1.00	8.20	0	--	0.050 in. wide
6-63-8B	68.6	1.00	0	6.50	52.8	0.045 in. wide
6-20-80	360	0.28	9.79	0	--	0.020 in. wide
6-28-8B	360	0.30	6.52	6.60	53.6	0.020 in. wide
6-26-80	360	0.48	9.42	0	--	0.020 in. wide
6-64-8B	360	0.525	0	6.62	53.7	45° vee

TABLE II. CIRCUMFERENTIAL FLAW DATA ON A 106 B PIPE

Wall Thickness, inch	Specimen Number Schedule	Diameter, inches	Tensile Data, Pressure			Burst Hoop Pressure		Flaw Data							
			Yield ksi	Ultimate, ksi	Elong, percent	Unflawed, ksi P_b (a)	Flawed, ksi P_f	Location	Type	Length, degrees	Average Length, inches 2c	Depth, inch d	$\frac{d}{t}$	$\frac{2c}{\sqrt{Rt}}$	$\frac{P_b}{P_f}$ (a)
0.434	6-20-80	6.66		9.79			9.79	Outside	a	360	20.54	0.122	0.28	17.67	1.00
0.429	6-21-80	6.66		8.78			8.60	Outside	a	360	20.32	0.193	0.45	17.58	1.02
0.429	6-22-80	6.67		8.75			4.81	Outside	a	360	19.85	0.352	0.82	17.12	1.82
0.435	6-23-80	6.66		9.20			9.20	Through	b	34	1.85	--	1.00	1.59	1.00
0.432	6-24-80	6.66		8.80			7.74	Outside	a	360	20.08	0.268	0.62	17.31	1.14
0.436	6-25-80	6.66		8.82			8.20	Through	b	68	3.69	--	1.00	3.17	1.08
0.428	6-26-80	6.66		--			9.42	Outside	a	360	20.28	0.205	0.48	17.56	--
0.449	6-29-80	6.68		--			8.58	Inside	c	180	10.02	0.301	0.67	8.47	--
0.321	8-20-40	8.66		5.63			4.275	Outside	a	360	26.59	0.196	0.61	22.98	1.32

Note: Flaw Type

a = 0.020-inch milled slot
b = 0.050-inch wide
c = 45 degrees Vee.

(a) Ultimate value used for P_b.

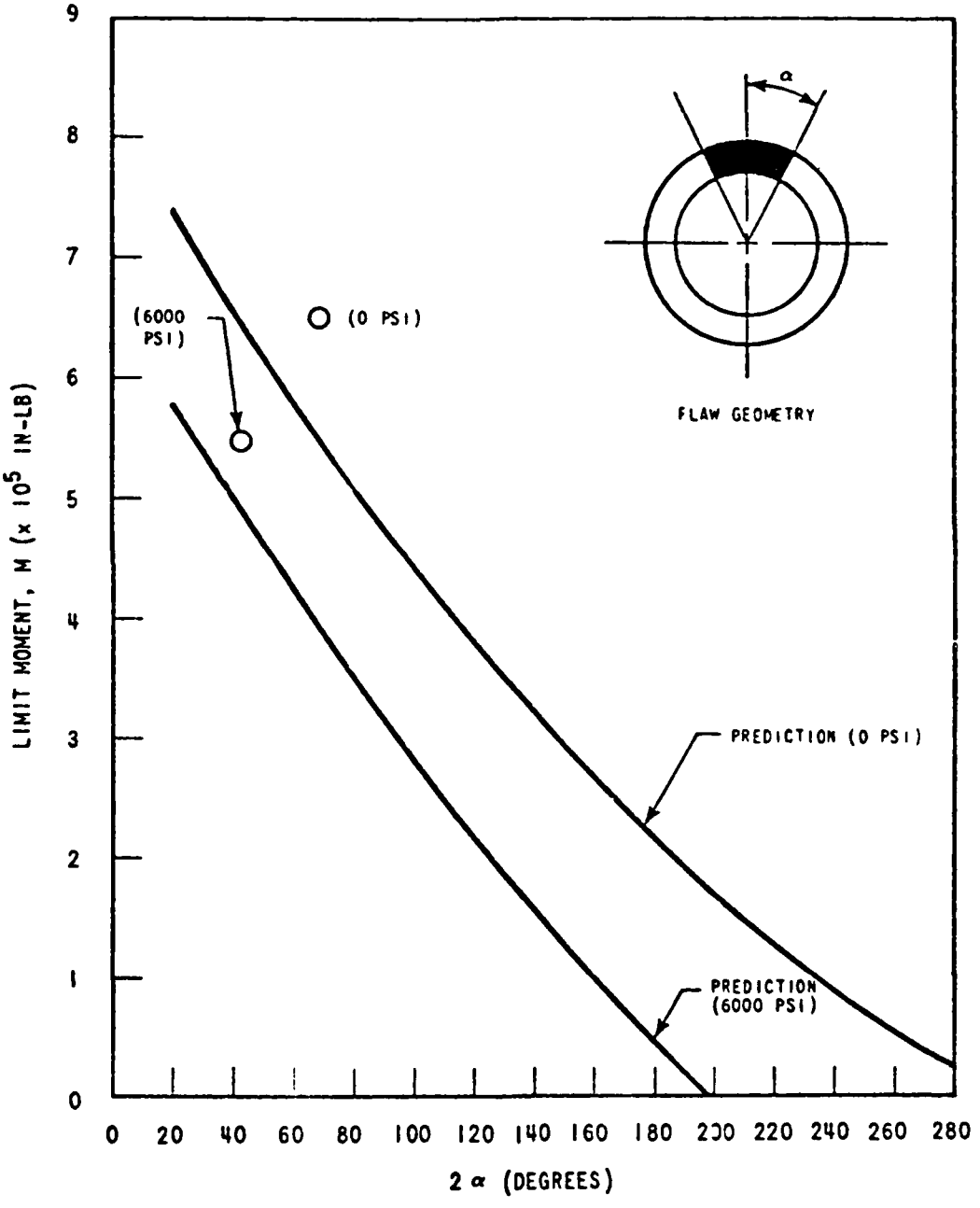

Fig. 29—Comparison of limit moment predictions with experimental results—A106B piping

3.4.1 Stable Crack Growth Criteria Based on the J-Controlled Growth

To treat elastic/plastic fracture initiation and propagation problems, crack opening displacement (COD), J controlled growth and energy method are candidates currently under intensive investigation. Although they have been proposed at different stages in the development of elastic/plastic fracture theory, there is strong correlation among them [47,48,49,50,51]. Because of the underlying assumption in these theories, extensive research effort is being carried on to establish the conditions under which they can be reliably utilized. To date, there is no single theory that can pass close scrutiny. However, provided certain requirements are satisfied, it is evident from the vast amount of available information that the J-controlled growth method can be employed as a useful tool to define structural stability against elastic/plastic fracture.

Following the introduction of the J-integral [7], J_{Ic} has been accepted as a elastic/plastic fracture initiation criterion [10,11,12,13] and the existence of a HRR (Hutchinson-Rice-Rosengren) field [8,9] has been identified as the necessary condition of a J-dominated stress field. In the J-integral derivation, it is assumed that no unloading occurs (deformation theory instead of incremental theory) and infinitesmal deformation (as opposed to finite strain) governs the kinematics relationship. Within the requirements of crack initiation, apparently both assumptions are acceptable. However, once the crack starts to propagate, further large deformation at the crack tip is expected and most of all, unloading is also experienced. Research efforts have been directed to extend J to a governing propagation parameter in spite of its underlying assumptions. Some efforts have been proven successful.

During crack growth there is some elastic unloading in the wake of advancing crack tip where the strains are strongly concentrated and where distinctly non-proportional plastic deformation occurs near the crack tip. Since the J-integral is theoretically based on the deformation theory of plasticity it does not adequately model any of these aspects of plastic behavior. Although, strictly speaking, J is restricted to the analysis of stationary cracks, a rationale is given by Hutchinson and Paris [53] for use of J

to analyze crack growth and stability under conditions which are called *J*-controlled growth. Assuming fully plastic situations for generally strain hardening materials, they considered the HRR (Hutchinson-Rice-Rosengren) type strain field based on the deformation theory for a growing crack, which is:

$$\epsilon_{ij} = K_n J^{\frac{n}{n+1}} r^{-\frac{n}{n+1}} \tilde{\epsilon}_{ij}(\theta) \tag{16}$$

where,

K_n = a constant

n = strain hardening coefficient

r, θ = local polar coordinates at the current crack tip.

The strain increments under a simultaneous increase in J and crack length are written as

$$d\epsilon_{ij} = K_n J^{\frac{n}{n+1}} r^{-\frac{n}{n+1}} \left\{ \frac{n}{n+1} \frac{dJ}{J} \tilde{\epsilon}_{ij} + \frac{da}{r} \tilde{\beta}_{ij} \right\} \tag{17}$$

where

$$\tilde{\beta}_{ij} = \frac{n}{n+1} \cos\theta \, \tilde{\epsilon}_{ij} + \sin\theta \frac{\partial}{\partial\theta} \tilde{\epsilon}_{ij} \tag{18}$$

da = increment of crack length, and $\Delta a << R$.

Equation (17) indicates that the loading increments will be proportional ($d\epsilon_{ij} \sim \epsilon_{ij}$) if the first term dominates, which may be assured when

$$\frac{da}{r} << \frac{dJ}{J}. \tag{19}$$

If there exists an annular region

$$D << r < R, \tag{20}$$

where

$$D = \left(\frac{dJ}{da} \frac{1}{J} \right)^{-1} \tag{21}$$

and R is a characteristic dimension for HRR field, then plastic loading is proportional and HRR singularity is dominant in this region. Therefore, deformation theory still remains as valid procedure for $r >> D$ and, the significance, for purpose of the present discussion, is that J uniquely measures or physically controls the fields specified by Eq. 20 for a growing crack. It may also be assumed that if predominantly proportional loading occurs throughout most of the singularity region, it will occur outside ($r > R$) this region as well [53]. Thus the requirements for the J-controlled growth are established.

If plane strain conditions are assumed to be present, which may be defined by the size requirement criterion,

$$\text{Size} \gtrsim 25\, J/\sigma_0, \tag{22}$$

the J-Resistance curve is size independent and may be reasonably configuration independent. Paris, et al. [54,59] proposed a Tearing Modulus to characterize a materials' stable tearing property,

$$T = \frac{E}{\sigma_0^2}\,\frac{dJ}{da} \tag{23}$$

where E is Young's modulus and a is the crack length. The behaviors of a structure during crack growth ($J_{app} > J_{I_c}$) is determined by the equilibrium condition

$$J_{\text{app}} = J_{\text{mat}}$$

and the stability criterion,

$$\begin{aligned} T_{\text{app}} &< T_{\text{mat}} = \text{stable} \\ T_{\text{app}} &> T_{\text{mat}} = \text{unstable} \end{aligned} \tag{24}$$

where

$$T_{\text{mat}} = \frac{E}{\sigma_0^2}\,\frac{dJ_{\text{mat}}}{da} \tag{25}$$

The onset of instability holds when $T_{\text{app}} = T_{\text{mat}}$.

For a bi-linear R-curve, dJ/da is simply the slope of the curve during crack extension; however, for arbitrary (non-linear) resistance curves, it should be noted that the Tearing Modulus (T) is dependent on the instantaneous J value.

Paris and his colleagues have demonstarated the applicability of the Tearing Instability Criterion for center cracked tension panels [56], HSST intermediate test vessels [56], and BWR pipe rupture test [55]. The effects of material strain hardening, small scale yield [54], and the correlation between tearing instability and Turner's η factor [57] have also been investigated. An experimental program utilizing three-point bend specimens was recently conducted and a good correlation between observed behavior and T-predicted instability response was noted [54].

Based on Rice's [60] J_2 flow theory for an ideally plastic material, similar studies have been conducted by Shih et. al. [61]. They considered the rate of change of the strain field crack growth in the form:

$$\frac{d\epsilon_{ij}}{da} = \frac{1}{r}\frac{d\delta}{da} f_{ij}(\theta) + \frac{\sigma_0}{E}\frac{1}{r}\ln\left[\frac{R(\theta)}{r}\right] g_{ij}(\theta) \tag{26}$$

where

δ = crack opening displacement

$R(\theta)$ = a measure of the plastic zone size

Δa = crack growth; $< < R$

σ_0 = flow stress

E = Young's modulus

$f_{ij}(\theta), g_{ij}(\theta)$ = dimensionless functions of order unity.

The first term in Eq. 26 represents the strain increment rate associated with crack tip blunting while the second term represents the strain increment rate caused by the crack advance. In Eq. 26, the strains at the crack tip may be characterized by the crack opening angle, $\frac{d\delta}{da}$, if the first term dominates that is,

$$\frac{d\delta}{da} >> \frac{\sigma_0}{E} \ln\left(\frac{R(\theta)}{r}\right). \tag{27}$$

Therefore, Eq. 27 becomes the requirement for a crack opening angle-controlled crack growth. It should be noted that the strain fields, Eq. 21 and Eq. 26, derived from two different approaches, viz, J_2 deformation theory and J_2 flow theory, have a very similar structure. Therefore, if the HRR field grows more rapidly than the advancing crack, either $\frac{d\delta}{da}$ or $\frac{dJ}{da}$ may characterize the crack tip environment for a growing crack. Based on the crack opening angle, Shih, et al. [61], proposed a tearing modulus,

$$T_\delta = \frac{E}{\sigma_0} \frac{d\delta}{da} \tag{28}$$

as a parameter to characterize the stable crack growth and its stability. Extensive studies on verification of the validity of the crack opening angle to characterize crack growth have been done both experimentally and numerically by Shih, et al. [61], and Hahn, et al. [62].

Sorensen [50] and Rice and Sorensen [51] formulated a ductile crack growth criterion which describes the critical magnitude of a crack tip opening angle during the crack growth. They assumed a Prandtl slip-line stress field centered at a moving crack-tip in an elastic perfectly-plastic von Mises material. As a consequence of having the Prandtl field zone translate through the material with the advancing crack, they derived a crack tip opening angle during crack growth as,

$$\frac{\delta}{\Delta a} = \frac{\alpha}{\sigma_0} \frac{dJ}{da} + \beta \frac{\sigma_0}{E} \ln\left(\frac{eR}{\Delta a}\right) \tag{29}$$

where

σ_o, E = as defined previously

R = plastic zone size; small scale yielding is assumed

Δa = increments of crack extension; $\Delta a << R$ is assumed

δ = crack surface displacement at the previous crack tip

α, β = constants.

If a stationary crack under monotonic loading is considered (i.e., $\Delta a = 0$), Eq. (29) integrates to the crack tip opening displacement,

$$\delta_t = \frac{\alpha}{\sigma_o} J. \tag{30}$$

The material dependent non-dimensional constant α correlates δ_t with J at the loading stage prior to the crack growth initiation. Another material constant β is theoretically defined as $\beta = 4\ (2-\nu)/\sqrt{3}$, where ν is Poisson's ratio. However, the theoretical value of β may not accurately fit the relation for the results obtained numerically, because the discretized numerical procedure can not precisely simulate the continuous crack extension. As demonstrated by Sorensen [50], β can be reestimated from finite element solutions according to the following analysis.

Let the crack be incremented by Δa at a constant external load level so that the first term in the right hand side of Eq. (29) is zero. Assuming the plastic zone size, R, is proportional to EJ/σ_o^2 as is in the case of monotonic loading of a stationary crack, β may be estimated by

$$\frac{\delta}{\Delta a}\frac{E}{\sigma_o} = \beta\, ln\left(\frac{\lambda e E J}{\sigma_o^2 \Delta a}\right) \tag{31}$$

where λ is a proportionality used for R, and may be fitted together with β.

Taking $\delta/\Delta a$ to be a material dependent constant during the crack growth, and assuming small scale yielding ($R = \lambda EJ/\sigma_o^2$) Sorensen derived the following crack growth criterion from Eq. (29):

$$\frac{dJ}{da} = \frac{\beta}{\alpha}\frac{\sigma_o^2}{E} ln\left(\frac{J_{ss}}{J}\right) \tag{32}$$

where J_{ss} denotes J at steady state conditions $\frac{dJ}{da} = 0$, so that

$$J_{ss} = \frac{\sigma_o^2 \Delta a}{\lambda eE} \exp\left[\frac{E}{\beta\sigma_o}\frac{\delta}{\Delta a}\right]. \tag{33}$$

The criterion, Eq. (32), describes the J requirement necessary to continue stable crack growth. Equation (32) is integrated to obtain the current crack length as a function of the required J level, i.e.,

$$\frac{\sigma_o^2}{E}\frac{a - a_o}{J_{ss}} = \frac{\alpha}{\beta}\left[Ei\, ln\left(\frac{J_{ss}}{J}\right) - Ei\, ln\left(\frac{J_{ss}}{J_{Ic}}\right)\right] \tag{34}$$

where

$$Ei(x) = \int_x^\infty \frac{e^{-u}}{u}\, du \text{ (Exponential integral)}$$

The crack growth criterion may be restated such that the necessary and sufficient condition to sustain crack extension is that the applied J equals the J required to meet the growth criterion (Eq. (34)), thus

$$J_A(Q,a) = J(a - a_o) \tag{35}$$

where Q denotes applied load. Likewise, instability will occur when applied value of dJ/da equals or exceeds the dJ/da required to meet the fracture criterion, thus

$$\frac{\partial J_A(Q,a)}{\partial a} \geqslant \frac{dJ(a-a_o)}{da}. \tag{36}$$

Wnuk [63] also formulated an instability criterion for a growing crack based on the concept of final stretch, which is defined as an incremental displacement continually generated at the crack tip during the stable crack growth, linked with the Dugdale-Bilby-Cottrell-Swinden model. He obtained a

resistance curve for plastic zone size R and J for a cracked panel of infinite width that experienced a large scale yielding:

$$R = R_i \left(\frac{a}{a_o}\right)^{\lambda_i+1} \exp\left[-\frac{1}{4} ln^2\left(\frac{a}{a_o}\right)\right]$$

or

$$J = J_i\left(\frac{a}{a_o}\right) + \frac{8\sigma_y^2}{\pi E} a\left[\lambda_i ln\left(\frac{a}{a_o}\right) - \frac{1}{4} ln^2\left(\frac{a}{a_o}\right)\right] \tag{37}$$

where σ_y is yield strength and the subscript i implies the value of the parameters at the moment of crack growth initiation. The parameter λ measures the distance of any state during the stable crack growth from the ultimate loss of stability. Thus, it is called "stability index". At crack growth initiation, the index λ is defined as,

$$\lambda_i = \frac{\pi E}{8\sigma_y^2}\left[\left(\frac{dJ}{da}\right)_i - \left(\frac{\partial J_A}{\partial a}\right)_i\right] \tag{38}$$

where $\frac{dJ}{da}$ is a measure of material resistance and the $\frac{\partial J_A}{\partial a}$ is an applied value. It is obvious that λ_i can be expressed in terms of tearing modulus T. Stable crack growth will occur if λ_i is greater than zero, and the crack will become unstable at the point where the λ drops to zero. However, for some types of cracked ductile specimens the crack may not grow to the critical size of instability. In such a case λ will never drop to zero and the specimen fails through a ductile tearing mechanism. Wnuk combined Eq. (37) with Eqs. (35) and (36) and derived the following expression for crack length at the terminal instability for a central crack panel:

$$a_f = a_o \exp[2\lambda_i]$$
$$a_f = \Delta a \exp[2(C-1)] \tag{39}$$

where

$$C = \frac{\delta}{\Delta a}\frac{\pi E}{8\sigma_Y} - \frac{1}{2}\ln(2e)$$

where δ denotes the final stretch. The terminal toughness is given by

$$J_f = J_i e^{2\lambda_i}\left(1 + \frac{a_o}{J_i}\frac{8\sigma_Y^2}{\pi E}\lambda_i^2\right)$$

or

$$J_f = \frac{J_i \Delta a}{a_o} e^{2(C-1)}\left\{1 + \frac{a_o}{J_i}\frac{8\sigma_Y^2}{\pi E}\left[(C-1)^2 - (C-1)\ln\left(\frac{a_o}{\Delta a}\right) + \frac{1}{4}\ln^2\left(\frac{a_o}{\Delta a}\right)\right]\right\}. \tag{40}$$

The advantage in these equations is that they can be used to predict the critical conditions in terms of known constants. It is interesting to note that similarities exist in the mathematical forms between the results obtained independently by Rice and Sorensen and by Wnuk. If Δa is assumed to be small compared to the plastic zone size R, Wnuk's equations can be modified and matched to those by Rice and Sorensen.

To summarize, although based on two different theories of plasticity, i.e., deformation theory and flow theory, the requirements of J-controlled crack growth and crack-tip opening displacement-controlled growth have been obtained by Hutchinson and Paris [54] and Shih et. al., [61] respectively. If these requirements are met, J and/or δ remain as valid tools to characterize stably growing cracks. Then Eqs. (24), (36), and (38), which are closely related to one another, give a fracture criterion in terms of tearing modulus T, J-resistance $\frac{dJ}{da}$, and stability index λ respectively. In addition, the instability condition is expressed in terms of terminal crack length by Eq. (39), and in terms of critical J value by Eq. (40).

3.4.2 Stable Crack Growth Criteria Based on the Griffith Energy Balance Equation

There exist other types of studies on stable crack growth whose associated failure criteria are not directly related to the J-controlled growth. Some of these are based on the Griffith energy balance concept extended to elastic-plastic materials undergoing slow crack growth in finite step sizes, Δa.

Neglecting dynamic and thermal effects on the structure, the energy balance for the structure during a step of crack advance may be written as

$$\frac{\Delta W_f}{\Delta a} = \frac{\Delta W_e + \Delta W_p + \Delta W_c}{\Delta a}, \tag{41}$$

where

ΔW_f = the external work increment applied to the structure

ΔW_e = the elastic energy increment stored in the structure

ΔW_p = the plastically dissipated energy increment in the structure

and

ΔW_c = the work dissipated due to separation of the crack surface over Δa.

Postulating Δa is finite, define

$$G^* = \frac{\Delta W_f - \Delta W_e - \Delta W_p}{\Delta a} \tag{42}$$

and

$$G^\Delta = \frac{\Delta W_c}{\Delta a} \tag{43}$$

then G^* may be interpreted as the rate of energy available for creating new crack surfaces, and G^Δ is the rate of work required to quasi-statistically release the cohesive tractions holding the crack surfaces. During the process of stable crack growth, G^* and G^Δ are equivalent. Atluri, et. al., [64] and Hahn, et. al., [62] studied the G^* by finite element analysis which simulated a resistance curve from existing experimental data. On the other hand, the G^Δ has been studied by Hahn et. al., [62] and Kfouri and Miller [65]. As predicted by Rice [66] that at least for non-hardening materials, both G^* and G^Δ

reduce to zero as crack growth step size, Δa, tends to zero, this phenomenon was recognized even for a low hardening material by Atluri, et. al., [64] in their numerical analyses. They discussed that Δa in finite element analyses of stable crack growth must by selected four to five times crack opening displacement at incipient growth condition to obtain meaningful results of G^* or G^Δ.

There may exist a small region ahead of a growing crack-tip in which some non-linear irreversible process occurs. This region is called a "crack-tip process zone." The rate of energy dissipated due to the irreversible process in the process zone can be thought as a material property. Denoting this energy dissipation rate by G_{pz}, the energy flow rate into the process zone, G^*_{pz} is equated to the sum of G^Δ and G_{pz}, i.e.,

$$G^*_{pz} = G^\Delta + G_{pz}. \tag{44}$$

This energy flow rate, G^*_{pz}, can be obtained by numerically evaluating change of the energy over the entire structure excluding the process zone, thus

$$G^*_{pz} = \frac{\Delta W_f}{\Delta a} - \frac{[\Delta W_e + \Delta W_p]_{\Omega - p}}{\Delta a} \tag{45}$$

or equivalently

$$G^*_{pz} = \int_{\partial\Gamma} T_i \frac{\Delta U_i}{\Delta a} ds \tag{46}$$

where T_i are the tractions at the boundary $\partial\Gamma$ of the process zone Γ, ΔU_i are increments of displacements on $\partial\Gamma$, and $[\ ]_{\Omega-p}$ in Eq. (45) denotes that the quantities in [ ] are integrated in the rest of the structure excluding the process zone. G^*_{pz} has been studied by Hahn et. al., [62] and Atluri et. al., [64]. The size of the process zone recommended by Hahn, et. al., is to be taken on the order of plate thickness, and maybe smaller for the plane strain case.

Another candidate for a criterion to characterize stable crack growth and possibly predict the onset of fracture is a crack tip nodal force. This has been proposed and studied by Hahn, et. al., [62]. Although this is intuitively appealing, the theoretical basis for use of the crack tip nodal force has not yet been established.

4.0 LEAK BEFORE BREAK CRITERIA

It is very desirable that pipe rupture is preceded by leakage so that necessary measures can be undertaken to remedy the situation. Therefore, there are two aspects to be considered: (1) the possibility of leak before break, and (2) the acceptable leakage rate. The state of art of pipe rupture in the elastic/plastic region is only at the semi-empirical stage. Therefore, effort has been devoted to the definition of critical crack length with only little emphasis to the mouth opening, which is one of the means to measure leakage rate.

For pipes fabricated from austenitic stainless steel or ferritic steels (at shelf temperature), pipe fracture is unlikely to occur unless the structure has reached its limit load capability. In that case, ductile tearing is the failure mode. From all the experimental and analytical results reviewed, the crack length that corresponds to limit load (flow stress criterion) is generally very large and excessive leakage would have been developed well before crack of such length is developed [3, 29].

For pipes fabricated from ferritic steels that operate in the transition temperature region, mixed mode failure consisting of brittle fracture and ductile tearing is observed. The leakage rate is determined by the degree of mouth opening. Analytically, the crack opening can be approximated as the sums of elastic displacement, plastic correction and bulging to pipe geometry. The following derivation is from Ref. 29.

$$A = \text{Mouth opening area} = A_1\ (\text{Elastic}) + A_2(\text{Plastic}) + A_3\ (\text{Bulging}), \tag{47}$$

$$\text{where } A_1 = \frac{2(1-\nu^2)}{E} \cdot \sqrt{\frac{c}{\pi}}\, K\pi c$$

$$A_2 = \frac{4\sigma_y c^2}{E}\, ln\, \text{Sec}\left[\frac{\pi}{2}\,\frac{\sigma}{\sigma_y}\right],$$

and

$$A_3 = \frac{2\pi}{3}\, y_o c\,(2y_0/R)^{1/2};$$

in which,

$2c$ = crack length

ν = Poisson's Ratio

E = Modulus

σ_y = yield strength

σ = applied stress

y_o = amount of bulging (Ref. 29)

K = stress intensity factor

R = pipe radius

5.0 CONCLUSIONS

An extensive literature review concerning experimental data and predictive capability of elastic/plastic pipe rupture has been completed. The materials used for nuclear reactor piping can be classified as high toughness and medium to high toughness materials. High toughness material, including austenitic stainless steel, exhibits no brittle to ductile transition temperature and ductile tearing is

the failure mode. Medium to high toughness materials, including ferritic steels, SA 106, SA 333 and SA 561, exhibit high ductility at the shelf temperature and fail in a mixed (brittle/ductile) fracture mode in the transition temperature region.

The predictive tools reviewed are classified into three major categories; the overall structural response computation, the semi-empirical method, and rigorous elastic/plastic fracture mechanics. Lack of adequate elastic/plastic fracture criteria and excessive computational expense limit the applicability of overall structural response computation. For the cases studied, the flow stress theory, which assumes pipe rupture from limit load, is adequate to predict failure of high toughness materials and medium to high toughness materials at the shelf temperature. The pseudo-toughness approach, K_c, has been used to describe pipe failure in the transition temperature region with limited success. Therefore, for those materials which operate in the transition region, the real solution is to ultilize rigorous elastic/plastic fracture mechanics methodology. Among the current theoretical developments in the analysis of advancing cracks, the *J*-controlled growth methods are one of the most promising and most widely accepted. All the criteria proposed to data, i.e., Tearing Modulus, COA, final stretch, and Stability Index, are capable of describing a small amount of crack growth and they are all mathematically related. To permit quantitative assessment of safety factors, *J*-integral resistance curves of current nuclear piping materials should be generated.

The high fracture toughness levels associated with existing nuclear piping configurations and materials suggests that extensive plastic deformation will precede failure. No sudden (catastrophic) ruptures are expected and a favorable leak-before-break condition should prevail. The mouth opening on the pipes of these materials in the transition region can be approximated by linear elastic mechanics modified by plasticity and geometry corrections.

6.0 REFERENCES

1. "Investigation and Evaluation of Cracking in Austenitic Stainless Steel Piping of Boiling Water Reactor Plants," US Nuclear Regulatory Commission, NUREG-75/067, October, 1975.

2. "Investigation and Evaluation of Stress-Corrosion Cracking in Piping of Light-Water Reactor Plants," US Nuclear Regulatory Commission, NUREG-0531, February, 1979.

3. F.J. Witt, W.H. Bamford, and T.C. Esselman, "Integrity of the Primary Piping Systems of Westinghouse Nuclear Power Plants During Postulated Seismic Events," Westinghouse Electric Corporation, WCAP-9283, March, 1978.

4. S.H. Bush, "Reliability of Piping in Light-Water Reactors," Nuclear Safety, Volume 17, Sept-Oct., 1976.

5. E.C. Rodabaugh, W.A. Maxey and R.J. Giles, "Review and Assessment of Research Relevant to Design Aspects of Nuclear Power Plant Piping Systems," Final Report for US Nuclear Regulatory Commission, NUREG-0307, Battelle Columbus Laboratory, July, 1977.

6. "Plane-Strain Fracture Toughness of Metallic Materials," ASTM Standard E-399.

7. J.R. Rice, "A Path Independent Integral and the Approximate Analysis of Strain Concentration by Notches and Cracks," J. App. Mech., Volume 14, June, 1968, pp. 379-386.

8. J.R. Rice and G.F. Rosengren, "Plane-Strain Deformation near a Crack Tip in a Power Law Hardening Material," J. Mech. Phys. Sol., Volume 16, 1968, pp. 1-12.

9. J.W. Hutchinson, "Plastic Stress and Strain Fields at a Crack Tip," J. Mech. Phys. Sol., Volume 16, 1968, pp. 337-347.

10. J.A. Begley, J.D. Landes, "The *J* Integral as a Fracture Criterion", in *Fracture Toughness*, ASTM STP 514, 1972, pp. 1-20.

11. J.D. Landes, J.A. Begley, "The Effect of Specimen Geometry on J_{Ic}," in *Fracture Toughness*, ASTM STP 514, 1972, pp. 24-39.

12. J.A. Begley, J.D. Landes, "The Effect of Specimen Geometry on J_{Ic}," in *Fracture Toughness*, ASTM STIP 560, 1974, pp. 170-186.

13. J.R. Rice, P.D. Paris, and J.G. Merkle, "Some Further Results of J-Integral Analysis and Estimates," in *Progress in Flaw Growth and Fracture Toughness Testing*, ASTM STP 536, 1973.

14. J.A. Begley and J.D. Landes, "A Comparison of the J-Integral Fracture Criterion with the Equivalent Energy Concept," in *Progress in Flaw Growth and Fracture Toughness Testing*, ASTM STP 536, 1973, pp. 246-263.

15. J.D. Landes and J.A. Begley, "Recent Developments in J_{Ic} Testing," in Developments in Fracture Mechanics Test Methods Standardization, ASTM STP 632, 1977, pp. 57-81.

16. C.A. Griffis and G.R. Yoder, "Initial Crack Extension in Two Intermediate Strength Aluminum Alloys," J. Engr. Mat'l and Tech., Volume 98, 1976, pp. 152-158.

17. W.H. Bamford and J.A. Begley, "Techniques for Evaluating the Flow Tolerance of Reactor Coolant Piping," ASME paper No. 76-PVP-48, American Society of Mechanical Engineers, 1976.

18. F. Erdogan, G.R. Irwin and M. Ratwani, "Ductile Fracture of Cylindrical Vessels Containing a Large Flaw," in Cracks and Fracture, ASTM STP 601, 1976.

19. F. Erdogan, F. Delale, and J.A. Owczarek, "Crack Propagation and Arrest in Pressurized Containers," J. Press. Vessel Technology, Feb. 1977, pp. 90-99.

20. A.F. Emery, W.J. Love, and A.S. Kobayashi, "Fracture in Straight Pipes under Large Deflection Conditions, Part I: Structural Deformations," J. of Press. Vessel Tech., Feb. 1977, pp. 122-127.

21. W.J. Love, A.F. Emery, and A.S. Kobayashi, "Fracture in Straight Pipes under Large Deflection Conditions, Part II: Pipe Pressures," J. of Press. Vessel Tech., Feb. 1977, pp. 128-136.

22. C. Popelar, A.R. Rosenfield, and M.F. Kanninen, "Steady State Crack Propagation in Pressurized Pipelines," J. Press, Vessel Tech., Feb. 1977, pp. 112-121.

23. A.R. Duffy, "Studies of Hydrostatic Test Levels and Defect Behavior," American Gas Association Publication L30000, 1966.

24. E.S. Folias, "On the Effect of Initial Curvature on Cracked Plate Sheets," Int. J. Fracture Mech., Volume 5, December, 1969.

25. T.N. Goodier, and F.A. Field, "Plastic Energy Dissipation in Crack Propagation," *Fracture of Solids*, Interscience Publishers, New York, 1963, pp. 103-118.

26. G.T. Hahn, M. Sarrate, and A.R. Rosenfield, "Criteria for Crack Extension in Cylindrical Pressure Vessels," Int. J. Fracture Mechanics, Volume 5, 1969, pp. 187-210.

27. J.C. Newman, "Fracture Analysis of Surface and Through-Cracked Sheets and Plates," Engr. Fracture Mech., Volume 5, 1973.

28. N.J.I. Adams, "Characterization of Fracture in Vessels and Piping," J. Press. Vessel Tech., Feb. 1977, pp. 114-148.

29. P.K. Nagata and F.W. Smith, "Code Assessment and Applications Program (A6166), Fracture Toughness Criteria Task," Report No. RE-M-78-029, EG and G Idaho, Inc., Idaho Falls, Idaho.

30. A. Quirk, "The Effect of Material Properties and Component Geometry on Fracture Behavior," UKAEA, AHSB(S)R, 1968.

31. R.J. Eiber, W.A. Maxey, A.R. Duffy, and T.J. Atterburg, "Review of Through-Wall Critical Crack Formulations for Piping and Cylindrical Vessels," BMI-1883, Battelle Memorial Institute, May, 1970.

32. "Fourth Symposium on Line Pipe Research, Pipeline Research Committee of the American Gas Association, Dallas, Texas, Nov. 18-19, 1969.

33. S.R. Vandenbergy, "Status of Pipe-Rupture Study at General-Electric II," GEAP-5653, AEC Research and Development Report, July, 1968.

34. "Reactor Primary Coolant System Rupture Study Quarterly Progress Report No. 14, July-September, 1968," GEAP-5716, AEC Research and Development Report, December, 1968.

35. "Reactor Primary Coolant System Rupture Study Quarterly Progress Report No. 16, January-March, 1969, GEAP-10024, AEC Research and Development Report, April, 1969.

36. F. Erdogan, J.J. Kibler, "Cylindrical and Spherical Shells with Cracks," Int. J. Fracture Mech., Volume 5, Sept., 1969.

37. R.J. Eiber, W.A. Maxey, A.R. Duffy, and T.T. Atterbury, "Investigation of the Initiation and Extent of Ductile Pipe Rupture," BMI-1908, Battelle Columbus Laboratory, July, 1969—June, 1971.

38. Ibid.

39. M.F. Kanninen, D. Broek, G.T. Hahn, C.W. Marschall, E.F. Rybicki, and G.M. Wilknowski, "Towards an Elastic-Plastic Fracture Mechanics Predictive for Reactor Piping," Nucl. Engr. Design, Volume 38, 1978, pp. 117-134.

40. M.F. Kanninen, D. Broek, C.W. Marschall, G.R. Rybicki, S.G. Sampath, F.A. Simonen, and G.M. Wilknowski, "Mechanical Fracture Prediction for Sensitized Stainless Steel Piping with Circumferential Cracks," EPRI, No. 192 Battelle Columbus Laboratory, Sept., 1976.

41. R.W. Nichols, W.H. Irvine, A. Quirk, and E. Bevitt, "A Limit Approach to the Presentation of Pressure Vessel Failure," Proc. First Int. Conf. on Fracture, Sendai, Japan, 1966 pp. 1673-1689.

42. M.B. Reynolds, "Reactor Primary Coolant System Rupture Study Task C Fracture Mechanics," Quarterly Progress Report 12, GEAP-5637, General Electric, January-March 1968.

43. D.C. McDermott, "Limit Analysis of Pressurized Cylinders with Slits," Ph. D. Thesis, Brown University, Providence, RI, 1969.

44. S. Wilson, "Estimating the Relative Probability of Piping Severance by Fault Causes," GEAP-20615, UC-78, AEC Research and Development Report, September, 1974.

45. Idem, Reference No. 34.

46. Idem, Reference No. 35.

47. J.G. Merkle, "Elastic-Plastic Fracture Criteria," Int. J. Press. and Piping, Volume 4, 1976, pp. 197-206.

48. C.F. Shih, "Relationship between the J-Integral and Crack Opening Displacement for Stationary and Extending Cracks," General Electric Report No. 79CRD075, April, 1979.

49. C.E. Turner, "Elastic/Plastic Fracture Analysis," presented at the ASTM 12th Symposium on Fracture Mechanics, May 1979, Washington University, St. Louis, MO.

50. E.P. Sorensen, "A Numerical Investigation of Plane-Strain Crack Growth Under Small Scale Yielding Conditions," in Elastic-Plastic Fracture, ASTM STP 668, pp. 151-174.

51. J.R. Rice and E.P. Sorenson, "Continuing Crack-Tip Deformation and Fracture for Plane-Strain Crack Growth in Elastic/Plastic Solids," J. Mech. Phys. Solids, Vol. 26, pp. 183-186.

52. "EPRI Ductile Fracture Research Review Document," EPRI NP-701-SR, Feb., 1978.

53. J.W. Hutchinson and P.C. Paris, "The Theory of Stability Analysis of J-Controlled Crack Growth," in ASTM STP 668, 1979, pp. 37-64.

54. P.C. Paris et al., H. Tada, A. Zahour, and H. Ernst, "A Treatment of the Subject of Tearing Instability," NUREG-0311, US. Nuclear Regulatory Commission, July 1977 and ASTM STP 668, 1979, pp. 5-36.

55. H. Tada, P.C. Paris. and R. Gamble, "Stability Analysis of Circumferential Cracks in Reactor Piping," NUREG/CR-0838, US Nuclear Regulatory Commission, June, 1979.

56. A. Zahoor and P.C. Paris, "Further Results on the Subject of Tearing Instability II" NUREG/CR-1220, Vol. 2, US Nuclear Regulatory Commission, Jan. 1980.

57. P.C. Paris, J.W. Hutchinson, H. Ernst, M. Rossow, C.E. Turner, D.D. Gorman, and B. Kong "Further Results on the Subject of Tearing Instability" NUREG/CR-1220, Vol. 1, US Nuclear Regulatory Commission, Jan. 1980.

58. H. Tada and P.C. Paris "Tearing Instability Analysis Handbook", NUREG/CR-1221, US Nuclear Regulatory Commision, Jan. 1980.

59. H.A. Ernst and P.C. Paris, "Techniques of Analysis of Load-Displacement Records by *J*-Integral-Methods" NUREG/CR-1222, US Nuclear Regulatory Commission, Jan. 1980.

60. J.R. Rice, "Elastic-Plastic Models for Stable Crack Growth," in *Mechanics* and Mechanism of Crack Growth," M.J. May, editor, 1975, pp. 14-39.

61. C.F. Shih, H.D. deLorenzi and W.R. Andrews, "Studies on Crack Initiation *and Stable Crack Growth*," in ASTM STP 668, 1979, pp. 65-120.

62. G.T. Hahn, D.D. Broek, M.F. Kanninen, C.W. Marschall, A.R. Rosenfield, E.F. Rybicki, and R.B. Stonesifer, "Methodology for Plastic Fracture," EPRI NP-701-SR, Battelle Columbus Laboratory, Feb., 1978.

63. M.P. Wnuk, "Stable and Unstable Cleavage Fracture in Fully Yielded Components," Mech. Res. Comm., Vol. 5, 1978, pp. 269-275.

64. M. Nakagaki, W.H. Chen, and S.N. Atluri, "A Finite-Element Analysis of Stable Crack Growth-I," ASTM STP 668, 1979, pp. 195-213.

65. A.P. Kfouri and K.J. Miller, in Proceeding, Institution of Mechanical Engineers, London, U.K., Vol. 190, 1976, pp. 571-586.

66. J.R. Rice, 'n Proceedings, 1st National Congress on Fracture, T. Yokobori et al., Eds, Sendai, Japan, 1965, Japanese Society for Strength and Fracture, Tokyo, Vol. 1, 1966, pp. 309-340.

67. D.M. Norris, Jr., B. Moran, D.F. Quinoes and J.E. Reaugh, "Fundamental Study of Crack Initiation and Propagation," EPRI NP-701-SR, Feb., 1978.

68. D.A. Shockey, L. Seaman, K.C. Dao and D.R. Curran, "A Computational Fracture Model for SA 533 Grade B Class 1 Steel Based upon Microfracture Processes," EPRI NP-701-SR, Feb., 1978.

Appendix A
LIST OF EXPERIMENTAL DATA
From Ref. 26

TABLE

Summay of flat-plate crack-extension measurements performed by Kihara et al. on 19.7-in.-long by 15.7-in.-wide hot-rolled steel plates with 3.14-in.-long edge cracks.

Plate thickness, in.	Test temp, C	σ^*, psi	K_c, ksi $\sqrt{\text{in.}}$[a]
0.25	−118	20,300	73
	−138	18,000	65
	−158	14,500	52
	−170	15,600	56
	−196	8,170	29
0.375	−118	25,200	90
	−138	20,200	73
	−158	15,600	56
	−180	12,400	45
0.500	−118	28,400	100
	−138	23,800	85
	−158	17,000	61
	−180	9,900	36

[a] $K_c = 1.14\,\sigma^*(\pi c)^{\frac{1}{2}}$, no plasticity correction was necessary since $\sigma^*/\sigma_Y < 0.4$ in all cases.

Compilations of pressure-vessel test data

TABLE

Data summary for Anderson and Sullivan for aluminum-alloy vessels

Material properties			Vessel geometry			Test conditions			Calculated values[a]		
Designation	σ_Y, ksi	σ_U, ksi	R, in.	t, in.	R/t	Temp, C	c, in.	σ_R^*, ksi	c^2/Rt	φ_3	$(\sigma_R^{*2}\pi c\varphi_3)^{-1} \times 10^{-10}$ (in.^{2}) (lb.$^{-2}$)
Aluminum 2014-T6	68	79	2.81	0.06	46.8	Room Temp.	0.06	64.4	0.02	2.42/1.55	5.29/ 8.26
Ditto	68	79	2.81	0.06	46.8	Ditto	0.25	34.0	0.37	1.2 /1.14	9.17/ 9.66
Ditto	68	79	2.81	0.06	46.8	Ditto	0.50	20.6	1.48	1.13/1.09	13.40/13.76
Ditto	68	79	2.81	0.06	46.8	Ditto	1.00	9.7	5.93	1.08/1.06	31.32/31.91
Ditto	68	79	2.81	0.06	46.8	−196	0.05	71.6	0.014	1.75/1.42	7.09/ 8.74
Ditto	82	93.9	2.81	0.06	46.8	−196	0.07	70.6	0.029	1.74/1.41	5.24/ 6.47
Ditto	82	93.9	2.81	0.06	46.8	−196	0.10	63.7	0.059	1.49/1.31	5.26/ 5.98
Ditto	82	93.9	2.81	0.06	46.8	−196	0.12	58.5	0.085	1.39/1.26	5.57/ 6.15
Ditto	82	93.9	2.81	0.06	46.8	−196	0.15	52.2	0.13	1.29/1.20	6.03/ 6.49
Ditto	82	93.9	2.81	0.06	46.8	−196	0.20	47.4	0.23	1.25/1.17	5.66/ 6.03
Ditto	82	93.9	2.81	0.06	46.8	−196	0.25	40.1	0.37	1.19/1.13	6.65/ 7.00
Ditto	82	93.9	2.81	0.06	46.8	−196	0.37	30.2	0.81	1.14/1.10	8.27/ 8.57
Ditto	82	93.9	2.81	0.06	46.8	−196	0.50	23.1	1.48	1.11/1.08	10.75/11.04
Ditto	82	93.9	2.81	0.06	46.8	−196	0.62	18.6	2.28	1.09/1.07	13.61/13.86
Ditto	82	93.9	2.81	0.06	46.8	−196	0.87	14.4	4.50	1.09/1.07	16.10/16.48
Ditto	82	93.9	2.81	0.06	46.8	−196	1.00	11.3	5.80	1.07/1.05	23.30/23.68
Ditto	90.5	93.9	2.81	0.06	46.8	−253	0.05	82.2	0.014	1.97/1.77	4.78/ 5.32
Ditto	90.5	93.9	2.81	0.06	46.8	−253	0.12	63.4	0.08	1.38/1.34	4.78/ 4.92
Ditto	90.5	93.9	2.81	0.06	46.8	−253	0.25	39.6	0.37	1.16/1.14	6.99/ 7.12
Ditto	90.5	93.9	2.81	0.06	46.8	−253	0.37	32.0	0.81	1.15/1.14	7.30/ 7.37
Ditto	90.5	93.9	2.81	0.06	46.8	−253	0.50	21.0	1.48	1.08/1.08	13.36/13.38
Ditto	90.5	93.9	2.81	0.06	46.8	−253	0.63	19.8	2.35	1.11/1.10	11.60/11.70
Ditto	90.5	93.9	2.81	0.06	46.8	−253	0.87	13.2	4.52	1.08/1.07	19.45/19.63
Ditto	90.5	93.9	2.81	0.06	46.8	−253	1.00	11.9	5.93	1.08/1.08	20.80/20.80

[a] Two values are computed for φ_3 and $\sigma_R^{*2}\pi c\varphi_3$ corresponding to the upper and lower bounds for $\bar{\sigma}$: $\bar{\sigma} = \sigma_Y$, $\bar{\sigma} = \sigma_U$.

TABLE

Data summary for Getz, Pierce, and Calvet for aluminum-alloy vessels

Material properties			Vessel geometry			Test conditions			Calculated values[a]		
Designation	σ_Y, ksi	σ_U, ksi	R, in.	t, in.	R/t	Temp, C	c, in.	σ_R^*, ksi	c^2/Rt	φ_3	$(\sigma_R^{*2}\pi c\varphi_3)^{-1}\times 10^{-10}$(in.^{3})(lb.$^{-2}$)
Aluminum 2014-T6	90.5	93.9	3.0	0.06	50	−253	0.05	81	0.013	1.86/1.70	5.21/ 5.71
Ditto	90.5	93.9	3.0	0.06	50	−253	0.05	83	0.013	1.97/1.80	4.70/ 5.14
Ditto	9.05	93.9	3.0	0.06	50	−253	0.05	86	0.013	2.54/2.05	3.39/ 4.20
Ditto	9.05	93.9	3.0	0.06	50	−253	0.07	73	0.027	1.53/1.46	5.57/ 5.84
Ditto	90.5	93.9	3.0	0.06	50	−253	0.12	63	0.08	1.36/1.31	4.91/ 5.10
Ditto	90.5	93.9	3.0	0.06	50	−253	0.25	40	0.34	1.14/1.13	6.98/ 7.04
Ditto	90.5	93.9	3.0	0.06	50	−253	0.25	39	0.34	1.13/1.12	7.41/ 7.47
Ditto	90.5	93.9	3.0	0.06	50	−253	0.37	33	0.76	1.12/1.11	7.05/ 7.18
Ditto	90.5	93.9	3.0	0.06	50	−253	0.50	21	1.38	1.06/1.06	13.63/13.63
Ditto	90.5	93.9	3.0	0.06	50	−253	0.61	20	2.06	1.08/1.07	12.08/12.20
Ditto	90.5	93.9	3.0	0.06	50	−253	0.87	14	4.20	1.06/1.06	17.63/17.63
Ditto	90.5	93.9	3.0	0.06	50	−253	1.0	11	5.50	1.05/1.04	25.06/25.18
Ditto	90.5	93.9	3.0	0.06	50	−253	1.0	13	5.50	1.07/1.06	17.63/17.79
Ditto	82.0	93.9	3.0	0.06	50	−196	0.06	70	0.02	1.65/1.40	6.5 / 7.7
Ditto	82.0	93.9	3.0	0.06	50	−196	0.06	72	0.02	1.80/1.45	5.69/ 7.06
Ditto	82.0	93.9	3.0	0.06	50	−196	0.06	75	0.02	2.10/1.50	4.49/ 6.29
Ditto	82.0	93.9	3.0	0.06	50	−196	0.07	72	0.027	1.90/1.45	4.62/ 6.05
Ditto	82.0	93.9	3.0	0.06	50	−196	0.10	65	0.055	1.50/1.35	5.02/ 5.58
Ditto	82.0	93.9	3.0	0.06	50	−196	0.14	60	0.10	1.40/1.30	4.51/ 4.86
Ditto	82.0	93.9	3.0	0.06	50	−196	0.15	54	0.12	1.35/1.20	5.39/ 6.06
Ditto	82.0	93.9	3.0	0.06	50	−196	0.20	45	0.22	1.20/1.15	6.55/ 6.84
Ditto	82.0	93.9	3.0	0.06	50	−196	0.20	50	0.22	1.30/1.20	4.89/ 5.30
Ditto	82.0	93.9	3.0	0.06	50	−196	0.25	39	0.34	1.20/1.10	6.98/ 7.62
Ditto	82.0	93.9	3.0	0.06	50	−196	0.25	41	0.34	1.20/1.10	6.31/ 6.89
Ditto	82.0	93.9	3.0	0.06	50	−196	0.37	30	0.76	1.10/1.10	8.69/ 8.69
Ditto	82.0	93.9	3.0	0.06	50	−196	0.50	23	1.38	1.10/1.07	10.95/11.26
Ditto	82.0	93.9	3.0	0.06	50	−196	1.00	20	5.50	1.05/1.04	30.33/30.60
Ditto	82.0	93.9	3.0	0.06	50	−196	1.00	11	5.50	1.06/1.04	24.89/25.37

[a] Two values are computed for φ_3 and $\sigma_R^{*2}\pi c\varphi_3$ corresponding to the upper and lower bounds for $\bar{\sigma}$: $\bar{\sigma}=\sigma_Y$, $\bar{\sigma}=\sigma_U$.

TABLE

Data summary for Duffy et al. for ductile crack extension in steel pipes

Material properties			Vessel geometry			Test conditions			Calculated values[a]			
Designation[b]	σ_Y, ksi	σ_U, ksi	R, in.	t, in.	R/t	Temp, C	c, in.	σ_R^*, ksi	c^2/Rt	φ_3	$(\sigma_R^{*2}\pi c\varphi_3)^{-1}\times 10^{-10}$(in.^{3})(lb^{-2})	$\sigma^{*-2}\times 10^{-10}$(in^4)(lb.$^{-2}$)
Steel RR, TR, BB	60	80	15	0.375	40	−20–24	0.5	70.6	0.044	α/2.00	0/0.638	2.00
Ditto	60	80	15	0.375	40	−20–24	0.5	69.8	0.044	α/2.00	0/0.654	2.05
Ditto	60	80	15	0.375	40	−20–24	1.65	56.2	0.483	α/1.85	0/0.331	3.16
Ditto	60	80	15	0.375	40	−20–24	1.65	55.8	0.483	α/1.85	0/0.335	3.20
Ditto	60	80	15	0.375	40	−20–24	2.25	46.8	0.90	α/1.70	0/0.380	4.50
Ditto	60	80	15	0.375	40	−20–24	2.70	42.6	1.30	α/1.85	0/0.351	5.50
Ditto	60	80	15	0.375	40	−20–24	3.20	38.8	1.82	α/2.0	0/0.329	6.64
Ditto	60	80	15	0.375	40	−20–24	4.40	28.2	3.34	α/1.60	0/0.569	12.50
Ditto	60	80	15	0.375	40	−20–24	4.40	27.8	3.34	α/1.55	0/0.604	12.90
Ditto	60	80	15	0.375	40	−20–24	4.40	27.6	3.34	α/1.55	0/0.613	13.10
Ditto	60	80	15	0.375	40	−20–24	4.40	27.6	3.34	α/1.55	0/0.613	13.10
Steel AF	68	84	15	0.375	40	−16–16	2.65	48.7	1.25	α/2.20	0/0.230	4.22
Ditto	68	84	15	0.375	40	−16–16	2.65	48.1	1.25	α/2.10	0/0.247	4.32
Ditto	68	84	15	0.375	40	−16–16	2.65	47.4	1.25	α/1.90	0/0.281	4.45
Ditto	68	84	15	0.375	40	−16–16	4.40	31.6	3.34	α/1.75	0/0.414	10.00
Ditto	68	84	15	0.375	40	−16–16	7.50	16.5	10.0	1.9 /1.35	0.82 /1.156	37.20
Ditto	68	84	15	0.375	40	−16–16	10.00	11.4	17.6	1.59/1.25	1.54 /1.96	76.90
Steel AC, AD	53	75	15	0.375	40	2–23	3.5	33.0	2.18	α/1.65	0/0.506	9.18
Ditto	53	75	15	0.375	40	2–23	3.5	32.8	2.18	α/1.65	0/0.512	9.30
Ditto	53	75	15	0.375	40	2–23	3.5	32.4	2.18	α/1.62	0/0.535	9.53
Steel UU	61.7	70	3.06	0.25	12.25	−2–0	2.20	25.3	6.35	α/α	0	15.60
Ditto	61.7	70	3.06	0.25	12.25	−2–0	3.55	15.3	16.4	α/α	0	42.70
Steel GP	51	73	13	0.281	46.4	17	2.55	37.9	1.78	α/α	0	6.90
Steel AH	60	80	18	0.406	45	−8–−4	2.7	43.9	1.0	α/1.55	0/0.394	5.10
Ditto	60	80	18	0.406	45	−8–−4	2.7	44.7	1.0	π/1.57	0/0.376	5.00
Ditto	60	80	18	0.406	45	−8–−4	2.7	46.0	1.0	α/1.65	0/0.337	4.70
Steel YY	62	74	18	0.861	21	62	4.85	33.6	1.50	2.6 /1.5	0.223/0.387	8.80

[a] Two values are computed for φ_3 and $\sigma_R^{*2}\pi c\varphi_3$ corresponding to the upper and lower bounds for $\bar{\sigma}$: $\bar{\sigma}=\sigma_Y$, $\bar{\sigma}=\sigma_U$.

[b] The steels employed in this study are X-50 and X-60 grade line-pipe steels.

TABLE

Data summary for Nichols et al. for ductile and semibrittle crack extension in steel, pressure vessels

Material properties			Vessel geometry			Test conditions			Calculated values[a]			
Designation	σ_Y, ksi	σ_U, ksi	R, in.	t, in.	R/t	Temp, C	c, in.	σ_R^*, ksi	c^2/Rt	φ_3	$(\sigma_R^{*2}\pi c\varphi_3)^{-1}\times 10^{-10}$(in.^{3})(lb^{-2})	$\sigma^{*-2}\times 10^{-10}$(in.^{4})(lb.$^{-2}$)
0.36 C Steel[b]	34.5	69.5	30	1.0	30	1–51	3	27.6	0.3	2.3 /1.12	0.6 /1.24	
Ditto	34.5	69.5	30	1.0	30	1–51	3	32.2	0.3	∝/1.16	0/0.88	
Ditto	34.5	69.5	30	1.0	30	1–51	6	18.8	1.2	1.8 /1.09	0.83/1.37	
Ditto	34.5	69.5	30	1.0	30	1–51	6	17.9	1.2	1.62/1.08	1.02/1.53	
Ditto	34.5	69.5	30	1.0	30	1–51	6	21.0	1.2	∝/1.12	0/1.07	
Ditto	34.5	69.5	30	1.0	30	1–51	6	15.9	1.2	1.4 /1.06	1.49/1.98	
Ditto	34.5	69.5	30	1.0	30	1–51	12.37	9.6	5.0	1.5 /1.07	1.86/2.61	
Ditto	34.5	69.5	30	1.0	30	62–88	3	33.0	0.3	—	—	9.8
Ditto	34.5	69.5	30	1.0	30	62–88	6	25.7	1.2	—	—	15.0
Ditto	34.5	69.5	30	1.0	30	62–88	6	27.7	1.2	—	—	13.0
Ditto	34.5	69.5	30	1.0	30	62–88	12	12.7	4.8	—	—	62.0
Ditto	34.5	69.5	30	1.0	30	62–88	12	15.2	4.8	—	—	43.28
Ditto	34.5	69.5	18	1.0	18	10–50	6	13.9	2.0	1.4 /1.06	1.96/2.59	
Ditto	34.5	69.5	18	1.0	18	10–50	6	17.4	2.0	2.15/1.08	0.81/1.62	
Ditto	34.5	69.5	18	1.0	18	79	6	23.4	2.0	—	—	18.2
Ditto	34.5	69.5	57	1.0	57	17	6	22.0	0.63	1.55/1.07	0.7 /1.02	
Ditto	34.5	69.5	57	1.0	57	80	6	27.2	0.63	—	—	13.5
0.13 C Steel[c]	40.0	63.5	30	1.0	30	16–79	6	29.9	1.2	—	—	11.1
Ditto	40.0	63.5	30	1.0	30	16–79	6	31.8	1.2	—	—	9.88
Ditto	40.0	63.5	30	1.0	30	16–79	6	29.4	1.2	—	—	11.56
Ditto	40.0	63.5	30	1.0	30	16–79	6	31.8	1.2	—	—	9.88
Ditto	40.0	63.5	30	1.0	30	16–79	12	19.5	4.8	—	—	26.2
0.16 C Steel[d]	31.0	64.0	30	1.0	30	39	6	28.5	1.2	—	—	13.5

[a] *Two values are computed for φ_3 and $\sigma_R^{*2}\pi c\varphi_3$ corresponding to the upper and lower bounds for $\bar{\sigma}$: $\bar{\sigma} = \sigma_Y$, $\bar{\sigma} = \sigma_U$.*

[b] Plain carbon steel; C: 0.36%, Mn: 0.44–0.46%, Si: 0.10–0.13%. The mode of crack extension in this steel was 100 percent ductile shear above 51 C, semibrittle below 51 C.

[c] Aluminum grain-refined steel; C: 0.13%, Mn: 1.14%, Si: 0.12%. Crack extension mode was 100 percent ductile shear in all cases.

[d] Silicon-killed steel; C: 0.16%, Mn: 1.22%, Si: 0.20%. Crack extension mode was 100 percent ductile shear in all cases.

TABLE

Data summary for Kihara, Ikeda, and Iwanga for brittle-steel vessels

Material properties			Vessel geometry			Test conditions			Calculated values		
Designation	σ_Y, ksi	σ_U, ksi	R, in.	t, in.	R/t	Temp, C	c, in.	σ_R^*, ksi	c^2/Rt	φ_3	$(\sigma_R^{*2}\pi c\varphi_3)^{-1}\times 10^{-10}$(in.^{3})(lb.$^{-2}$)
Steel[a]	115	125	4.3	0.25	17	−196	2.44	3.98	5.56	1.00	82.64
Ditto	115	125	4.3	0.25	17	−196	1.96	4.95	3.59	1.00	66.22
Ditto	115	125	4.3	0.25	17	−196	1.35	8.25	1.70	1.00	34.6
Ditto	115	125	4.3	0.25	17	−196	0.86	13.2	0.69	1.00	21.17
Ditto	115	125	8.0	0.25	32	−196	3.22	4.95	5.18	1.00	40.48
Ditto	115	125	8.0	0.25	32	−196	2.53	5.60	3.20	1.00	40.16
Ditto	115	125	8.0	0.25	32	−196	1.85	8.52	1.71	1.00	23.69
Ditto	115	125	8.0	0.25	32	−196	1.16	9.60	0.67	1.00	29.76
Ditto	115	125	6.0	0.25	25	−196	1.65	7.56	1.80	1.00	33.78
Ditto	115	125	6.4	0.375	17	−196	2.0	4.40	1.66	1.00	81.96
Ditto	115	125	6.4	0.375	17	−196	2.0	5.70	1.66	1.00	49.01
Ditto	115	125	4.3	0.375	11.4	−196	1.65	7.40	1.68	1.00	35.21
Ditto	115	125	8.0	0.375	21.3	−196	2.24	9.90	1.67	1.00	14.42
Ditto	115	125	4.3	0.50	8.6	−196	2.30	3.42	5.44	1.00	176.0
Ditto	115	125	4.3	0.50	8.6	−196	2.63	3.50	3.20	1.00	99.0
Ditto	115	125	4.3	0.50	8.6	−196	1.94	4.20	1.75	1.00	92.99
Ditto	115	125	4.3	0.50	8.6	−196	1.16	9.20	0.62	1.00	31.46
Ditto	115	125	8.0	0.50	16	−196	3.62	2.40	3.27	1.00	153.8
Ditto	115	125	8.0	0.50	16	−196	2.53	4.80	1.60	1.00	54.64
Ditto	115	125	8.0	0.50	16	−196	1.55	7.20	0.60	1.00	39.58
Ditto	115	125	6.4	0.50	12.8	−196	2.34	4.90	1.71	1.00	56.49

[a] Hot-Rolled Steel; C: 0.25%, Si: 0.02%, Mn: 0.85%.

TABLE

Data summary for Almond et al. for ductile-steel vessels

Material properties			Vessel geometry			Test conditions			Calculated values			
Designation	σ_y, ksi	σ_U, ksi	R, in.	t, in.	R/t	Temp, C	c, in.	σ_H^*, ksi	c^2/Rt	φ_3	$(\sigma_H^{*2}\pi c\varphi_3)^{-1}\times 10^{-10}$(in.^{3})(lb.$^{-2}$)	$c^{*-2}\times 10^{-10}$(in.^{4})(lb.^{2})
Steel[a]	45.7	66.0	2.5	0.5	5.0	−25	1.125	32.0	1.01	—	—	9.75
Ditto	45.7	66.0	2.5	0.5	5.0	−25	1.125	35.5	1.01	—	—	7.94
Ditto	45.7	66.0	2.5	0.5	5.0	−25	1.125	36.0	1.01	—	—	7.70
Ditto	47.0	70.6	2.5	0.5	5.0	−5-5	1.125	38.0	1.01	—	—	6.94
Ditto	47.0	70.6	2.5	0.5	5.0	−5-5	1.125	36.5	1.01	—	-	7.50
Ditto	47.0	70.6	2.5	0.5	5.0	−5-5	1.125	35.5	1.01		—	7.94
Ditto	49	77	2.5	0.5	5.0	−68	1.125	42.5	1.01	—	—	5.54
Ditto	66	88	2.5	0.5	5.0	−120	1.125	45.7	1.01	—	—	4.80

[a] Hot Rolled Steel; C: 0.14%, Si: 0.26%, Mn: 0.47%. Crack extension occurred by ductile fibrous mode, at least initially.

TABLE

Data summary for Peters and Kuhn for aluminum-alloy vessels

Material properties			Vessel geometry			Test conditions			Calculated values		
Designation	σ_y, ksi	σ_U, ksi	R, in.	t, in.	R/t	Temp. C	c, in.	σ_H^*, ksi	$50(c^2/R^2)\tanh(R/50t)$	φ_3	$(\sigma_H^{*2}\pi c\varphi_3)^{-1}\times 10^{-10}$(in.^{3})(lb.$^{-2}$)
Aluminum 2024-T3	36.5	65.0	14.4	0.015	960	Room Temp	0.31	41.3	0.023	∝/1.25	0/ 4.81
Ditto	36.5	65.0	14.4	0.015	960	Ditto	0.64	29.8	0.098	1.74/1.12	3.21/ 4.99
Ditto	36.5	65.0	14.4	0.015	960	Ditto	1.25	20.4	0.37	1.2?/1.07	4.67/ 5.71
Ditto	36.5	65.0	14.4	0.015	960	Ditto	2.55	11.3	1.56	1.18/1.04	8.28/ 9.39
Ditto	36.5	65.0	14.4	0.015	960	Ditto	3.85	8.2	3.57	1.18/1.05	10.42/11.71
Ditto	36.5	65.0	3.6	0.025	144	Ditto	0.50	21.9	0.96	2.62/1.15	5.06/11.54
Ditto	36.5	65.0	3.6	0.025	144	Ditto	1.0	10.4	3.84	1.41/1.08	20.85/27.23
Ditto	36.5	65.0	3.6	0.025	144	Ditto	2.81	3.4	29.50	1.25/1.06	78.43/92.48
Ditto	36.5	65.0	3.6	0.015	230	Ditto	0.31	29.3	0.37	∝/1.18	0/10.13
Ditto	36.5	65.0	3.6	0.015	230	Ditto	0.60	17.2	1.38	1.6?/1.11	11.20/15.14
Ditto	36.5	65.0	3.6	0.015	230	Ditto	1.20	8.7	5.50	1.39/1.08	25.24/32.48
Ditto	36.5	65.0	3.6	0.012	300	Ditto	0.49	22.9	0.92	∝/1.16	0/10.68
Ditto	36.5	65.0	3.6	0.012	300	Ditto	1.0	12.8	3.85	2.18/1.14	8.90/17.03
Ditto	36.5	65.0	3.6	0.012	300	Ditto	2.0	5.7	15.40	1.46/1.09	33.57/44.97
Ditto	36.5	65.0	3.6	0.012	300	Ditto	1.90	5.4	13.90	1.32/1.07	43.53/53.7
Ditto	36.5	65.0	3.6	0.012	300	Ditto	0.48	22.8	0.88	2.62/1.15	4.86/11.09
Ditto	36.5	65.0	3.6	0.012	300	Ditto	0.95	10.2	3.48	1.34/1.07	23.99/30.05
Ditto	36.5	65.0	3.6	0.012	300	Ditto	0.28	40.2	0.05	∝/1.24	0/ 5.67
Ditto	36.5	65.0	3.6	0.012	300	Ditto	0.12	41.4	0.05	∝/1.26	0/12.28
Ditto	36.5	65.0	3.6	0.012	300	Ditto	0.25	30.6	0.25	∝/1.16	0/11.72
Ditto	36.5	65.0	3.6	0.012	300	Ditto	0.25	26.4	0.25	1.41/1.11	12.96/16.46
Ditto	36.5	65.0	3.6	0.012	300	Ditto	0.48	20.0	0.80	1.57/1.10	10.56/15.07
Ditto	36.5	65.0	3.6	0.012	300	Ditto	0.93	10.7	3.35	1.37/1.08	21.78/27.63
Ditto	36.5	65.0	3.6	0.012	300	Ditto	1.91	4.9	12.50	1.22/1.66	56.92/65.51
Ditto	36.5	65.0	3.6	0.012	300	Ditto	3.80	2.6	50.0	1.24/1.66	99.56/116.46
Ditto	36.5	65.0	3.6	0.012	300	Ditto	0.48	20.4	0.80	1.62/1.11	9.82/14.34
Ditto	36.5	65.0	3.6	0.012	300	Ditto	0.48	21.0	0.80	1.71/1.12	8.79/13.42
Ditto	36.5	65.0	3.6	0.06	600	Ditto	0.12	44.4	0.05	∝/1.32	0/10.39
Ditto	36.5	65.0	3.6	0.06	600	Ditto	0.23	27.3	0.15	1.56/1.10	11.89/16.86
Ditto	36.5	65.0	3.6	0.06	600	Ditto	0.48	20.7	0.80	1.67/1.11	9.26/13.94
Ditto	36.5	65.0	3.6	0.06	600	Ditto	0.98	10.2	3.50	1.34/1.07	23.32/29.2

TABLE

Data summary for Peters and Kuhn for aluminum-alloy vessels

Materials properties			Vessel geometry			Test conditions			Calculated values[a]		
Designation	σ_y, ksi	σ_U, ksi	R, in.	t, in.	Rt	Temp, C	c, in.	σ_H^*, ksi	$50(c^2/R^2)\tanh(R/50t)$	φ_3	$(\sigma_H^{*2}\pi c\varphi_3)^{-1}\times 10^{-10}$(in.^{3})(lb.$^{-2}$)
Aluminum 7075-T6	65	80	3.6	0.016	225	Room Temp	0.33	19.4	0.40	1.06/1.04	24.68/ 24.65
Ditto	65	80	3.6	0.016	225	Ditto	0.65	11.7	1.60	1.05/1.03	34.08/ 34.74
Ditto	65	80	3.6	0.016	225	Ditto	1.28	5.5	4.50	1.02/1.01	80.60/ 81.43
Ditto	65	80	3.6	0.025	144	Ditto	0.50	16.6	0.50	1.05/1.03	22.01/ 22.44
Ditto	65	80	3.6	0.025	144	Ditto	1.0	8.4	3.90	1.06/1.03	42.57/ 43.81
Ditto	65	80	3.6	0.025	144	Ditto	2.0	3.7	15.50	1.04/1.02	111.84/114.03
Ditto	65	80	14.4	0.016	960	Ditto	0.31	37.2	0.02	2.02/1.39	3.67/ 5.34
Ditto	65	80	14.4	0.016	960	Ditto	0.65	24.9	0.09	1.08/1.05	7.31/ 7.52
Ditto	65	80	14.4	0.017	847	Ditto	1.30	13.6	0.40	1.03/1.02	12.85/ 12.98
Ditto	65	80	14.4	0.017	847	Ditto	2.50	8.5	1.40	1.02/1.01	17.29/ 17.46

[a] Two values are computed for φ_3 and $\sigma_H^{*2}\pi c\varphi_3$ corresponding to the upper and lower bounds for $\bar{\sigma}: \bar{\sigma} = \sigma_y$, $\bar{\sigma} = \sigma_U$.

TABLE

Data summary for Crichlow and Wells for titanium-alloy vessels

Material properties			Vessel geometry[a]			Test conditions			Calculated values[b]		
Designation	σ_Y, ksi	σ_U, ksi	R, in.	t, in.	R/t	Temp, C	c, in.	σ_H^*, ksi	$50(c^2/R^2)\tanh(R/50t)$	φ_3	$(\sigma_H^{*2}\pi c\varphi_3)^{-1}\times 10^{-10}$ (in.^{3})(lb.$^{-2}$)
Ti-8AC-1Mo-1V	138	149	15	0.05	300	Room Temp	2.25	30.0	1.125	1.06/1.05	1.48/1.49
Ditto	138	149	15	0.05	300	Ditto	3.40	25.0	2.568	1.08/1.06	1.38/1.41
Ditto	138	149	15	0.05	300	Ditto	4.20	19.0	3.920	1.06/1.05	1.98/2.0
Ditto	138	149	15	0.05	300	Ditto	8.0	11.3	14.220	1.07/1.06	2.91/2.94
Ditto	138	149	15	0.05	300	Ditto	9.2	10	18.800	1.07/1.06	3.23/3.26
Ditto	138	149	33.3	0.03	1100	Ditto	2.6	30	0.30	1.02/1.02	1.33/1.33
Ditto	138	149	33.3	0.03	1100	Ditto	5.5	15	1.36	1.02/1.02	2.54/2.54
Ditto	138	149	70	0.03	2325	Ditto	4.25	30	0.18	1.05/1.04	0.79/8.0
Ditto	138	149	70	0.03	2325	Ditto	9.20	15	0.86	1/1	1.53

[a] The $R = 15$-in. tests involved cylindrical vessels, the $R = 33.3$-in. and 70-in. tests involved curved panels.
[b] Two values are computed for φ_3 and $\sigma_H^{*2}\pi c\varphi_3$ corresponding to the upper and lower bounds for $\bar{\sigma}$: $\bar{\sigma} = \sigma_Y$, $\bar{\sigma} = \sigma_U$.

TABLE

Data summary for Anderson and Sullivan for titanium-alloy vessels

Material properties			Vessel geometry			Test conditions			Calculated values[a]		
Designation	σ_Y, ksi	σ_U, ksi	R, in.	t, in.	R/t	Temp, C	c, in.	σ_H^*, ksi	$50(c^2/R^2)\tanh(R/50t)$	φ_3	$(\sigma_H^{*2}\pi c\varphi_3)^{-1}\times 10^{-10}$ (in.^{3})(lb.$^{-2}$)
Ti-5Al-2.5 Sn	193	220	3.0	0.02	150	−196	0.06	190.4	0.02	∞/1.76	0/0.83
Ditto	193	220	3.0	0.02	150	−196	0.12	164.9	0.08	1.90/1.49	0.51/0.65
Ditto	193	220	3.0	0.02	150	−196	0.11	156.6	0.06	1.63/1.38	0.72/0.85
Ditto	193	220	3.0	0.02	150	−196	0.22	115.5	0.26	1.32/1.14	0.82/0.95
Ditto	193	220	3.0	0.02	150	−196	0.23	105.1	0.29	1.26/1.18	0.99/1.06
Ditto	193	220	3.0	0.02	150	−196	0.37	84.9	0.75	1.25/1.18	0.95/1.01
Ditto	193	220	3.0	0.02	150	−196	0.38	74.6	0.80	1.18/1.13	1.27/1.33
Ditto	193	220	3.0	0.02	150	−196	0.47	71.8	1.22	1.24/1.16	1.05/1.13
Ditto	193	220	3.0	0.02	150	−196	0.49	66.2	1.33	1.21/1.14	1.22/1.30
Ditto	193	220	3.0	0.02	150	−196	0.74	44.1	3.00	1.16/1.11	1.90/1.99
Ditto	193	220	3.0	0.02	150	−196	0.73	35.9	2.90	1.09/1.07	3.10/3.16
Ditto	219	240	3.0	0.02	150	−253	0.04	171.5	0.01	1.46/1.34	1.61/1.75
Ditto	219	240	3.0	0.02	150	−253	0.07	160.9	0.03	1.39/1.30	1.14/1.22
Ditto	219	240	3.0	0.02	150	−253	0.09	133.9	0.05	1.23/1.18	1.51/1.58
Ditto	219	240	3.0	0.02	150	−253	0.13	121.4	0.10	1.20/1.16	1.30/1.34
Ditto	219	24	3.0	0.02	150	−253	0.14	114.2	0.10	1.16/1.13	1.50/1.54
Ditto	219	240	3.0	0.02	150	−253	0.26	84.6	0.37	1.11/1.09	1.54/1.56
Ditto	219	240	3.0	0.02	150	−253	0.24	76.0	0.32	1.08/1.06	2.12/2.15
Ditto	219	240	3.0	0.02	150	−253	0.40	63.6	0.88	1.09/1.08	1.79/1.82
Ditto	219	240	3.0	0.02	150	−253	0.47	63.0	1.22	1.13/1.09	1.52/1.55
Ditto	219	240	3.0	0.02	150	−253	0.38	61.5	0.80	1.08/1.07	2.05/2.06
Ditto	219	240	3.0	0.02	150	−253	0.49	51.6	1.33	1.08/1.06	2.25/2.30
Ditto	219	240	3.0	0.02	150	−253	0.80	40.6	3.55	1.11/1.09	2.17/2.21
Ditto	219	240	3.0	0.02	150	−253	0.78	37.7	3.38	1.08/1.07	2.65/2.68

[a] Two values are computed for φ_3 and $\sigma_H^{*2}\pi c\varphi_3$ corresponding to the upper and lower bounds for $\bar{\sigma}$: $\bar{\sigma} = \sigma_Y$, $\bar{\sigma} = \sigma_U$.

TABLE

Data summary for Sechler and Williams for brass vessels

Material properties			Vessel geometry			Test conditions			Calculated values[a]		
Designation	σ_y, ksi	σ_u, ksi	R, in.	t, in.	R/t	Temp, C	c, in.	σ_H^*, ksi	$50(c^2/Rt)\tanh$ $(R/50t)$	φ_3	$(\sigma_H^{*2}\pi c\varphi_3)^{-1}$ 10^{-10}(in.^{3})(lb.$^{-2}$)
Brass[b]	45	57	1.5	0.001	1500	Room Temp	0.03	50.6	0.02	$\pi/1.86$	0/22.3
Ditto	45	57	1.5	0.001	1500	Ditto	0.04	45.4	0.03	$\pi/1.52$	0/25.4
Ditto	45	57	1.5	0.001	1500	Ditto	0.06	37.1	0.08	1.74/1.71	22.18/29.47
Ditto	45	57	1.5	0.001	1500	Ditto	0.10	30.0	0.22	1.44/1.21	24.53/29.2
Ditto	45	57	1.5	0.001	1500	Ditto	0.10	30.0	0.22	1.44/1.21	24.13/29.2
Ditto	45	57	1.5	0.001	1500	Ditto	0.12	25.5	0.32	1.31/1.16	31.15/35.18
Ditto	45	57	1.5	0.001	1500	Ditto	0.12	25.7	0.32	1.31/1.16	30.65/34.62
Ditto	45	57	1.5	0.001	1500	Ditto	0.13	26.8	0.37	1.39/1.19	24.55/24.68
Ditto	45	57	1.5	0.001	1500	Ditto	0.15	24.0	0.50	1.33/1.17	27.74/31.53
Ditto	45	57	1.5	0.001	1500	Ditto	0.15	21.7	0.50	1.25/1.13	36.03/39.86
Ditto	45	57	1.5	0.001	1500	Ditto	0.17	19.1	0.64	1.20/1.11	42.73/46.2
Ditto	45	57	1.5	0.001	1500	Ditto	0.21	19.1	0.98	1.28/1.15	32.55/36.23
Ditto	45	57	1.5	0.001	1500	Ditto	0.25	14.2	1.38	1.17/1.10	54.09/57.53
Ditto	45	57	1.5	0.001	1500	Ditto	0.30	13.3	2.00	1.21/1.11	49.48/53.94
Ditto	45	57	1.5	0.001	1500	Ditto	0.35	11.0	2.70	1.16/1.09	64.81/68.97
Ditto	40	53.7	2.5	0.001	2500	Ditto	0.032	48.0	0.008	$\pi/1.86$	0/23.17
Ditto	40	53.7	2.5	0.001	2500	Ditto	0.032	46.1	0.008	$\pi/1.66$	0/25.14
Ditto	40	53.7	2.5	0.001	2500	Ditto	0.062	40.0	0.03	$\pi/1.40$	0/22.89
Ditto	40	53.7	2.5	0.001	2500	Ditto	0.094	37.0	0.07	2.6/1.36	9.52/18.2
Ditto	40	53.7	2.5	0.001	2500	Ditto	0.094	38.7	0.07	$\pi/1.40$	0/16.16
Ditto	40	53.7	2.5	0.001	2500	Ditto	0.10	35.0	0.08	1.98/1.30	13.11/19.98
Ditto	40	53.7	2.5	0.001	2500	Ditto	0.125	32.2	0.12	1.76/1.26	13.96/19.50
Ditto	40	53.7	2.5	0.001	2500	Ditto	0.125	30.2	0.12	1.54/1.21	18.13/23.09
Ditto	40	53.7	2.5	0.001	2500	Ditto	0.15	27.5	0.18	1.44/1.18	19.50/25.80
Ditto	40	53.7	2.5	0.001	2500	Ditto	0.156	26.2	0.20	1.39/1.16	21.41/25.65
Ditto	40	53.7	2.5	0.001	2500	Ditto	0.156	27.0	0.20	1.43/1.18	19.58/23.75
Ditto	52	63.2	2.5	0.003	833	Ditto	0.048	56.4	0.018	$\pi/1.66$	0/11.2
Ditto	52	63.2	2.5	0.003	833	Ditto	0.098	50.0	0.076	$\pi/1.60$	0/8.11
Ditto	52	63.2	2.5	0.003	833	Ditto	0.115	48.4	0.10	$\pi/1.54$	0/7.67
Ditto	52	63.2	2.5	0.003	833	Ditto	0.125	42.5	0.12	$\pi/1.54$	0/9.15
Ditto	52	63.2	2.5	0.003	833	Ditto	0.125	45.0	0.12	2.24/1.44	5.61/8.73
Ditto	52	63.2	2.5	0.003	833	Ditto	0.125	43.2	0.12	1.88/1.22	8.25/11.18
Ditto	52	63.2	2.5	0.003	833	Ditto	0.148	41.3	0.17	1.85/1.38	8.10/9.13

[a] Two values are computed for φ_3 and $\sigma_H^{*2}\pi c\varphi_3$ corresponding to the upper and lower bounds for $\bar{\sigma}$, $\bar{\sigma} = \sigma_y$, $\bar{\epsilon} = \epsilon_L$.

[b] Brass shim stock.

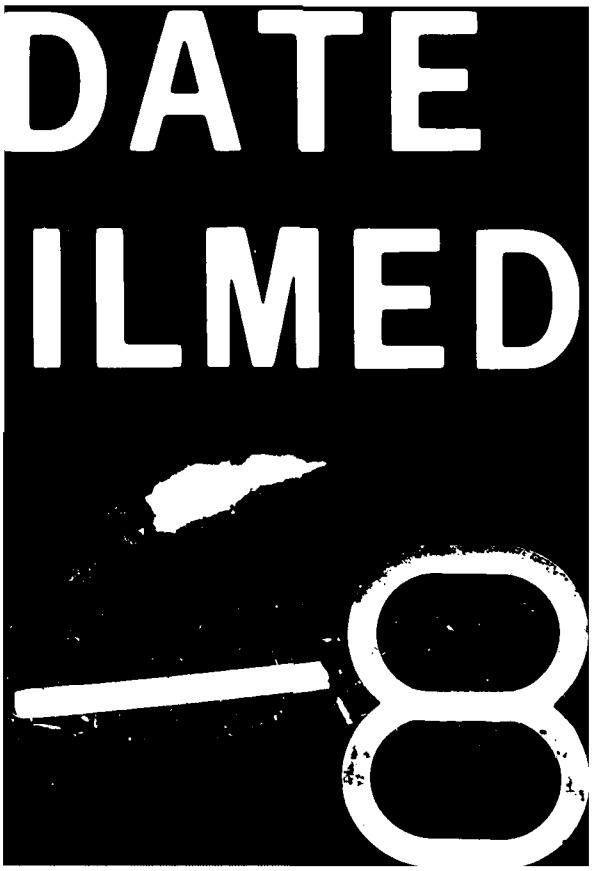
DATE
ILMED
8